Alma Mater Studiorum · University of Bologna

School of Science
Department of Physics and Astronomy
Master Degree in Physics

Study of a 2D Bose-Fermi mixture with Quantum Monte Carlo methods

Supervisor:
Prof. Pierbiagio Pieri

Co-supervisor:
Dr. Gianluca Bertaina

Submitted by:
Jacopo D'Alberto

Academic Year 2020/2021

Abstract

Ultracold gases are an exceptionally versatile platform to test novel physical concepts. Thanks to the development of new experimental techniques, they have greatly advanced our understanding of the physics of many-body systems and allowed precision measurements of fundamental constants. Bose-Fermi mixtures can then be introduced in this context. This novel quantum many-body system is essentially an ultracold gas made up by both bosons and fermions, where tunable attractive or repulsive interactions between the components can be introduced. At T = 0 and for weak interactions the bosons condense while the fermions behave as a Fermi liquid. In particular, a recent system of interest is given by two-dimensional Bose-Fermi mixtures with both Bose-Fermi and Bose-Bose repulsive interactions. In the present work, a Quantum Monte Carlo study is conducted, for a fixed value of boson concentration, at zero-temperature from the weak to the strong Bose-Fermi coupling limit. Variational Monte Carlo and Fixed-Node Diffusion Monte Carlo are applied using an optimized Jastrow-Slater wavefunction, extending previous methodology developed for the three-dimensional case. The results are then compared with perturbative predictions, showing very good agreement in the weak coupling region. Variational Monte Carlo agrees with the analytic predictions only for extremely weak coupling, while Diffusion Monte Carlo proves necessary to recover good agreement over the whole perturbative regime. For stronger couplings, our simulations indicate the tendency of the mixture to form bosonic clusters. This finding would definitively deserve further investigation, which is postponed to future works.

Contents

Introduction

All particles in nature can be distinguished between bosons, obeying Bose-Einstein statistics, and fermions, obeying Fermi-Dirac statistics. These different statistics determine a very different behaviour in the quantum regime, namely when the thermal wavelength $\lambda_T = h/\sqrt{2\pi m k_B T}$ associated to a particle of mass m at temperature T (h and k_B being the Planck and Boltzmann constants, respectively) becomes comparable to the average interparticle distance $n^{-1/d}$ (where n is the particle density and d the dimensionality of the system). At sufficiently low temperature, noninteracting bosons condense in a single quantum state, with all particles sharing the same single-particle wavefunction. For fermions this is strictly forbidden by Pauli exclusion principle. The first phenomenon, known as Bose-Einstein condensation (BEC), is at the heart of superfluidity and superconductivity. Fermi statistics, on the other hand, guarantees the existence and stability of atomic structures, including the elements and molecules of which we are made. Furthermore, for fermions, a microscopic theory for pairing in charged systems was introduced in 1957 by Bardeen, Cooper and Schrieffer [1]. In their celebrated BCS theory, the (conventional) superconductivity, discovered in 1911, was explained in terms of the formation of electronic pairs (Cooper pairs) below a certain critical temperature, giving a good description of the phenomenology observed in experiments with conventional superconductors. The subsequent discovery of the first cuprate superconductor in 1986 by Bednorz and Müller gave a large impetus to the search for a theory able to connect the conventional superconductor to such novel systems and motivated the exploration of the so called BCS-BEC crossover.

All these physical phenomena find an excellent testing platform in ultracold gases. In fact, thanks to the recent development of experimental techniques, such as laser cooling, it has been possible to cool down to near absolute zero atomic and molecular gases and explore in this way the quantum regime where these interesting phenomena occur. In addition, ultracold gases allow one to test theories and to address fundamental issues of quantum mechanics as well as to reproduce physical systems relevant to other areas in physics, with a flexibility and a degree of tunability of parameters unimaginable in the original system of interest. Furthermore ultracold gases offer the possibility to construct novel many-body systems, which are not commonly found in nature.

Bose-Fermi mixtures can be introduced within this florid framework. These novel

quantum systems have attracted much attention over the last fifteen years. It is essentially an ultracold gaseous mixture made up by both bosons and fermions, where attractive or repulsive interactions between the two components can be introduced. A new experimental technique, which exploits Feshbach resonances in the scattering between atoms, has made it possible to tune the interaction between bosons and fermions by simply changing the value of external parameters (such as the magnetic field) [2], and explore almost all the interaction regimes of the system. The situation of most interest is that of a Bose-Fermi mixture with an attractive interaction between bosons and fermions (and a reciprocal repulsive interaction between bosons). At zero temperature, one expects that for weak Bose-Fermi attraction a Fermi sea will coexist with a BEC of bosons. By increasing the interaction strength, molecular bound states of one boson and one fermion will be created. Such molecular bound states are fermionic Feshbach molecules which, contrary to the case of the BCS-BEC crossover in fermionic systems, cannot condense because they obey the Fermi-Dirac statistics. By increasing the coupling, the condensate will be progressively depleted by the conversion of bosons (and fermions) to composite fermions. By increasing further the coupling and assuming that the number of bosons does not exceed the number of fermions, the conversion of bosons into composite fermions will be complete, and the original Bose-Fermi mixture will behave as a Fermi-Fermi mixture in such molecular regime. For systems with majority of fermions, a first order phase transition has been found to divide the molecular region from the region where a BEC is present at $T = 0$ [3], contrary to the case of the BCS-BEC crossover in ultracold fermions for which the weakly-interacting regime is connected to the strongly-interacting regime with a crossover.

Bose-Fermi mixtures with an attractive boson-fermion interaction have already been studied in three dimensions both theoretically and experimentally. In particular, Bose-Fermi mixtures can be treated, from a numerical point of view, through Quantum Monte Carlo techniques (QMC). Variational Monte Carlo (VMC) and Fixed-Node Diffusion Monte Carlo (FN-DMC) are both used to obtain upper bounds for the ground state energy of the gas. For three-dimensional Bose-Fermi mixtures, Quantum Monte Carlo studies have been developed at zero temperature from the weak to the strong-coupling limit, providing a good description of the system both in the condensed and in the molecular phase [3, 4].

The possibility to confine ultracold gases in a two-dimensional trap geometry prompted interest in two-dimensional mixtures. Fermi-Fermi mixtures in two dimensions have already been studied in some theoretical works [5, 6]. Two-dimensional Bose-Fermi mixtures are, instead, still marginally explored in the literature. A recent paper by Bazak and Petrov [7], has motivated great interest on two-dimensional Bose-Fermi mixtures with an attractive BF interaction and a repulsive BB interaction. The authors, in fact, showed an important result: the composite fermionic dimers (boson + fermion), formed in the two-dimensional mixture, may exhibit a strong p-wave mutual attraction, which should lead to a stable p-wave superfluid gas. Thus, a complete and exhaustive study

of this system, both with theoretical and numerical techniques, may be helpful to develop guidelines for future experiments with the aim of realizing the first high-T_C p-wave superfluid in ultracold fermionic matter.

This is the context in which the present thesis sets in. Before studying the system described by Bazak and Petrov, however, a preliminary study must be conducted for a simpler system, that is, a two-dimensional Bose-Fermi mixture with both repulsive BF and BB interactions. Compared to the system considered in [7], this system does not foresee the formation of the fermionic dimers but, instead, is characterized only by a homogeneous phase, which is very similar to the condensed phase of the previous mixture. Thus, the purpose of this thesis is to carry out a Quantum Monte Carlo study of a Bose-Fermi mixture with both BF and BB repulsive interactions, by extending and adapting the methodology developed for three-dimensional Bose-Fermi mixtures. The results of the simulations are then compared with perturbative predictions [8], for which agreement is expected at least for low values of the BF interaction.

The dissertation is organized as follows. In Chapter 1 we introduce the reader into the field of ultracold gases, paying particular attention to the phenomenon of Feshbach resonances and to the recent theoretical and experimental interest in Bose-Fermi mixtures.

Chapter 2 is entirely devoted to the vast world of Quantum Monte Carlo. In particular, after a brief review of some fundamental concepts of statistics, we face the problem of the generation of random numbers according to a generic probability distribution function, which can be solved by introducing an important algorithm: the Metropolis algorithm. Then we show how the integral of a function can be dealt using Monte Carlo methods, introducing the fundamental concept of importance sampling. Variational Monte Carlo and Diffusion Monte Carlo are thus introduced, paying particular attention to how the simulations must be implemented and which trial function best approximates the true ground state wavefunction. Furthermore, some sections are devoted to the approximations used during our simulations and how these affect our results.

Chapter 3 is mainly dedicated to the results of our simulations. We first show the conventions used during our work in order to clarify the notation. Then the results of VMC and DMC simulations, together with the results of all the preliminary analyses carried out, are presented. Finally, the last section is reserved for the comparison between QMC results and theoretical predictions ([8]).

Chapter 1

Ultracold Bose-Fermi mixtures

1.1 Ultracold Gases

Ultracold gases [9, 10, 11] are a relatively young field in atomic and molecular physics. They became world-wide known after the experimental achievement of Bose-Einstein condensation in 1995 [12, 13]. In more recent years, these systems have attracted a great deal of attention also in other areas of physics, such as condensed matter physics, nuclear physics and quantum information. This is mainly due to the high degree of control that can be achieved experimentally. Feshbach resonances, for example, can be used to tune the interaction strength between atoms. Furthermore, optical potentials allow to vary the magnitude of the interactions as well as the effective dimensionality of the system.

The physics of ultracold gases concerns atomic systems with low densities and with temperatures close to absolute zero. Three length scales are used to identify the physical regime of ultracold gases: the range of the interaction potential between atoms r_0, the mean interparticle distance l_m and the thermal de Broglie wavelength λ_T.

The quantum degeneracy regime is achieved when the thermal de Broglie wavelength (which represents the size of the wavepacket associated to a particle) is on the order of or larger than the interparticle distance ($\lambda_T \gtrsim l_m$). In such regime quantum effects will dominate, in the sense that particles become indistinguishable and can no longer be described by classical Maxwell-Boltzmann statistics.

The diluteness condition is also fundamental in the context of ultracold gases and it is reached when both the thermal wavelength λ_T and the interparticle distance l_m are larger than r_0. In particular, this condition guarantees universality in the description of the scattering of particles: the scattering problem does not depend on the features of the interatomic potential, but only on the lowest angular momentum scattering length a.

1.2 Feshbach resonances

In this section we show the main aspects that characterize the phenomenon known as Feshbach resonance. It is not the purpose of this thesis to present a thorough review of scattering theory and of all the resulting phenomena (we refer the reader to references [14, 15]).

In a scattering process, the internal states of the particles in the initial or final states are described by a set of quantum numbers, such as those for the spin, the atomic species, and their state of excitation. Generally, a possible choice of these quantum numbers identifies the so called *channel*. Clearly, this implies that scattering processes can be divided into single-channel scattering problems or multi-channel scattering problems. To give an example, at the temperature of interest for Bose-Einstein condensation, atoms are in their electronic ground states and the only relevant internal states are therefore the hyperfine states. Because of the existence of several hyperfine states for a single atom, the scattering of cold alkali atoms is a multi-channel problem.

In a multi-channel scattering problem, the elastic scattering in one channel can be altered dramatically if there is a low-energy bound state in a second channel which is closed (in the sense that its energy is higher than the available energy when the particles are free at large distance). This phenomenon, generally known as Feshbach resonance, was first investigated in the context of nuclear physics. Then, thanks to its versatility, it has become a fundamental tool in investigations of the basic atomic physics of cold atoms. In particular, Feshbach resonances appear when the total energy of two scattering particles in an open channel is approaching the energy of a bound state in a closed channel. Two particles in an open channel can scatter to an intermediate state in a closed channel, which subsequently decays to give two particles in one of the open channels. This second-order processes give rise to a contribution to the scattering amplitude which has the form of a sum of terms of the type

$$a \sim \frac{1}{E - E_{res}} , \tag{1.1}$$

where E is the energy of the particles in the open channel and E_{res} is the energy of a bound state in the closed channels modified by the coupling between closed and open channels. Consequently, the closer the bound closed state energy is to the energy of the incoming particles in the open channels, the greater the effect on the scattering length. The effective interaction between particles in the open channel can thus become attractive or repulsive, depending on the side of the resonance. Since the energies of states depend on the external parameters, such as the magnetic field, these resonances make it possible to tune the effective interactions between atoms.

Given an external magnetic field B applied to the system under study, we call B_0 the value of the field at which the threshold energy of the open channel matches the modified bound-state energy (E_{ref}) in the closed channel. The expression for the scattering length

in presence of a Feshbach resonance is given by:

$$a = a_{bg}\left(1 - \frac{\Delta B}{B - B_0}\right) , \tag{1.2}$$

where a_{bg} is the background scattering length far from the resonance and ΔB is the width parameter. The scattering length a is thus changed by the resonance for variations of the magnetic field of the order of ΔB, which represents the width of the resonance. This parameter depends on the coupling between the channels and on the different magnetic moments in the channels (for further detail see Ref. [15]). Eq. 1.2 shows that, for $B = B_0$, the scattering length has a divergence. In the context of ultracold gases, one refers to this particular situation as the *unitarity limit*. Notice also that, because of the dependence of the scattering length on $1/(B - B_0)$, large changes in the interaction as well as changes in the sign of the interaction can be obtained just by slightly varying the magnetic field.

1.3 Bose-Fermi mixtures

After an exploration of a rich variety of systems, entirely composed by the same species of bosons or fermions, nowadays the attention is focusing on a new interesting kind of systems, the mixtures, which include ultracold gases composed by bosons and fermions, or by bosons of two different atomic species, or by multi-component fermions (for example fermions of the same atomic species in two or more different hyperfine levels). Feshbach resonances play again a relevant role, since they can be exploited to tune the interaction between particles, allowing the realization of numerous experiments. The first heteronuclear boson-fermion Feshbach molecules were obtained in Hamburg [16] and later in Boulder [17], with a Bose-Fermi mixture of ^{40}K $-$ ^{87}Rb in presence of a Feshbach resonance. The creation of Feshbach molecules in B-F mixtures was achieved also with ^{23}Na $-$ ^{6}Li [18] and ^{23}Na $-$ ^{40}K [19] mixtures, in the latter case observing lifetimes of the order of 100 ms, sufficient for the setup of many-body effects.

On the theoretical side, the initial works on boson-fermion mixtures studied, mainly with mean-field and perturbative approaches, the problem of instability (for collapse or phase-separation) of the systems [20, 21, 22]. Subsequent research started to consider what happens in the presence of a Feshbach resonance and to study strongly interacting systems, approaching the problem in several ways: within mean-field approximation, with the diagrammatic formalism or with fully numerical methods (Quantum Monte Carlo methods).

The case of broad Fano-Feshbach resonance attracted a lot of attention in recent years. This is because broad resonances imply the smallness of the effective range parameter r_0 of the boson-fermion interaction with respect to both the average particle

distance l_m and the boson-fermion scattering length a_{BF} [23]. Then, under these conditions, the system can be described simply by a Hamiltonian made just by bosons and fermions mutually interacting via a contact potential, without explicitly describing internal degrees of freedom of the atoms.

The most relevant case of Bose-Fermi mixture in literature is the one in which there is an attractive Bose-Fermi (BF) interaction and a repulsive Bose-Bose (BB) interaction. In particular, it is expected that for weak attraction, at sufficiently low temperature the bosons condense, while the fermions behave like a Fermi liquid, and the BF interaction can be treated with perturbative methods [24, 25]. Instead, for sufficiently strong attraction, bosons and fermions pair into molecules. The two above opposite regimes of a Bose-Fermi mixture have thus been explored already to some extent in experiments. The intermediate (unitary) region, instead, has remained inaccessible so far, essentially because of the large losses due to the three-body recombination into deep energy levels, favored by the presence of three-body (Efimov) bound states. Some control of these losses should, however, be achieved by working with small concentrations of bosons (the dominant recombination process being proportional to the square of the density of the bosons), and by considering isotopic mixtures, for which Efimov states are relevant only very close to the resonance [26].

The Bose-Fermi mixtures described above were studied also with numerical and diagrammatic approaches. In particular, in [27, 3] the competition between Bose-Fermi pairing and boson condensation in a broadly resonant three-dimensional Bose-Fermi mixture was analysed. The authors showed that for increasing Bose-Fermi attraction, the boson-fermion pairing correlations progressively reduce the boson condensation temperature and make it eventually vanish at a critical coupling above which the condensate is completely depleted. Furthermore, in the case of a Bose-Fermi mixture with a prevalence of fermions, a first-order quantum phase transition was found from a state with condensed bosons immersed in a Fermi sea, to a Fermi-Fermi mixture of composite fermions and unpaired fermions.

1.3.1 Two-dimensional case

Thanks to the possibility of confining mixtures in two dimensions using optical potentials, a new interest has arisen towards two-dimensional mixtures. A peculiarity of these systems is the presence of an additional resonance (confinement-induced resonance) which offers greater flexibility in tuning the interactions between the components of the mixture.

A very important theoretical study was conducted by Bazak and Petrov [7], where it was shown that in a two-dimensional Bose-Fermi mixture, for a sufficiently strong Bose-Bose repulsion, two- and three-molecule collisions are elastic. Furthermore, according to that paper, the composite fermionic dimers, formed in the two-dimensional mixture,

may exhibit a strong p-wave mutual interaction, which should lead to a stable p-wave superfluid gas. However, apart from these results, two dimensional mixtures have been studied only marginally.

This motivates the present thesis' work, which will focus on the study of two-dimensional Bose-Fermi mixtures with QMC techniques, in particular in a regime where the interactions are repulsive both between bosons and bosons, and between fermions and bosons. The Hamiltonian to be considered in the QMC simulations will be:

$$\begin{aligned}\hat{H} = &-\frac{\hbar^2}{2m_F}\sum_{i=1}^{N_F}\nabla_i^2 - \frac{\hbar^2}{2m_B}\sum_{i'=1}^{N_B}\nabla_{i'}^2 \\ &+\sum_{i,i'}^{N_F,N_B} V_{BF}(r_{ii'}) + \sum_{i'<j'}^{N_B} V_{BB}(r_{i'j'})\ ,\end{aligned} \tag{1.3}$$

where $i, j, ...$ and $i', j', ...$ label, respectively, fermions and bosons, and the laplacian operators $\nabla_i^2 = \frac{\partial^2}{\partial x_i^2} + \frac{\partial^2}{\partial y_i^2}$ for two-dimensional Bose-Fermi mixtures. The specific form of the interaction potentials $V_{BF}(r)$ and $V_{BB}(r)$ is irrelevant in the dilute regime of interest to experiments with ultracold gases. In our simulations we will then simply take a soft-disk potential for both interactions: $V_{BB}(r) = V_{BB}^0$ for $r < R^{BB}$ and zero elsewhere, and similarly for $V_{BF}(r)$, and parametrize the strength of the interactions in terms of the scattering lengths a_{BB} and a_{BF}.

Chapter 2

Quantum Monte Carlo methods

Quantum Monte Carlo (QMC) techniques include a large family of computational methods whose common aim is the study of complex quantum systems. One of the major goals of these approaches is to provide a reliable solution (or an accurate approximation) of the quantum many-body problem, studying the properties of microscopic systems made of many interacting particles. QMC methods allow for a direct treatment and description of complex many-body effects encoded in the wave function, going beyond mean-field theory and offering an exact solution of the many-body problem in some circumstances.

There are different types of Quantum Monte Carlo approaches but all share the common use of the Monte Carlo method, which is exploited to compute multidimensional integrals or to solve differential equations of many variables. In particular, in this chapter we will see only two QMC techniques that have been used during this thesis work: Variational Monte Carlo (VMC) and Diffusion Monte Carlo (DMC).

Due to the high flexibility of these computational methods, Quantum Monte Carlo techniques find application in various research fields such as nuclear physics, condensed matter physics or quantum chemistry.

Before describing these powerful techniques, we need to briefly introduce some basic standard definitions and concepts of Statistics such as random variables, probability distribution functions, etc. Of course, this will be only an introduction and exploring the vast world of statistics and probability theory will certainly not be the purpose of this thesis. Classical texts in mathematical statistics have been written by Feller [28] and Gnedenko [29]. The introductory part of the book by Hammersley and Handscomb [30] is both concise and precise.

2.1 Basic concepts of Statistics

In the following, we are going to deal extensively with the basic concepts of Statistics and its mathematical foundation, probability theory.

2.1.1 Events and probability

In probability theory, an *event* is an outcome or defined collection of outcomes of an experiment. In principle, by using classical physics laws, we can make exact predictions of events by knowing exactly the initial conditions. In practice, there are several events that are unpredictable, essentially because it is impossible to have the exact knowledge of the initial conditions.

In the definition of probability, it is important to assume that there exist reproducible experiments, that, under very similar initial conditions, produce different events (denoted here by E_i). It is therefore natural to introduce the *probability* of the event E_i as:

$$P(E_i) = p_i = \frac{\text{Number of successful events}}{\text{Total number of experiments}} \ . \tag{2.1}$$

It is worth to repeat again that this is only a brief review of the key notions of probability theory and for an exhaustive discussion we refer to the books [28] and [29]. However, one can see that the number p_i, i.e., the probability of the event E_i, is consistently defined in the limit of a large number of experiments [31].

Two events E_i and E_j are said to be *mutually exclusive events* if and only if the occurrence of E_i implies that E_j does not occur and vice versa. If E_i and E_j are mutually exclusive, then:

$$P(E_i \text{ and } E_j) = 0 \quad \text{and} \quad P(E_i \text{ or } E_j) = p_i + p_j \ . \tag{2.2}$$

A whole class of events can be mutually exclusive for all i and j. When the class is exhaustive, that is all possible events have been enumerated, being M the number of exclusive events characterizing the experiment, then, by using (2.2) clearly:

$$P(\text{some } E_i) = \sum_{i=1}^{M} p_i = 1 \ . \tag{2.3}$$

In order to characterize all possible exclusive events one can define *composite* events. For composite events, the probability is labeled by more than one index and it is called *joint probability*. In the particular case where composite events are independent, the joint probability can be factorized into a product of the corresponding *marginal probabilities* (the probabilities of individual events occurring). Thus we can define as composite events the ones obtained by two or more realizations of the same experiment. In fact, by definition, we assume that different realizations of the same experiment are always independent, otherwise there should exist some particular external condition that has a clear influence on the experiment and has not been correctly taken into account to classify exhaustively the events of the experiment.

2.1.2 Random variables and probability distribution functions

Before giving the rigorous definitions, it might be useful to address these concepts using practical examples. The typical example is the result of throwing a die. If we place ourselves in a purely deterministic point of view, we could imagine being able to exactly determine the motion of the die and, in consequence, the result of the throwing once the initial conditions are fixed (such as height, angle, velocity and so on). It is, however, simpler to imagine our incapacity and, consequently, it is commonly stated that the result of throwing a die is unexpected, or random. This is an example of the concept of *random variable*. Usually a random variable is related to the outcome of a given physical action of a special nature, such that we have not a precise control on all the conditions which make unique the result of the referred action. This incapacity does not mean that we have absolute ignorance about the outcome, and the partial knowledge of the action is related to the so-called *probability distribution function*, which is usually abbreviated as *pdf*. Thus, if it is assumed that the die has a perfect regular form, and is perfectly homogeneous, and other additional requirements (assuming the *equiprobability* of the results), the outcome of the action throwing a die is a number of the set $\{1, 2, 3, 4, 5, 6\}$, each result having a *probability* of value $1/6$.

When we toss two dice simultaneously, then the possible result for the sum of values is an integer between 2 and 12. A simple combinatorial calculation shows that there is a different number of ways of obtaining a particular result. Thus, to this new physical action we must assign a random variable with values between 2 and 12, but with different probabilities for each result. As a consequence, we understand that there is a double information to be supplied in order to define a random variable: the *domain* and the *probability distribution function*. The domain will represent the set of accessible values, and the pdf the probability or frequency with which these values appear.

Once for a given experiment E all the possible exclusive events E_j are classified, for each realization of the experiment there is only one integer i such that E_i is verified. Therefore we can define a *random variable* $i \to x_i$, as a real-valued function associated to any possible successful event E_i. There are some conditions to be taken in consideration with respect to the definition of a random variable. The domain must contain all possible values that the random variable may take. Moreover, the probability related to a given value must be positive or null and, finally, the sum of all probabilities must be unity, indicating certitude.

So far we have implicitly discussed about variables which take only a discrete set of values, however one may define random variables also in the continuum. If one makes this extension, it is no longer possible to talk of probability of a given value, and instead one must limit oneself to talk of probability that the result is contained in a interval $[x, x + \Delta x]$. When dealing with continuous random variables, the relevant concept of probability distribution function is replaced by the *density of probability distribution function*, again abbreviated by *pdf*. This function represents the limit of the ratio between

the probability of having a value in the interval $[x, x + \Delta x]$ and Δx, when $\Delta x \to 0$.

Another concept which we will see later applied and which is closely related to the pdf is the *cumulative distribution function*, P_i or $F(x)$. This function represents the probability that the random variable takes a value less than or equal to x_i or x, for the cases of discrete and continuous distributions, respectively. In particular, in the continuum, it is related to the pdf through the following relation:

$$F(x) = \int_a^x f(y)\, dy \ ,$$

where a is the lower boundary of the domain. The previous definitions regarding pdf's have been explicitly written for a single random variable. These distributions are then called *univariate*. A logical extension is to consider *multivariate* pdf, just by replacing the random variable x by the random vector $\boldsymbol{x}$, as well as other related quantities. A multivariate pdf is said to define *uncorrelated* random variables if it may be factorized in the form:

$$f(\boldsymbol{x}) \equiv f(x_1, x_2, \ldots, x_d) = \prod_{i=1}^{d} f_i(x_i) \ .$$

2.1.3 Examples of distribution functions

The *Uniform Distribution* $U(a, b)$ corresponds to the domain $[a, b]$ and the related pdf is a constant, with value $1/(b - a)$. By using the step function θ it may be described by a single equation:

$$f(x) = \frac{1}{b-a}\theta(x - a)\theta(b - x) \ . \tag{2.4}$$

The standard form of the uniform distribution is $U(0, 1)$. This function is of primary interest in Monte Carlo methods, being the basic tool to generate random numbers and random deviates from the required distributions.

The *Normal* or *Gaussian Distribution* $N(\mu, \sigma)$ characterizes a pdf of Gaussian shape, defined in the interval $[-\infty, +\infty]$, and given by:

$$f(x) = \frac{1}{\sqrt{2\pi}\sigma} \exp\left(-\frac{(x-\mu)^2}{2\sigma^2}\right) \ . \tag{2.5}$$

We write the Gaussian distribution in this special form because the parameters μ and σ have a specific meaning, as the mean and standard deviation of the distribution, to be defined later. The standard form of the normal distribution is $N(0, 1)$. Furthermore, this distribution is particularly interesting in relation with the central limit theorem, to be described later.

The *Exponential Distribution* is given by:

$$f(x) = \gamma \exp(-\gamma x) \ , \tag{2.6}$$

and defined in the domain $[0, +\infty]$. This distribution is of particular relevance in physics, being related with the radioactive decay and with the collisions of particles moving in material media.

2.1.4 Expectation values

Let $f(x)$ be a pdf with domain $[a, b]$ and $h(x)$ a function defined in the same domain. The *expectation value* of $h(x)$ with respect to $f(x)$ is defined by the integral

$$\mathbb{E}[h] = \langle h \rangle = \int_a^b f(x)h(x)\,dx \ . \tag{2.7}$$

There is a special class of expectation values, known with the name of *moments* of the pdf, and defined as follows

- *Mean* is the expectation value of $h(x) = x$, and it is normally represented by the letter μ,
$$\mu = \int_a^b x f(x)\,dx \ . \tag{2.8}$$
- *Moments* of a pdf are defined as the expectation value of x^n, and usually are represented by μ'_n,
$$\mu'_n = \langle x^n \rangle \ . \tag{2.9}$$
- *Centered Moments* are usually represented by μ_n, $n = 0, 1, 2, \ldots$, and correspond to the expectation value of the function $h(x) = (x - \mu)^n$. For low values of n the centered moments have particular names.
- *Variance* is the centered moment μ_2 of a distribution function. Its square root is known as the *standard deviation*, being usually represented by the letter σ,
$$\sigma = \sqrt{\langle (x - \mu)^2 \rangle} \ . \tag{2.10}$$

2.1.5 Distribution of mean values and central limit theorem

In many applications of statistics pdf's are characterized by giving just the values of the lowest moments μ and σ of the distribution. The Quantum Monte Carlo theory is not an exception to this rule. In practice this means that instead of studying the full distribution, one limits himself to less complete information. Certainly, this is almost necessary when dealing with multivariate distributions or with expectation values of functions of many variables. This is possible because there is a connection between μ and σ and the full pdf. In order to understand this connection, it is convenient to study the distribution of averages of a given random variable.

From a generic univariate pdf $f(x)$, one may define another univariate pdf related to the mean of N random values of x,

$$z = \frac{x_1 + x_2 + ... + x_N}{N} \ ,$$

and the question is which is the pdf g of the new random variable z.
In general it is not possible to get a precise expression of $g(z)$ when considering an arbitrary value of N and a general starting distribution $f(x)$. It is possible, however, to get an approximate result for $N \to \infty$, and this limit result is the so called *central limit theorem*. A formal proof can be found in Ref. [32].

Theorem (Central limit theorem)**.** *The pdf $g(z)$ of the average of N independent random values corresponding to a pdf $f(x)$, in the limit of large N, is a Gaussian distribution whose mean is the mean μ of the pdf $f(x)$ and whose variance is the variance σ^2 of the distribution $f(x)$ divided by the number of values N used to compute the average.*

This theorem is satisfied by a large class of pdf, but not all of them fulfill the conditions for its validity (e.g., the Cauchy distribution is one of the exceptions). It is a theorem of asymptotic or limit validity, the larger N the better the fulfillment.

In addition to the central limit theorem, there are two other theorems which serve to empirically determine the pdf: the *Chebyshev Inequality* and the *Law of Large Numbers*. For further details we refer to Guardiola's paper [32]. All these three properties establish the link between the empirical analysis of a given pdf and the mathematical knowledge of it.

The previous discussion has been limited to the study of the distribution of the mean of a pdf, and we have specifically considered univariate distributions. The theorem can certainly be generalized to deal with other kind of expectation values as well as with multivariate distributions. However, it is not within the scope of this thesis to demonstrate how this extension is possible.

Before concluding this section, it is worth to underline the consequences of the central limit theorem. This theorem can be used as a measure of the mean of the original distribution and a confidence limit related to the new variance σ^2/N. The square root of this quantity, $\sigma/\sqrt{N}$, is normally appended to the estimator of the mean with a $\pm$ sign. The *error* thus written must be interpreted as a confidence limit.
The dependence on N from the central limit theorem may also inform about the amount of work to be done so as to have a predetermined error. For example, in order to halve the error the empirical sampling must deal with four times more samples. Increasing the number of samples is not always the best way of improving the quality of the results, and the creativity in Monte Carlo work resides in the search of procedures to lower the variance σ, which is the quantity which fixes the error scale.

2.2 Generation of random numbers

Any physical problem tied to a probability distribution function may be dealt with a *simulation* by means of a random number generator (RNG). The simulation consists in statistically evolving the system through the generation of sequences of random numbers which are distributed with the pdf. This is certainly valid also for Monte Carlo simulations, thus it is worth to see how random numbers, related to a given pdf, are generated.

Of course, if random numbers are generated by means of a deterministic algorithm, they are no longer random numbers, so the usual name is *pseudo-random* numbers. However, the fact that we can predict the sequence is independent of its randomness, as witnessed by correlations between subsequent numbers (one of the basic references regarding the analysis of randomness is the book of Knuth [33]). For ease of exposition, from now on, we will refer to all pseudo-random numbers by simply calling them random numbers.

2.2.1 Uniform distribution

Algorithms to generate random numbers with a precise pdf are based on the generation of random numbers from the uniform distribution $U[0,1]$. Therefore, in this section, we first introduce the main features of a uniform random generator and then we will see some methods to transform the random numbers to another pdf. The main characteristics of a uniform RNG are the following:

- *Randomness.* The generated sequence must pass a large number of tests of randomness, including their consideration as pairs, triplets, ... nth-tuples of numbers.
- *Periodicity.* Random generators are periodic, so that after a certain number of sequential generations the results repeat and randomness properties are lost. Consequently, a random number generator is better the greater is its period.
- *Speed of generation.* This is a feature to be taken into account when one has to deal with very large simulations.
- *Portability.* The ability to generate the same sequence of random numbers by another computer or another programming language, just by coding appropriately the algorithm.
- *Repeatability.* The possibility of generating again a previous sequence of random numbers.

The main reason to demand the last two properties is that a large part of the computer work is devoted to checking and tuning the code, thus the presence of these two features in the random number generator allows to simplify these jobs.

In our Monte Carlo simulations we use one of the random number generators present in the Intel MKL libraries with period of order 10^{57}, which provides a fair compromise between the characteristics described above and which allows also to safely manage parallel simulations.

2.2.2 The method of Change of Variables

We introduce now the method of Change of Variables which allows to generate random numbers, according to a certain pdf, starting from uniformly distributed random numbers. The advantage of this method is that the associated algorithm is quite simple, however it is not so general, being applicable only to some pdf.

Let $x \in U[0,1]$ and apply a one-to-one transformation $y = h(x)$ which maps monotonically the domain $[0,1]$ into a new domain $[a,b]$. A first question is to determine the pdf corresponding to y, which will be represented by $g(y)$. The link with the starting distribution is the equality of the probabilities:

$$dx = g(y)\, dy \ .$$

From here it is simple to obtain the form of the new pdf,

$$g(y) = \frac{dx}{dy} = \frac{dh^{-1}(y)}{dy} \ , \tag{2.11}$$

where h^{-1} is the inverse function of $h(y)$.
However, Eq. (2.11) does not solve our problem because we typically know $g(y)$, but need to determine the change of variables $h(y)$ appropriate to our pdf. This can be done by solving (2.11) for h:

$$h^{-1}(y) = \int_a^y g(z)\, dz \equiv G(y) \ , \tag{2.12}$$

where $G(y)$ is the cumulative pdf of $g(y)$.
The resulting algorithm is simple and can be briefly summarized as follows: the change of variables is the inverse of the cumulative function of the pdf of interest. It is now evident that the drawback of this method is that the algorithm will only be practical if both cumulative function and its inverse are simple to obtain.
Some examples of the use of the method of Change of Variables are the following:

- *Uniform distribution* $U[a,b]$, with sampling method $y = a + (b-a)x$, for $x \in [0,1]$.
- *Exponential distribution* $\gamma \exp(-\gamma y)$, with sampling method $y = -\log(x)/\gamma$, for $x \in [0,1]$.

- *Gaussian distribution.*

The Gaussian distribution is a particular example of this method. In fact, in this case, the cumulative distribution is given in terms of the complementary error function, which has not a simple form and its inversion requires the solution of a transcendental equation. However, this problem can be overcome using a method known as the *Box-Muller method*. This technique still exploits the method of Change of Variables but uses the trick of considering a bivariate Gaussian distribution, whose cumulative distribution function is simpler and easily reversible. Thus, starting with two uniform random numbers, x_1 and x_2, one can obtain an independent pair of Gaussian distributed numbers, y_1 and y_2. The associated algorithm, known in literature as the Box-Muller algorithm [34], consists of the following steps:

1. Sample x_1 and x_2 independently from the uniform distribution $U[0, 1]$;
2. calculate $y_1 = \sqrt{-2 \log x_1} \cos(2\pi x_2)$ and $y_2 = \sqrt{-2 \log x_1} \sin(2\pi x_2)$;
3. y_1 and y_2 are two independent Gaussian random variables, with $\mu = 0$ and $\sigma = 1$. For a generic mean and variance one takes $y_i \to \sigma y_i + \mu$.

2.2.3 Acceptance-Rejection method

Another important method, which is worth mentioning, for the generation of random numbers is the *Acceptance-Rejection method*. This technique, due to von Neumann, is a general purpose method valid for bounded distributions with finite domains. It may be used also in multivariate distributions, but its efficiency tends to decrease with the number of variables.
Assume the pdf $f(x)$ defined in the domain $[a, b]$, and let M be an upper bound to the distribution, i.e. $f(x) \leq M$, $x \in [a, b]$. To obtain a sequence of random numbers of $f(x)$ proceed as follows:

1. Draw $z \in U[a, b]$;
2. draw $p \in U[0, M]$;
3. if $f(z) \geq p$ then accept z as the random number, else discard both z and p and go to the point 1.

For further details regarding the proof of this method and the generalization to the modified von Neumann method (in order to have efficiency one) we refer the reader to Guardiola's paper [32].

2.2.4 Markov chains and Metropolis Algorithm

When the probability distribution function to be sampled is complicated and possibly multivariate, a general sampling method, known as *Metropolis algorithm*, can be used. This method is closely related to the Variational Monte Carlo theory, thus it will receive special attention in the following.

Before describing the main steps of the algorithm, it is worth to review the Markov chain theory, that is the context in which the method is settled in (for a more exhaustive description regarding Markov chains see Ref. [35]).

Markov chains

Roughly speaking, a *Markov chain* is a stochastic model describing a sequence of possible events in which the probability of each event depends only on the state attained in the previous event. A possible way of visualizing a Markov chain is through its interpretation as a *random walk*: random walks are an example of Markov chains, in which future behaviour is independent of past history. A typical example is the drunkard's walk, in which a point beginning at the origin of the Euclidean plane moves a distance of one unit for each unit of time, the direction of motion, however, being random at each step. One may walk at random in many different systems. For this reason, these concepts find enormous application in the world of physics and in many other scientific or financial fields. Interesting examples of random walks may be found in Ref. [36].
More rigorously, a Markov chain is defined in terms of a discrete set of states $\{s_1, \dots, s_N\}$ and a rule governing the transition from a given state s_i to any other state of the set s_j. This rule is expressed in terms of a *transition matrix* $T(j \leftarrow i) \equiv T_{ji}$ so that T_{ji} is the probability of transition from the state s_i to the state s_j. Some transition probabilities may be null, and the matrix may also contain non-null diagonal terms representing the probability of remaining at the initial state. Given that the matrix elements are transition probabilities and that the transition probability from s_i to any final state must be unity, this matrix must fulfill the following two properties

$$0 \leq T_{ji} \leq 1 \quad \text{and} \quad \sum_j T_{ji} = 1 \ ,$$

so that the sum of any column is 1. Matrices fulfilling these two conditions are termed *stochastic*. If it happens that a given column has all its elements null, but the diagonal, then the state corresponding to this column is referred to as an *absorbing state*. Once it is reached, it will never move from there.

Of course, Markov chains can be generalized to deal also with continuous set of states. In cases like this, called *Markov processes*, instead of referring to a transition probability one must deal with a density of probability, $T(x', x)$, which must in turn satisfy the two

properties

$$T(x', x) \geq 0 \quad \text{and} \quad \int T(x', x)\, dx' = 1 \ .$$

We will be interested, for our purposes, in *endless chains* (i.e. with no absorbing states) and we will consider only *irreducible chains*. A chain is called *reducible* if the set of states may be divided into two disjoint sets so that there cannot be a transition from the first set to the second one, and inversely.

The Direct problem

At this point, a crucial question could be which is the probability of staying at a given state s_i after a long random walk. The answer is very simple: the probability of arriving to s_i is the product of the probability of arriving to any state s_j times the transition probability from s_j to s_i :

$$P_i = \sum_j T_{ij} P_j \ , \tag{2.13}$$

where we have assumed that the probability distributions before and after the transition are the same, namely the probability is stationary. This is an homogeneous linear system whose solution is not uniquely defined unless an additional normalization condition is introduced $\sum_i P_i = 1$.
Solving this system of linear equations, by implementing an appropriate algorithm, allows to determine the stationary probabilities P_i related to a Markov chain. We can then interpret this algorithm as a method of generating random numbers corresponding to a pdf P_i, without knowing the actual distribution (the generation being controlled by the Markov chain, which is determined by its transition matrix T_{ij}).

In the case of a Markov process, the equivalent to the matrix equation (2.13) is the linear integral equation

$$P(x) = \int T(x, x') P(x')\, dx' \ , \tag{2.14}$$

with the supplementary normalization condition $\int P(x)\, dx = 1$. This latter case is more complicated because one cannot store the whole space of random variables as in the discrete case. Instead, the function $P(x)$, which is a pdf, is represented by a set of random numbers $\{\xi_i\}$ obtained sequentially, in such a form that the number ξ_{i+1} of the sequence is obtained by drawing a random number from the pdf $f(x) \equiv T(x, \xi_i)$, which is a *conditional probability* [1] of obtaining x from a given ξ_i. Certainly, it is not the same to know the complete pdf $P(x)$ for any x, and to consider a finite sequence of random numbers which are distributed according to $P(x)$. However, knowing the set of random numbers permits the determination of expectation values related to $P(x)$ (assuming the

[1] In probability theory, conditional probability is a measure of the probability of an event occurring, given that another event (by assumption, presumption, assertion or evidence) has already occurred.

central limit theorem holds).
Both of these methods, the discrete one and the continuous one, are practical only when it is possible to sample from the transition matrix T_{ij} and the pdf $T(x, \xi_i)$, respectively.

Equation (2.13) is a relation defining the concept of *stationary distribution*. This means that the pdf P_i is invariant under the action of the transition matrix T_{ij} . The existence of such a stationary distribution is guaranteed if each state i can be reached by any other state j in a finite number of steps (irreducibility). If moreover there is no characteristic period of recurrence, the chain is called *aperiodic*, and the stationary distribution is also an equilibrium distribution, in the sense that for any initial distribution the recursive action of the transition matrix asymptotically drives the chain to P_i. The previous conditions for the existence of an equilibrium distribution are necessary and sufficient and are equivalent to saying that the Markov chain is ergodic.

The Inverse problem and Metropolis method

Our initial goal was to find a method to sample random numbers from a generic probability distribution function. We have seen above that one possibility is to solve the system of linear equations (2.13) (or its continuous version (2.14)). However, in most cases of interest we do not know a priori the transition matrix corresponding to a certain stationary pdf and, consequently, the applications of this method are few and limited to particular exceptions.
So, at this point, a question arises naturally: given a pdf P_i or $P(x)$, is it possible to find a stochastic matrix T_{ij} or $T(x, x')$ defining a random walk which gives rise to the mentioned pdf?
This question, known with the name of *Inverse problem*, was answered by N. Metropolis, A. W. Rosenbluth, M. N. Rosenbluth, A. H. Teller and E. W. Teller in 1953 [37], giving a specific rule to construct it. The method, known as *Metropolis* or MR^2T^2 method, allows to generate random numbers from an arbitrary pdf.

For discrete distributions the solution is as follows. Let S_{ji} be an auxiliary stochastic and symmetric matrix. The seeked stochastic matrix is given by

$$\begin{aligned} T_{ji} &= S_{ji} && if\ \ P_j \geq P_i\ , && i \neq j \\ T_{ji} &= S_{ji}\, P_j/P_i && if\ \ P_j < P_i\ , && i \neq j \\ T_{ii} &= S_{ii} + {\sum_k}' S_{ki}(1 - P_k/P_i) && for\ \ k \in \{P_k < P_i\}\ . \end{aligned} \tag{2.15}$$

The prime on the sum indicates that only states k such that $P_k < P_i$ are considered. The values of the diagonal elements have been fixed so as to fulfill the property $\sum_j T_{ji} = 1$.

In order to prove that the matrix so defined satisfies the wanted relation $\sum_i T_{ji} P_i = P_j$, an intermediate step is to prove the *detailed balance* property:

$$T_{ji} P_i = T_{ij} P_j\ , \tag{2.16}$$

where there is no sum over repeated indices. To check this relation it is convenient to distinguish the two cases

$$\begin{aligned} P_j &\geq P_i\,, \quad T_{ji}P_i = S_{ji}P_i & T_{ij}P_j = S_{ij}\frac{P_i}{P_j}P_j = S_{ij}P_i\,, \\ P_j &< P_i\,, \quad T_{ji}P_i = S_{ji}\frac{P_j}{P_i}P_i = S_{ji}P_j & T_{ij}P_j = S_{ij}P_j\,. \end{aligned}$$

Exploiting the symmetry of the auxiliary transition matrix S_{ij}, both left relations are equal to their respective right relations, proving the detailed balance property. At this point, summing up on i in Eq. (2.16), one obtains the desired condition $P_j = \sum_i T_{ji}P_i$.

In the case of continuous processes one may write down a similar derivation.
Let us consider a stochastic and symmetric auxiliary transition function $S(y,x)$ and define

$$\begin{aligned} T(y,x) &= S(y,x)\theta(P(y)-P(x)) \\ &+ S(y,x)\frac{P(y)}{P(x)}\theta(P(x)-P(y)) \\ &+ \delta(y-x)\int S(z,y)\left(1-\frac{P(z)}{P(y)}\right)\theta(P(x)-P(z))\,dz\,. \end{aligned} \tag{2.17}$$

This again satisfies the detailed balance property:

$$T(x,y)P(y) = T(y,x)P(x)\,. \tag{2.18}$$

Metropolis algorithm

The Metropolis solution to the Inverse problem was extended to more general cases, involving asymmetric transition matrices, by W. K. Hastings in 1970 [38], and for this reason the complete version of the algorithm takes the name of *Metropolis-Hastings* algorithm.
In the symmetric case, the algorithm can be summarized in the following few steps:

- Let I, starting state.
- Draw J from $S(J,I)$.
- If $P(J)/P(I) >$ RAND( )[2] then $I = J$.
- I is the next state.

[2]Here RAND( ) is a generic procedure generating $U[0,1]$ uniform random numbers.

Essentially, we select a candidate s_j for the next state from the auxiliary transition matrix S_{ji}. Then, we compute the probability P_j of the candidate and we compare it with the probability of the starting state P_i. If P_j is greater than P_i, the transition is accepted (i.e. , the next state of the chain is s_j), otherwise, if P_j is smaller than P_i the new state is accepted with probability P_j/P_i . In case of rejection this means that we remain in s_i, i.e. , the next state in the chain is the same as the old state, and it should be counted again. We have seen here, for ease of discussion, the discrete version of the algorithm, however, even in the case of continuous variables the procedure is quite similar.

Of course, the algorithm will be practical if we know how to generate random numbers from the auxiliary distribution S. Anyway, thanks to the freedom in choosing the auxiliary transition function, we are able to choose the most convenient one. Usually, but not necessary, the transition operator S is taken as an uniform distribution in a box centered on the previous point or as a Gaussian distribution.

There are technical issues regarding the asymptotic nature of this algorithm and the strong correlation between consecutive moves, but they will be addressed comprehensively in the next section.

2.3 Monte Carlo method

In studying the properties of few- and many-body systems we are quite often driven to the calculation of multidimensional integrals, either needed for solving differential equations of motion, or involved in the evaluation of expectation values. Such integrals can be calculated analytically in few relevant cases, but as soon as the number of degrees of freedom is large most of the problems need some simplifications in order to be analytically solved, thus introducing some approximations, which are not always controllable. When exact analytical results are not available or not accurate enough, a possibility is to resort to numerical methods. The drawback of these methods is that the free parameters of the problem have to be specified from the beginning for each simulation so that the solution is known only in a discrete set of points in parameter space, and one needs to use fitting methods in order to give a more exhaustive answer.

There are several numerical techniques and among these, the Monte Carlo method is very competitive if the number of degrees of freedom is very large or in presence of very complicated integration domains (see [39] and [40]).

The essence of this stochastic method is to interpret multidimensional integrals as expectation values of some functions (observables) of the multidimensional configurations, associated to certain probability distribution functions. These expectation values are therefore estimated by sampling a relevant population of points in configuration space (walkers), which are distributed according to the given pdf, and taking the average of the observables calculated on the sampled walkers. An uncertainty in the estimated observables is intrinsic, given the numerical and stochastic nature of the calculation, but

it can be systematically estimated and reduced with longer samplings or more efficient algorithms.

The original idea behind Monte Carlo methods was introduced in Nuclear Physics by Fermi and then studied by Metropolis and Ulam (see [41] for a general introduction). Several years later, these techniques were also applied in Quantum Physics and Quantum Chemistry. In these contexts, major developments were the Variational Monte Carlo, introduced by McMillan [42], and the Diffusion Monte Carlo, introduced by Anderson [43] and refined by Reynolds, Ceperley and Alder [44], [45].

2.3.1 Crude Monte Carlo

We now see the easiest application of Monte Carlo methods to the solution of integrals. This technique is called *Crude Monte Carlo* and it is simply based on the direct application of the central limit theorem.
For ease of discussion, we consider the integral of a continuous univariate function $h(x)$, which can be written as follows

$$\int_a^b h(x)\,dx = (b-a)\int_a^b \frac{1}{b-a}\,h(x)\,dx\ .$$

This apparently useless trick of multiplying and dividing the integral by the same quantity $(b-a)$, turns out to be of fundamental importance. In fact, at this point, the expression on the right can be interpreted as the expectation value of the function $h(x)$ with respect to the uniform distribution function $U[a,b]$. Thus, in order to solve the integral, one can simply implement an algorithm that calculates the average of $\{h(x_i)\}$, where $x_i \in U[a,b]$. Of course, along with the calculation of the average one may also compute the variance by evaluating the expectation value of $h(x)^2$.
The equations, in summary, to be used to correctly implement the algorithm are the following:

$$\langle h\rangle = \int_a^b h(x)\,dx = \lim_{N\to\infty}\frac{b-a}{N}\sum_{i=1}^{N} h(x_i)\ \ ,\ \ x_i \in U[a,b]\ , \tag{2.19}$$

$$\sigma^2 = \lim_{N\to\infty}\frac{b-a}{N}\left[\frac{1}{N}\sum_i h(x_i)^2 - \left(\frac{1}{N}\sum_i h(x_i)\right)^2\right]\ . \tag{2.20}$$

We can see, from Eq. (2.20), that the variance of the mean σ^2 is inversely proportional to the number of samples N. Thus, in order to lower the variance, the only solution to achieve this goal is to perform longer samplings, and consequently larger simulations.

2.3.2 Importance sampling

In reality the variance can be lowered, without increasing the sampling, by using another Monte Carlo method. We now introduce the fundamental technique known as *Importance Sampling*, which is just another application of the central limit theorem to the calculation of integrals.
We consider again the integral of a continuous univariate function $h(x)$ which, this time, can be written as

$$\int h(x)\,dx = \int f(x)[h(x)/f(x)]\,dx\ .$$

We still used the trick of multiplying and dividing the integral by a same quantity, but this time we have introduced an *ad hoc* pdf $f(x)$ which cannot be pulled out of the integral due to its dependence on x. Again, the expression on the right can be interpreted as an expectation value of the function $[h(x)/f(x)]$ but, this time, with respect to the pdf $f(x)$. This is, of course, the main difference with Crude Monte Carlo (i.e., the use of a non-uniform pdf).
Another difference from the previous method is that the variance of its expectation values can be smaller. In fact, while one should get roughly the same value for the expectation value $\langle h\rangle$ using both procedures, Crude MC will give for the variance the value

$$\sigma^2 = \int h(x)^2\,dx - \langle h\rangle^2\ ,$$

whereas the importance sampling method will give a different value

$$\sigma^2 = \int f(x)[h(x)/f(x)]^2\,dx - \langle h\rangle^2\ .$$

Thus, by cleverly choosing the importance sampling function $f(x)$ one may design a better calculation from the MC point of view. Clearly, the search for the optimal importance sampling function is an important step in implementing Monte Carlo methods. The best function to use, in principle, is $f(x) = C|h(x)|$, where C is a proportionality constant, however this solution is not always practical. Of course, in order to implement the importance sampling method, an algorithm capable of drawing points from an arbitrary probability distribution function, such as the Metropolis-Hastings algorithm, is needed.

In addition to lowering the variance, there is a side benefit of this method, namely, that it allows to deal with (null-measure) infinite integrands and/or infinite intervals, just by choosing an appropriate pdf.

Before concluding this section, in order to give an idea of the power of this method, we report the example 3.1 present in Guardiola's paper [32].

Example 2.3.1. *Consider the six-dimensional integral of the function*

$$F(\boldsymbol{x}, \boldsymbol{y}) = \exp[-\boldsymbol{x}^2 - \boldsymbol{y}^2 - (\boldsymbol{x} - \boldsymbol{y})^2/2]$$

extended to the full space. The exact value is 10.9626.
Table 2.1 presents the calculation using the Crude MC method (each variable integrated between -5 *to* $+5$*), and the calculation with the importance sampling function* $\exp(-\boldsymbol{x}^2 - \boldsymbol{y}^2)$*, adequately normalized. It is absolutely clear the advantage of using the importance sampling algorithm, so that the extra work required to sample from the importance sampling pdf is largely compensated by the smallness of the error. Just by comparing the errors quoted in the last row of the table, we may conclude that the importance sampling method is about* 250 *times more efficient.*

Crude MC	Importance Sampling
12.80 ± 4.51	10.46 ± 0.26
8.93 ± 2.96	11.23 ± 0.26
21.90 ± 8.43	11.02 ± 0.26
12.70 ± 3.06	11.15 ± 0.26
13.84 ± 4.48	10.90 ± 0.25
4.58 ± 1.02	10.94 ± 0.26
14.84 ± 4.68	10.72 ± 0.25
8.17 ± 2.38	10.89 ± 0.25
6.79 ± 1.35	10.87 ± 0.26
5.56 ± 1.11	10.75 ± 0.25
11.01 ± 1.27	10.89 ± 0.08

Table 2.1: Results of the integral of example 2.3.1. The left column shows the Crude MC method, whereas the right column the importance sampling MC method. Each row corresponds to one hundred thousand samples, and the last row is the full average corresponding to one million samples.

2.3.3 Markov Chain Monte Carlo

Combining the Metropolis-Hastings algorithm together with the importance sampling method we obtain a general Monte Carlo method known as *Markov Chain Monte Carlo* (MCMC). Thus, thanks to the Metropolis algorithm, we have a method to generate random numbers according to a generic pdf and this allows to choose the optimal importance sampling function capable to reduce significantly the variance.

Even if we have already seen in the previous sections how these two methods work, it is important to dwell for a moment on the asymptotic nature of the Metropolis algorithm.

In section 2.2.4 we have seen the important concepts of stationary distribution and equilibrium distribution, the existence of which is guaranteed if the considered Markov chain is ergodic. However, starting with a collection of points (called *walkers*), arbitrary distributed in configuration space, and evolving them[3] thanks to the repeated action of the transition matrix, the equilibrium distribution is reached only after a *transient*. Then, after the transient, averages can be taken using all walkers at subsequent times.
We can now see how to practically apply this algorithm in order to determine the expectation value of a function, or observable, $h(x)$ with respect to the pdf $P(x)$:

- Start from a population of m walkers randomly distributed in space.
- Start iteration *iter*. For each walker *ipop* at position x do:
  - Sample a point y' from the auxiliary transition function $S(y', x)$.
  - Calculate the quotient $P(y')/P(x)$ (if S is symmetric).
  - If it is bigger than RAND( ) then accept the move ($y = y'$), else reject the move ($y = x$).
  - Calculate $h_{ipop} = h(y)$.
- If the transient is finished, compute the partial sum $\bar{h}_{iter} = \frac{1}{m} \sum_{ipop} h_{ipop}$.
- Go to the next iteration.
- The estimated expectation value is $\langle h \rangle = \frac{1}{n} \sum_{iter>transient} \bar{h}_{iter}$, where n is the number of iterations after the transient.

We have seen that, in general, the auxiliary transition function S can be arbitrary but, in practice, the choice of S determines the length of the transient after which the equilibrium distribution is reached. Moreover, if for example S is a Gaussian distribution of the variable $(x - y)$, then a small variance of it will cause high acceptance ratio, but high correlation between the moves, while a big variance will cause a small correlation of the moves, but a small acceptance ratio. Very high or very low acceptance rates are a sign that the Markov chain is not moving appreciably. There are not specific rules to say when a certain rate of acceptances is reasonable, but a good compromise is obtained with an acceptance ratio around $40\% - 60\%$. Generally speaking, one could optimize the transition matrix by optimizing the effective measured variance obtained in a chosen wall time.
The issue of the correlation between successive moves is an insidious problem, especially in the continuous case where the algorithm is prone to stronger correlations. Furthermore, the correlation between moves reflects itself in a high correlation between subsequent values $\bar{h}_{iter}$, so that the central limit theorem cannot be immediately used to

[3]Each walker evolves independently under the action of the transition matrix.

estimate the variance of $\langle h \rangle$. There are, in principle, two ways to overcome this problem. The first solution exploits an interesting property of stochastic matrices which states that any integer power of a given stochastic matrix, which is again stochastic, gives rise to a stationary pdf which is the same as the stationary pdf related to the original transition matrix. This property allows to *thermalize* the random walk, in the following sense. Starting at a given state s_i we proceed carrying out a given number n of steps, $\{s_{i+1}, s_{i+2}, \dots, s_{i+n}\}$, but we only count or collect the state s_{i+n} after n steps, and so on. In other words, $n-1$ intermediate steps are discarded. In this way, the resulting collection of states is again a set of random numbers corresponding to the pdf under study and, thanks to this process of thermalization, we have minimized the effect of correlation among successive states. Suitable correlation tests have to be performed to choose n.
The second solution, instead, consists in dividing the calculation into n_b blocks such that iterations from different blocks are not correlated anymore; this is true if the length l_b of a single block is longer than the correlation time of the estimated quantity h. Therefore one can sum the contributions to $\langle h \rangle$ coming from the iterations within a block $\bar{h}_{i_b} = \frac{1}{l_b} \sum_{iter \in i_b} \bar{h}_{iter}$, and use their variance to estimate the variance of $\langle h \rangle \equiv \bar{h} = \frac{1}{n_b} \sum_{i_b} \bar{h}_{i_b}$:

$$\sigma_h^2 \approx \frac{1}{n_b} \left(\frac{1}{n_b - 1} \sum_{i_b} (\bar{h}_{i_b} - \bar{h})^2 \right) . \tag{2.21}$$

A longer correlation time forces to use longer blocks. This causes having less independent contributions for calculating the observable and, consequently, an increase in variance.

Both solutions are correct. However, especially in the case of strong correlations, the second method turns out to be more effective from a computational point of view. In fact, longer correlation time implies more intermediate steps discarded, thus increasing the number of random deviates to be generated in order to have independent samples.

See Appendix A for more details regarding Eq. (2.21) and the estimate of the correlation time.

2.4 Variational Monte Carlo

Variational Monte Carlo (VMC) is the direct application of Monte Carlo integration, in particular the MCMC method, to problems of Quantum Physics. In fact, when studying quantum many-body systems such as those introduced in Chapter 1, we need a practical tool able to calculate the expectation values of observables, even if this requires the solution of complicated multidimensional integrals. It is then clear that a technique such as the MCMC method is an optimal candidate for this purpose. Typical observables to be calculated are, for example, the energy of the system or the correlation functions. Usually these quantities need to be computed in the ground state or at thermal equilibrium. For

a historical and pedagogical review about the Variational Monte Carlo method see Ref. [46], for applications of VMC to systems of many bosons and fermions see [42] and [47], respectively.

2.4.1 Variational method

Variational Monte Carlo is based on an important approximation method in Physics, known as the *Variational method*, which is very useful in obtaining the bound state energies and wave functions of a time-independent Hamiltonian $\hat{H}$. See the book by B. H. Bransden and C. J. Joachain [48] for a complete overview regarding this method and other approximation methods in Quantum Physics.

Let $\hat{H}$ be a time-independent Hamiltonian. We denote by E_n its eigenvalues and by ϕ_n the corresponding orthonormal eigenfunctions. Assuming that $\hat{H}$ has at least one discrete eigenvalue, we consider an arbitrary normalizable function ψ such that the following functional $E[\psi]$ can be defined as

$$E[\psi] = \frac{\langle\psi|\hat{H}|\psi\rangle}{\langle\psi|\psi\rangle} = \frac{\int \psi^* \hat{H}\psi}{\int \psi^*\psi} \,, \tag{2.22}$$

where the integration is extended over the full range of all coordinates of the system. The functional above is independent of the normalization and of the phase of ψ. In particular, it is often convenient to impose the condition $\langle\psi|\psi\rangle = 1$.

It is clear that if the function ψ is identical to one of the exact eigenfunctions ϕ_n of $\hat{H}$, then $E[\psi]$ will be equal to the corresponding exact eigenvalue E_n. It is also worth stressing that if ψ and ϕ_n differ by $\delta\phi$, it could be shown (see again Ref. [48]) that the leading term of the difference between $E[\psi]$ and the true eigenvalue E_n is quadratic in $\delta\phi$.

A very important important property of the functional (2.22) is that it provides an upper bound to the exact ground state energy E_0.
To prove this result, we expand the arbitrary, normalizable function ψ in the complete set of orthonormal eigenfunctions ϕ_n of $\hat{H}$. That is,

$$\psi = \sum_n a_n \phi_n \,, \tag{2.23}$$

where a_n are complex coefficients. Substituting (2.23) into (2.22), we find that

$$E[\psi] = \frac{\langle \sum_m a_m \phi_m | \hat{H} | \sum_n a_n \phi_n \rangle}{\langle \sum_m a_m \phi_m | \sum_n a_n \phi_n \rangle}$$

$$= \frac{\sum_m \sum_n a_m^* a_n \langle \phi_m | \hat{H} | \phi_n \rangle}{\sum_m \sum_n a_m^* a_n \langle \phi_m | \phi_n \rangle}$$

$$= \frac{\sum_n |a_n|^2 E_n}{\sum_n |a_n|^2} \ ,$$

where, in the last equality, we have used the relation $\hat{H}\phi_n = E_n \phi_n$ and the orthonormality of the eigenfunctions ϕ_n. If we now subtract E_0, the lowest energy eigenvalue, from both sides of the expression above we obtain:

$$E[\psi] - E_0 = \frac{\sum_n |a_n|^2 (E_n - E_0)}{\sum_n |a_n|^2} \ . \tag{2.24}$$

Since $E_n \geq E_0$, the right-hand side of (2.24) is non-negative and, consequently

$$E_0 \leq E[\psi] \tag{2.25}$$

proving that the functional $E[\psi]$ gives an upper bound for the ground state energy.

The property (2.25) constitutes the basis of the variational method for the approximate calculation of E_0. This method consists in evaluating the quantity $E[\psi]$ by using trial functions ψ which depend on a certain number of variational parameters, and then to minimize $E[\psi]$ with respect to these parameters in order to obtain the best approximation of E_0 allowed by the form chosen for ψ.

Clearly the energy of the ground state is not the only observable that can be evaluated through the Variational Monte Carlo. However, in order to apply the variational method to other measurable quantities, relations similar to the property (2.25) must hold.

2.4.2 Monte Carlo integration and local energy

Before the expectation value of a certain observable may be computed, the integral must be transformed into a form suitable for Monte Carlo integration. In the following we are mainly interested in studying the energy of the ground state, thus, for ease of discussion, we proceed by considering as an example the expectation value of the Hamiltonian of the system.

The two-dimensional Bose-Fermi mixture is described by the Hamiltonian (1.3). We consider, for the moment, a generic trial wavefunction ψ_T which is dependent on the set

of $N_F + N_B$ particle positions, $\boldsymbol{R} = \{\boldsymbol{r}_1, \boldsymbol{r}_2, ..., \boldsymbol{r}_{N_F}, \boldsymbol{r}_{1'}, \boldsymbol{r}_{2'}, ..., \boldsymbol{r}_{N'_B}\}$. The expectation value is then given by

$$E = \langle \hat{H} \rangle = \frac{\int \psi_T^* \hat{H} \psi_T \, d\boldsymbol{R}}{\int \psi_T^* \psi_T \, d\boldsymbol{R}} \, . \tag{2.26}$$

Multiplying and dividing the numerator by the same quantity ψ_T, Eq. (2.26) may be rewritten in an importance sampled form in terms of the probability density $|\psi_T|^2$:

$$\langle \hat{H} \rangle = \frac{\int \psi_T^* \frac{\psi_T}{\psi_T} \hat{H} \psi_T \, d\boldsymbol{R}}{\int \psi_T^* \psi_T \, d\boldsymbol{R}} = \frac{\int |\psi_T|^2 \frac{\hat{H}\psi_T}{\psi_T} \, d\boldsymbol{R}}{\int |\psi_T|^2 \, d\boldsymbol{R}} \, . \tag{2.27}$$

Thus the expectation value of the Hamiltonian can be expressed in the following compact form

$$\langle \hat{H} \rangle = \int f(\boldsymbol{R}) E_L(\boldsymbol{R}) \, d\boldsymbol{R} \, , \tag{2.28}$$

where we have named the multivariate pdf as

$$f(\boldsymbol{R}) = \frac{|\psi_T(\boldsymbol{R})|^2}{\int |\psi_T(\boldsymbol{R})|^2 \, d\boldsymbol{R}} \tag{2.29}$$

and we have introduced the quantity called *local energy* E_L, given by

$$E_L(\boldsymbol{R}) = \frac{1}{\psi_T(\boldsymbol{R})} \hat{H} \psi_T(\boldsymbol{R}) \, . \tag{2.30}$$

The expression (2.28) allows then to apply the Markov Chain Monte Carlo method, in the sense that the variational energy can be obtained by averaging the local energy E_L over the set of configurations $\{\boldsymbol{R}_i\}$ sampled from the modulus square of the trial wavefunction:

$$E = \frac{1}{N} \sum E_L(\boldsymbol{R}_i) \, . \tag{2.31}$$

A transition matrix which converges to the above probability distribution can be a Gaussian in configuration space, that is

$$S(\boldsymbol{R}', \boldsymbol{R}) = \frac{1}{(2\pi\sigma^2)^{dN/2}} \exp\left[-\frac{|\boldsymbol{R} - \boldsymbol{R}'|^2}{2\sigma^2} \right] , \tag{2.32}$$

where, in our case, $d = 2$ and $N = N_F + N_B$.

The local energy E_L, introduced in Eq. (2.30), is one of the central quantities in Quantum Monte Carlo methods. It occurs, in fact, in both the Variational and Diffusion Monte Carlo algorithms and its properties are exploited to optimize trial wavefunctions.

The local energy has the useful property that for an exact eigenstate of the Hamiltonian, the local energy is constant, and thus its variance is null. For a general trial wavefunction the local energy is not constant and the associated variance is a measure of how well the trial wavefunction approximates an eigenstate.
The determination of the local energy is one of the most computationally costly operations performed in QMC calculations. For typical Hamiltonians, which are the sum of a kinetic energy term and a momentum-independent interaction potential, the contribution to the local energy is the computation of the second derivatives of the wavefunction and the numerical value of the potential, respectively. There is a second way of estimating the kinetic energy which provides also a check for the stationarity of the distribution to be sampled. This alternative method relies on the possibility to transform the expectation value $\langle\psi_T|\boldsymbol{\nabla}^2|\psi_T\rangle$ into $-\langle\boldsymbol{\nabla}\psi_T|\boldsymbol{\nabla}\psi_T\rangle$ by integration by parts. The transformed contribution to the local kinetic energy will then be proportional to $|\boldsymbol{\nabla}\psi_T/\psi_T|^2$. Although this second procedure leads to simpler and faster calculations, the resulting variance will probably be greater (this is shown in Ref. [32]). It is useful to accumulate both the estimators in order to check the correctness of the implementation of the VMC algorithm.

Lastly, before concluding this section, it is worth to underline that the probability distribution $f(\boldsymbol{R})$ described above is well defined (in the sense that it is positive and normalized) even if the variational trial wavefunction is negative for some regions in configuration space, due to the appearance of the modulus square of the wavefunction. This fact is very important and, as we will see in the following, will be one of the main differences between the VMC and the DMC methods.

2.5 Diffusion Monte Carlo

Variational Monte Carlo is a very efficient and fast algorithm, however its effectiveness depends drastically on the accuracy of the chosen many-body trial wavefunction. We then need a more refined method which is, in principle, independent from the choice of the trial wavefunction, in order to obtain accurate results also for those situations where we are unable to find a suitable many-body function. Diffusion Monte Carlo (DMC) method is a good solution to this problem. This method allows to solve the many-body Schroedinger equation in imaginary time by means of a stochastic procedure. In principle the DMC method is exact, although in practice, several well-controlled approximations must be introduced for calculations to remain tractable. The Diffusion Monte Carlo algorithm was introduced by Anderson [43], [49] and refined by Reynolds, Ceperley and Alder [45]. For general introductions see [32, 50, 51, 52, 53].

2.5.1 Introduction

The Schroedinger equation in imaginary time, with proper boundary condition, has the following form:

$$\begin{aligned} -\frac{\partial}{\partial\tau}\Psi(\boldsymbol{R},\tau) &= (\hat{H}(\boldsymbol{R}) - E_{ref})\Psi(\boldsymbol{R},\tau) \ , \\ \Psi(\boldsymbol{R},\tau=0) &= \Psi_i(\boldsymbol{R}) \ . \end{aligned} \tag{2.33}$$

$\boldsymbol{R}$ represents the set of all coordinates, $\tau = it/\hbar$ is the imaginary time in units of inverse energy and E_{ref} is an energy shift introduced for convenience. The formal solution of the previous differential equation is

$$\Psi(\boldsymbol{R},\tau) = e^{-[\hat{H}-E_{ref}]\tau}\Psi(\boldsymbol{R},0) \ , \tag{2.34}$$

where the evolution operator $\exp\left[-(\hat{H} - E_{ref})\tau\right]$ is also called *Green's function*.

The expression (2.34) allows the interpretation of imaginary time evolution of states, in the sense that the initial state $\Psi_i(\boldsymbol{R}) = \Psi(\boldsymbol{R},0)$ evolves to the state $\Psi(\boldsymbol{R},\tau)$ thanks to the action of the Green's function $\exp\left[-(\hat{H} - E_{ref})\tau\right]$. Let us decompose $\Psi_i(\boldsymbol{R})$ in terms of the eigenstates $\phi_n(\boldsymbol{R})$ of the Hamiltonian $\hat{H}$

$$\Psi_i(\boldsymbol{R}) = \Psi(\boldsymbol{R},0) = \sum_n c_n\phi_n(\boldsymbol{R}) \ ,$$

then the imaginary time evolution of the arbitrary starting state $\Psi(\boldsymbol{R},0)$ is given by

$$\Psi(\boldsymbol{R},\tau) = \sum_n c_n e^{-[E_n-E_{ref}]\tau}\phi_n(\boldsymbol{R}) \ , \tag{2.35}$$

where we have used the fact that the eigenstates satisfy the relation $\hat{H}\phi_n(\boldsymbol{R}) = E_n\phi_n(\boldsymbol{R})$. So the imaginary time evolution consists of an exponential decay of each component of the initial wavefunction (provided $E_{ref} < E_n$, $\forall n$), with the interesting property that the longest-living component is the lowest energy one, which is the ground state, if the initial wavefunction has non-zero overlap c_0 with the ground state.

Again, as in the case of VMC, the wave function is represented by a set of random vectors or walkers, in such a form that the time evolution of the wave function is actually represented by the evolution of the set of walkers.

Thus the resulting scheme of the DMC method is, in principle, quite simple: once one has found an appropriate approximation for the short time Green's function, and a starting state has been determined[4], the job consists in representing the starting state by a collection of walkers and letting them evolve in time, i.e. obtaining a new collection

[4]In our case, we use as starting configurations those obtained from previous VMC simulations.

of walkers from the previous one, up to a time large enough[5] so that only the ground state amplitude is relevant.

The energy can then be estimated by the mixed estimator

$$E = \frac{\langle \phi_0 | \hat{H} | \psi_T \rangle}{\langle \phi_0 | \psi_T \rangle} = \frac{\int \phi_0^*(\boldsymbol{R}) E_L^T(\boldsymbol{R}) \psi_T(\boldsymbol{R})\, d\boldsymbol{R}}{\int \phi_0^*(\boldsymbol{R}) \psi_T(\boldsymbol{R})\, d\boldsymbol{R}} \,, \tag{2.36}$$

which is, in the case of bosonic systems, an exact estimator, in the sense that the resulting energy does not depend from the chosen trial wavefunction ψ_T (see Appendix B for more details about estimators of observables in MC methods and Section 2.5.6 for the relevant case of fermionic systems).

It is worth to address, before concluding this introduction, an important issue related to the imaginary time evolution, in particular with the non unitarity of the evolution operator $\exp\left[-(\hat{H} - E_{ref})\tau\right]$. This particular aspect of imaginary evolution implies that the norm of the state is not anymore conserved in time, growing without limit or going to zero depending on the value of E_{ref}. If E_{ref} equals the ground state energy, $E_{ref} = E_0$, then all amplitudes will go to zero at large time, with the exception of the amplitude of ϕ_0. On the other hand, if $E_{ref} > E_0$, all amplitudes will go to infinity and, conversely, for $E_{ref} < E_0$, all amplitudes will go to zero. In any case, the c_0 amplitude will always dominate. A way of determining the ground state energy is then to adjust E_{ref} so that the norm of the state tends to a constant. This could be achieved, in practice, by choosing as starting value for E_{ref} the resulting energy of a preliminary VMC simulation and by periodically setting E_{ref} equal to the average energy of the previous n-iterations of the algorithm (where this n is chosen in order to ensure maximum simulation stability).

2.5.2 Green's function and small-time approximation

In general, an explicit expression for the Green's function is not known analytically, due to the presence of both the kinetic energy operator and the potential energy operator, which do not commute. However, one may obtain approximations to the value of the Green's function for short time intervals. We will see below that a fundamental step, in order to obtain these approximations, will be to make the coordinate representation of the Green's function explicit. Thus, in coordinate representation the Green's function is given by the matrix-element:

$$G(\boldsymbol{R}', \boldsymbol{R}, \tau) = \langle \boldsymbol{R}' | e^{-(\hat{H} - E_{ref})\tau} | \boldsymbol{R} \rangle \,, \tag{2.37}$$

which, at $\tau = 0$, becomes

[5] We still have a transient time τ_t to wait for the population of walkers to represent the stationary distribution corresponding to ϕ_0. However, unlike the VMC method, this is a physical transient as it corresponds to a physical time evolution.

$$G(\boldsymbol{R}', \boldsymbol{R}, 0) = \delta(\boldsymbol{R}' - \boldsymbol{R}) \, . \tag{2.38}$$

The time evolution equation (2.34) can be then written in terms of $G(\boldsymbol{R}', \boldsymbol{R}, \tau)$ as

$$\Psi(\boldsymbol{R}', \tau) = \int G(\boldsymbol{R}', \boldsymbol{R}, \tau)\Psi(\boldsymbol{R}, 0) \, d\boldsymbol{R} \, . \tag{2.39}$$

From the operatorial representation of the Green's function one may easily obtain the formal differential equation

$$-\frac{\partial}{\partial \tau} G = [\hat{H} - E_{ref}]G \, ,$$

which is transformed in coordinate representation to the differential equation

$$-\frac{\partial G(\boldsymbol{R}', \boldsymbol{R}, \tau)}{\partial \tau} = \left[-\frac{\hbar^2}{2m} \sum_i \nabla_i^2 + \sum_{(i,j)} V_{ij} - E_{ref} \right] G(\boldsymbol{R}', \boldsymbol{R}, \tau) \, , \tag{2.40}$$

with the boundary condition (2.38). $\sum_{(i,j)}$ refers to the sum over all pairs of particles. We have thus obtained an equation which is the equivalent of Eq. (2.33) but now it is expressed in terms of the Green's function in coordinate representation. Even if we have obtained this expression, we still are unable to determine the exact Green's function. However, the above equation is a starting point to get a small-time approximation. In fact the Green's functions related exclusively to the kinetic or potential operators may be readily determined.

For the kinetic operator we have the following coordinate representation

$$G_K(\boldsymbol{R}', \boldsymbol{R}, \tau) = \langle \boldsymbol{R}' | e^{-\hat{K}\tau} | \boldsymbol{R} \rangle = \frac{1}{(4\pi D\tau)^{dN/2}} \exp\left[-\frac{|\boldsymbol{R} - \boldsymbol{R}'|^2}{4D\tau} \right] \, , \tag{2.41}$$

where the last equality is obtained by expressing the quantity $\langle \boldsymbol{R}' | e^{-\hat{K}\tau} | \boldsymbol{R} \rangle$ in terms of its momentum representation and then by solving the resulting integral. Here we have introduced the constant $D = \hbar^2/2m$ and we have generalized the expression for arbitrary vector components dN (in our case we just replace dN with $2(N_F + N_B)$ and we assume that the mass of all the particles is the same).

The case of the Green's function related to the potential energy is even simpler, for momentum-independent interactions. It is then a local operator with coordinate representation given by

$$G_V(\boldsymbol{R}', \boldsymbol{R}, \tau) = e^{-(\hat{V}(\boldsymbol{R}) - E_{ref})\tau} \delta(\boldsymbol{R} - \boldsymbol{R}') = G_V(\boldsymbol{R}, \tau)\delta(\boldsymbol{R} - \boldsymbol{R}') \, . \tag{2.42}$$

At this point, if the commutator between the kinetic operator and the potential operator were null, it would be possible to compute the exact Green's function since we have

all the necessary elements. However, this is not the case, so an approximate solution consists in performing a perturbative expansion in terms of small time step. We start from the exact factorization

$$e^{-[\hat{H}-E_{ref}]\tau} = \prod_{i=1}^{n} e^{-[\hat{H}-E_{ref}]\frac{\tau}{n}} \ , \tag{2.43}$$

with arbitrary n. For sufficiently large n, corresponding to a small time step $d\tau = \tau/n$, each factor in the product can in turn be expanded in the following way

$$e^{-[\hat{H}-E_{ref}]d\tau} = e^{-\hat{K}d\tau} e^{-(\hat{V}-E_{ref})d\tau} + \mathcal{O}(d\tau^2) \ , \tag{2.44}$$

which is Trotter formula (see [54]). The above approximation introduces a systematic error in the Green's function which is quadratic in the time step, so that suitable extrapolations to $d\tau \to 0$ have to be produced in order to avoid a bias in the results of the simulation. An approximate form for the full Green's function, in coordinate representation, is then obtained by replacing in Eq. (2.37) the relation (2.44) and using the expressions of kinetic and potential Green's function (2.41), (2.42) :

$$G(\boldsymbol{R}', \boldsymbol{R}, d\tau) = G_K(\boldsymbol{R}', \boldsymbol{R}, d\tau) G_V(\boldsymbol{R}, d\tau) + \mathcal{O}(d\tau^2) \ . \tag{2.45}$$

We have finally obtained the so called *small-time* or *primitive approximation* of the Green's function.

It can been shown that a Green's function with an error of order $d\tau^2$ will produce an estimated energy with a linear time-step dependence (see Ref. [32] for further details).

2.5.3 Diffusion interpretation of Schroedinger equation

The Schroedinger equation in imaginary time (2.33) can be written as

$$-\frac{\partial \Psi(\boldsymbol{R}, \tau)}{\partial \tau} = [-D\boldsymbol{\nabla}^2 + V(\boldsymbol{R}) - E_{ref}]\Psi(\boldsymbol{R}, \tau) \ , \tag{2.46}$$

where we have just divided the Hamiltonian operator into the kinetic and potential operators and we have introduced the constant $D = \hbar^2/2m$. The above equation is the starting point of this stochastic approach, in fact Eq. (2.46) can be interpreted as a diffusion equation in a $dN-$dimensional space (we still remind that, in our case, $dN = 2(N_F + N_B)$), with $\Psi(\boldsymbol{R}, \tau)$ playing the role of the density of diffusing particles.

If the $[E_{ref} - V(\boldsymbol{R})]\Psi$ term were absent, Eq. (2.46) would be the usual diffusion equation, with D acting as a diffusion constant. This simple equation can then be simulated by a random walk of particles through configuration space. On the other hand, if the term $[E_{ref} - V(\boldsymbol{R})]\Psi$ were present alone on the right-hand side, Eq. (2.46) would be a rate equation, describing branching processes such as radioactive decay or

exponential birth and death processes in a population. Thus, the entire equation can be simulated as a combination of a diffusion and a branching process, in which the number of diffusers increases or decreases at a given point proportional to the density of diffusers already there. This branching serves to decrease the probability density in regions where $V(\boldsymbol{R})$ is large, and enhance it in regions of favorable potential energy.

For the diffusion interpretation to be valid, however, Ψ must always be positive, since it is a population density. In reality, if the overall phase of the wavefunction is arbitrary, Ψ may also be everywhere negative. Thus, at first glance, it seems that the process is restricted to wavefunctions that have no nodes, such as for Bose systems in their ground state. This is one of the main differences from the Variational Monte Carlo, where it is not important whether the considered wavefunction has nodes or not. If, however, the ground state $\phi_0(\boldsymbol{R})$ does have nodes, the apparent limitation of the diffusion analogy can be dealt with by treating positive and negative regions separately and prohibiting the diffusion between them, thus introducing an approximation which takes the name of *fixed-node approximation* (for further details see section 2.5.6 below).

In the previous sections we have introduced the Green's functions and we have seen how the time evolution operator in coordinate representation can be approximated thanks to the use of both the kinetic and the potential Green's functions. We now want to make apparent the link between the diffusion interpretation of the Schroedinger equation and the Green's functions. Thus, the term G_K is responsible for the diffusion process, acting as a conditional transition probability: given a walker at position $\boldsymbol{R}$, one draws a random number ξ from the Gaussian distribution (2.41) and moves the walker to

$$\boldsymbol{R} \to \boldsymbol{R}' = \boldsymbol{R} + \xi \,.$$

The term G_V, instead, can be interpreted as a branching factor, that is a probability for the creation or destruction of copies of the walker at point $\boldsymbol{R}$. Operatively the number of created walkers is taken to be

$$n_{copy} = \mathrm{Int}[G_V(\boldsymbol{R}, d\tau) + \xi'] \,,$$

where Int[x] gives the biggest integer number smaller than x and ξ' is a random number distributed according to $U[0,1]$. Figure 2.1 naively represents the diffusion-branching process.

For completeness, there is also another possible interpretation for the potential Green's function G_V. This consists of considering G_V as a weight when accumulating the observables, without changing the number of walkers. This second possibility should, in principle, produce the same result, it has however been noticed that the branching technique gives a lower variance for the observables than the weighting technique. Moreover the second interpretation tends to favor the dominance of a single walker (see [55] for more details).

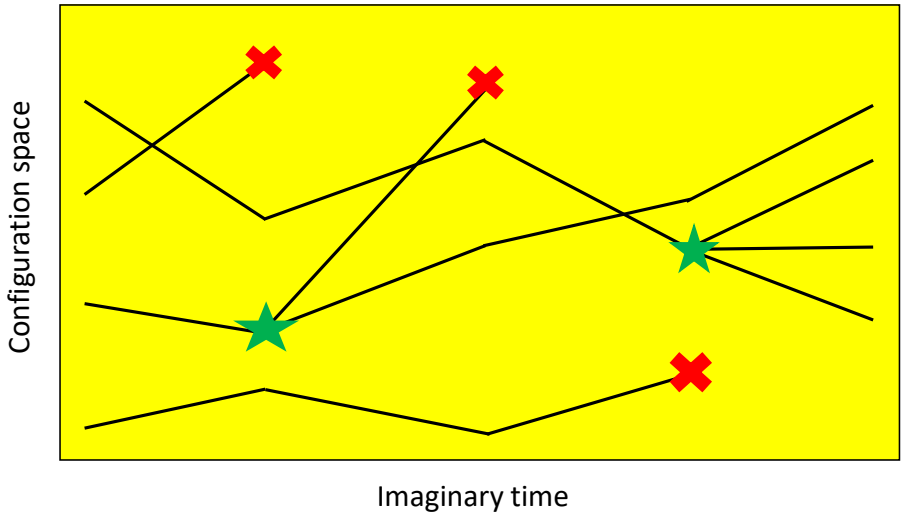

Figure 2.1: Pictorial view of the diffusion-branching process. The lines represent the diffusion process governed by G_K, the red crosses the death of a walker, the green stars the birth of new walkers, governed by G_V. The total number of walkers can change in time. For large enough time the walkers are distributed as ϕ_0 .

2.5.4 Importance sampling

The concept of importance sampling can be introduced also for Diffusion Monte Carlo. As we have seen in section 2.3.2, its use may help in lowering the variance of the energy estimators, reducing the required number of samples for a given value of the desired error. There are several ways to introduce importance sampling in DMC. We will consider Guardiola's paper [32] as a guideline.

Instead of considering the wavefunction Ψ alone, let us now introduce the new quantity (according to Ref. [56])

$$f(\boldsymbol{R}, \tau) = \psi_T(\boldsymbol{R})\Psi(\boldsymbol{R}, \tau) \ , \tag{2.47}$$

where Ψ is a wavefunction satisfying the Schroedinger equation and ψ_T is a time-independent trial wavefunction, which should be close to the exact ground state wavefunction. It is not necessarily the starting wavefunction Ψ_i, even if normally it is taken also as the starting wavefunction. We then consider the (imaginary) time evolution of $f(\boldsymbol{R}, \tau)$, which is given by the following differential equation

$$-\frac{\partial f(\boldsymbol{R}, \tau)}{\partial \tau} = -D\boldsymbol{\nabla}^2 f(\boldsymbol{R}, \tau) + D\boldsymbol{\nabla} \cdot [\boldsymbol{F}(\boldsymbol{R}) f(\boldsymbol{R}, \tau)] + [E_L(\boldsymbol{R}) - E_{ref}] f(\boldsymbol{R}, \tau) \ , \tag{2.48}$$

where we have used again the local energy E_L and we have introduced a new quantity

$\boldsymbol{F}(\boldsymbol{R})$ called *drift force*. This new term appearing in the evolution equation is given by

$$\boldsymbol{F} = \frac{2}{\psi_T(\boldsymbol{R})}\boldsymbol{\nabla}\psi_T(\boldsymbol{R}) \; . \tag{2.49}$$

The right-hand side of Eq. (2.48) represents the action of the transformed Hamiltonian $\hat{H}$ on the new probability distribution f. We can then express $\hat{H}$ as the sum of three terms

$$\begin{aligned}
\hat{H} &= \hat{K} + \hat{F} + \hat{L} \; , \\
\hat{K} &= -D\boldsymbol{\nabla}^2 \; , \\
\hat{F} &= D[(\boldsymbol{\nabla}\cdot\boldsymbol{F}(\boldsymbol{R}) + \boldsymbol{F}(\boldsymbol{R})\cdot\boldsymbol{\nabla}] \; , \\
\hat{L} &= E_L(\boldsymbol{R}) \; ,
\end{aligned}$$

corresponding respectively to the kinetic part, the drift part and the local energy part. To obtain the previous non importance sampling formula, one only has to put $\psi_T = 1$, implying $\boldsymbol{F} = \boldsymbol{0}$ and $E_L(\boldsymbol{R}) = V(\boldsymbol{R})$. In other words, one gets the equation (2.48) just by multiplying the time evolution equation (2.33) by the trial wavefunction ψ_T and rearranging the terms appropriately.

One may define as above a Green's function corresponding to this transformed operator, obeying a similar, but more complicated, differential equation. Formally, the new Green's function is given by the following expression

$$\hat{G} = e^{-[\hat{K}+\hat{F}+\hat{L}-E_{ref}]\tau} \; . \tag{2.50}$$

Also in this case, we are not able to calculate the exact expression for the total Green's function. Thus we can proceed as in section (2.5.2) considering the coordinate representation of each single piece of $\hat{G}$. The term $G_K(\boldsymbol{R}', \boldsymbol{R}, \tau)$ is the same as in the section above. The term $G_L(\boldsymbol{R}', \boldsymbol{R}, \tau)$ is obtained from $G_V(\boldsymbol{R}', \boldsymbol{R}, \tau)$ replacing V with the local energy E_L. The Green's function related to the drift force $G_F(\boldsymbol{R}', \boldsymbol{R}, \tau)$ is instead given by (see [57])

$$\langle \boldsymbol{R}'|G_F|\boldsymbol{R}\rangle = \delta(\boldsymbol{R}' - \boldsymbol{\mathcal{R}}(\tau)) \; , \tag{2.51}$$

where $\boldsymbol{\mathcal{R}}(\tau)$ is the solution of the following differential equation

$$\frac{d\boldsymbol{\mathcal{R}}(\tau)}{d\tau} = D\,\boldsymbol{F}(\boldsymbol{\mathcal{R}}(\tau)) \tag{2.52}$$

with the boundary condition $\boldsymbol{\mathcal{R}}(0) = \boldsymbol{R}$. Let us focus on solving the differential equation (2.52). If the quantum force were a constant vector, then the solution would simply be the initial condition shifted with constant velocity $\boldsymbol{F}$ (that is why the drift force is also called drift velocity):

$$G_F(\boldsymbol{R}', \boldsymbol{R}, \tau) = \delta(\boldsymbol{R} + \tau D\boldsymbol{F} - \boldsymbol{R}') \; . \tag{2.53}$$

We will adopt this approximation, which is good provided that τ is small and $\boldsymbol{F}$ not too large. However, when the trial wavefunction goes to zero but has finite gradient, so that $\boldsymbol{F}$ diverges, this is a very bad approximation and suitable cut-offs have to be artificially introduced, or more refined methods have to be used (see Ref. [58] for further details). We can finally obtain the approximate total Green's function for small time-step $d\tau$, which is given by the product of the three terms described above:

$$\begin{aligned} G(\boldsymbol{R}', \boldsymbol{R}, d\tau) &= \int G_V(\boldsymbol{R}, d\tau) G_F(\boldsymbol{R}_1, \boldsymbol{R}, d\tau) G_K(\boldsymbol{R}_1, \boldsymbol{R}', d\tau)\, d\boldsymbol{R}_1 \;+\; \mathcal{O}(d\tau^2) \\ &= G_K(\boldsymbol{R}', \boldsymbol{R} + d\tau D\boldsymbol{F}, d\tau) G_V(\boldsymbol{R}, d\tau) \;+\; \mathcal{O}(d\tau^2)\ . \end{aligned} \tag{2.54}$$

Even after introducing the importance sampling, the diffusion-branching interpretation of the (imaginary) time evolution equation still be valid but with some little modifications. Equation (2.48), which incorporates importance sampling through ψ_T, is a diffusion equation for a density function $f(\boldsymbol{R}, \tau)$ with diffusion constant $D = \hbar^2/2m$. The branching term is now proportional to the "excess local energy" $[E_L(\boldsymbol{R}) - E_{ref}]$, which, unlike the original one, with a good choice of ψ_T does not become singular when $V(\boldsymbol{R})$ does. Also, an additional term $\frac{\hbar^2}{2m}\boldsymbol{\nabla} \cdot [\boldsymbol{F} f]$ now appears in Eq (2.48). This new term acts to impose a directed drift velocity on diffusion with consequences on the sampling regions, in the sense that, in regions of low probability (where ψ_T is small) one has a large drift force $\boldsymbol{F}$ and hence any diffusers reaching such a region are driven away. Thus, the advantage of Eq. (2.48) over Eq. (2.33) is that the diffusion process for $f(\boldsymbol{R}, \tau)$ is guided by ψ_T (through the force $\boldsymbol{F}$), so that the sampling is performed preferentially in regions where ψ_T is large.
Therefore, summing up, if ψ_T is a good approximation of the ground state with this algorithm we have two benefits: the drift accelerates the dynamics towards the ground state and the branching term becomes a very smooth factor. These improvements yield averages with much lower statistical uncertainties than those obtained without importance sampling.

2.5.5 DMC algorithm

Here we collect and resume all the results that we have seen in the previous sections in order to present a scheme of the algorithm of the DMC method. Of course, before implementing the code, an importance sampling trial function must be determined. Also, adequate procedures must be devised in order to compute the local energy and the drift force. We postpone the discussion of these important issues to section 2.6.

The algorithm can therefore be schematized in this way:

- Initialization:

- Get a proper value for the time step;
- Guess a value for the energy shift E_{ref};
- Create a starting set of walkers, representing the function $f(\boldsymbol{R}, \tau = 0)$;
- For each walker $\boldsymbol{R}$ compute and store the local energy and the drift function;
- Initialize accumulators for energy and its square[6], as well as for other observables.

- Start time evolution loop. For each walker do:
  - Generate a trial move

$$\boldsymbol{R}' = \boldsymbol{R} + Dd\tau \boldsymbol{F}(\boldsymbol{R}) + \boldsymbol{\xi} \ ,$$

    where $\boldsymbol{\xi}$ is drawn from the multivariate Gaussian distribution with null mean and variance $\sigma^2 = 2Dd\tau$;
  - Compute the replication factor

$$n = [\exp\{d\tau(E_L(\boldsymbol{R})/2 + E_L(\boldsymbol{R}')/2 - E_{ref})\}] \ ,$$

    where the square brackets mean *integer part* and both the initial and the final configurations contribute, as it can be shown that this reduces the time-step bias;
  - Unless $n = 0$ make n copies of $\boldsymbol{R}'$, $E_L(\boldsymbol{R}')$ and $\boldsymbol{F}(\boldsymbol{R}')$ to the new set of walkers;
  - Copy the new set of walkers to the old set;
  - Test the growth of the population and, if necessary, adjust the energy E_{ref};
  - If the transient is finished, update the accumulators for averages and errors.

- Go to the next time iteration and repeat all the previous operations belonging to the time evolution loop until a sufficiently long time has passed.

- Compute averages and errors.

It is worth to stress that, usually, DMC simulations are performed after preliminary VMC simulations. Thus one can determine both the initial energy shift E_{ref} and the starting configuration of walkers from Variational Monte Carlo results.
Another point that requires special attention and which should be discussed here is the correlation between successive positions. We have seen that the correctness of the DMC

[6]Necessary for the calculation of the variance.

method is strictly related to the small-time approximation of the total Green's function. Then it is necessary to implement the algorithm with ever smaller time-steps. However, if the time-step is very small, successive positions are strongly correlated. Even if the source of the correlation is in principle different, this correlation problem is very similar to the one already seen in VMC section. Thus we have again two solutions, which are a thermalization loop or a block analysis. Also for this case the second solution is the most convenient one for the reasons already mentioned in the section 2.3.3.

2.5.6 Fixed-node approximation

When we talked about the diffusion interpretation of the Schroedinger equation we said that a necessary condition for its validity is the absence of nodes in the ground-state wavefunction. This condition is always guaranteed for bosonic systems, whose ground-state wavefunction is everywhere positive and thus can be interpreted as a probability distribution function. However, in the case of fermionic systems, the antisymmetry of the wavefunction imposes the presence of positive and negative regions in configuration space. The problem of the sign of the wavefunction, which goes under the name of "sign problem", is a very famous issue in the context of Quantum Monte Carlo simulations.

One possible approach is to consider the sign of the wavefunction as a factor that multiplies the contribution of the single walker to the observables. This has been proven to result in a increasing fluctuation of the estimators of the observables with increasing imaginary time, reducing the signal with respect to the noise, so that a refined analysis has to be performed (see [44, 59, 60, 61]). Many other approaches to overcome this problem have been proposed, even if it has been demonstrated [62] that there is not a general solution, that is an algorithm both exact and convergent in a time which is polynomial in the number of degrees of freedom.

An approximate solution, which has been proven to be very precise for the ground state of ultracold gases, is obtained through the *fixed-node approximation* (FN). This approximation strongly relies on importance sampling and the use of a good trial function ψ_T, which can usually be constructed for dilute systems. Before going into the details of the FN approximation it is good to introduce some important definitions:

- *nodal surface*, region in the configuration space where a wavefunction is zero;
- *nodal pocket*, connected region in configuration space whose boundary is a part of the nodal surface.

In light of these new definitions, the problem of fermionic wavefunctions is that the sign of the wavefunction changes from a nodal pocket to the next one and the position of the nodal surface is not known a priori. Perhaps, it might be helpful to know the symmetry properties of the wavefunction (which sometimes are known from the physical knowledge of the considered system), however it is in general impossible to determine in a precise

way the complete nodal surface of an unknown function Ψ. It is therefore fundamental to use the FN approximation.

The essence of the fixed-node approximation is to fix the nodal surface of the studied wavefunction Ψ (the one that satisfies the Schroedinger equation (2.33)) to be equal to that of a trial wavefunction ψ_T, so that the nodal pockets of Ψ and ψ_T coincide. Then the Diffusion Monte Carlo, with the help of the importance sampling algorithm, is applied to the distribution $f = \psi_T \Psi$ which turns to be everywhere positive, except on the nodal surface. Thus the branching-diffusion interpretation of the many-body Schroedinger equation is preserved, provided that the nodal surface is never crossed. In other words, this is essentially equivalent to having a constraint defining impenetrable barriers which cannot be crossed by the walkers: every time a walker attempts to cross the nodal surface, it is killed (i.e., its replication factor n is made zero).

Ceperley [45] and almost simultaneously Moskowitz and collaborators [63] proved that the energy obtained with the mixed estimator (see Appendix B) in the fixed-node approximation is an upper bound to the fermion ground state energy.
If the nodal surface of the trial wavefunction were equal to the exact surface, then this upper bound would coincide with the ground state energy. The proof of this statement, for the case of spin independent wavefunctions is the following.
Let the trial wavefunction $\psi_T(\boldsymbol{R})$ be antisymmetric in the spatial variables. Further, let v_α be the connected volumes in configuration space bounded by the nodes of ψ_T. In each of these volumes there is a unique ground state eigenfunction $\Psi_\alpha(\boldsymbol{R})$ with eigenvalue ϵ_α, which satisfies the equations

$$\begin{cases} \hat{H}\Psi_\alpha(\boldsymbol{R}) = \epsilon_\alpha \Psi_\alpha(\boldsymbol{R}) & \boldsymbol{R} \in v_\alpha \ , \\ \Psi_\alpha(\boldsymbol{R})\psi_T(\boldsymbol{R}) > 0 \end{cases}$$

and

$$\Psi_\alpha(\boldsymbol{R}) = 0 \qquad\qquad \boldsymbol{R} \in \Sigma \ ,$$

where we have denoted the nodal surface with the Greek capital letter Σ.
The fixed node procedure solves this problem exactly in each volume element:

$$\Psi(\boldsymbol{R}, \tau) \xrightarrow[\tau \to \infty]{} \Psi_\alpha(\boldsymbol{R}) \ .$$

For each α we can then define an antisymmetric function

$$\widetilde{\Psi}_\alpha(\boldsymbol{R}) = \sum_P (-)^P \Psi_\alpha(P\boldsymbol{R}) \ ,$$

whose variational energy[7] is

$$\frac{\int \widetilde{\Psi}_\alpha^* \hat{H} \widetilde{\Psi}_\alpha \, d\boldsymbol{R}}{\int \widetilde{\Psi}_\alpha^* \widetilde{\Psi}_\alpha \, d\boldsymbol{R}} = \epsilon_\alpha \geq E_0 \ .$$

[7]By construction the variational energy is bigger or equal to the ground state energy.

Here E_0 is the fermion ground state energy and P simply represents a permutation of the fermions. We have thus shown that each eigenvalue ϵ_α is an upper bound to the ground state energy E_0.

In the fixed node approximation, one usually attempt to populate as many volumes v_α as possible. This is a consequence of the fact that the best upper bound (for a given ψ_T) is obtained if all volumes v_α have been populated (see [45] for further information).

2.6 Trial wavefunctions

The choice of the trial wavefunction is critical in both VMC and DMC calculations. In the first case, the trial wavefunction has to be as close as possible to the ground state solution in order to obtain precise results. In the second case, instead, we need a wavefunction which is able to reproduce the nodal surface of the solution of the many-body Schroedinger equation in the best possible way. Also, refined trial wavefunctions improve the importance sampling algorithm, reducing the cost of obtaining a certain statistical accuracy without increasing the number of sampling. Of course, this does not mean that any function can be used. In fact, only wavefunctions which are physical and for which the gradient and the laplacian may be efficiently computed, can be used.

For bosons in the ground state, the Jastrow wavefunction [42, 64] was able to capture the few-body correlations which dominate the dilute systems physics, while for fermions the Slater [47] or BCS determinants [65, 66, 67] proved very accurate in describing the nodal surface. For systems containing both bosons and fermions (such as Bose-Fermi mixtures) a good ansatz for the wavefunction is given by the Jastrow-Slater wavefunction [3, 4].

Jastrow wavefunction

The *Jastrow wavefunction* is a symmetrized product of few-body wavefunctions. The simplest form, which is suitable for describing dilute systems, contains only the two-body correlation terms and reads as

$$\psi_J(\boldsymbol{R}) = \prod_{i<j} f(r_{ij}) \ , \tag{2.55}$$

where the product is extended over all the pairs of interacting particles. In this form the two-body term depends only on the distance between the particles in the pair $r_{ij} = |r_i - r_j|$. In case of short range interactions the function f is taken to be a solution of the two-body problem with suitable boundary conditions (see Appendix C for the details of the calculation). Notably, this choice of f allows to deal also with Coulomb-like potentials, which show a divergence when $r_{ij} = 0$, guaranteeing the exactness of the wavefunction at the two-body level at short distances. In case one considers two generic

species of particles (let us call them up, $\uparrow$, and down, $\downarrow$), the general (two-body) Jastrow function is:

$$\psi_J(\boldsymbol{R}) = J_{\uparrow\uparrow}(\boldsymbol{R})J_{\downarrow\downarrow}(\boldsymbol{R})J_{\uparrow\downarrow}(\boldsymbol{R}) = \prod_{i<j} f_{\uparrow\uparrow}(r_{ij}) \prod_{a<b} f_{\downarrow\downarrow}(r_{ab}) \prod_{i,a} f_{\uparrow\downarrow}(r_{ia}) \ , \tag{2.56}$$

where the indices i, j refer to the $\uparrow$ particles and the indices a, b refer to the $\downarrow$ particles.

Once the wavefunction has been chosen, an important step is the calculation of the explicit form of the drift force and of the local energy (in particular of the kinetic term). Thus the drift forces $F^{\alpha}_{i,a}$, where the index $\alpha = x, y$ refers to the spatial coordinate, reduce to

$$F^{\alpha}_{\uparrow\uparrow i} = 2\frac{\partial_{\alpha_i} J_{\uparrow\uparrow}}{J_{\uparrow\uparrow}} = 2\sum_{j\neq i} \frac{\partial_{\alpha_i} f_{\uparrow\uparrow}(r_{ij})}{f_{\uparrow\uparrow}(r_{ij})} = 2\sum_{j\neq i} \frac{f'_{\uparrow\uparrow}(r_{ij})}{f_{\uparrow\uparrow}(r_{ij})} \frac{\alpha_i - \alpha_j}{r_{ij}} \ , \tag{2.57}$$

for the $\uparrow\uparrow$ case and analogously for the other cases.
The local kinetic energy of the Jastrow wavefunction is instead given by

$$\begin{aligned} K = D \Bigg\{ & 2\sum_{i<j} \left[e^L_{\uparrow\uparrow}(r_{ij}) + \left(\frac{f'_{\uparrow\uparrow}(r_{ij})}{f_{\uparrow\uparrow}(r_{ij})} \right)^2 \right] + 2\sum_{a<b} \left[e^L_{\downarrow\downarrow}(r_{ab}) + \left(\frac{f'_{\downarrow\downarrow}(r_{ab})}{f_{\downarrow\downarrow}(r_{ab})} \right)^2 \right] \\ & + 2\sum_{i,a} \left[e^L_{\uparrow\downarrow}(r_{ia}) + \left(\frac{f'_{\uparrow\downarrow}(r_{ia})}{f_{\uparrow\downarrow}(r_{ia})} \right)^2 \right] - \frac{1}{4}(\boldsymbol{F}_S \cdot \boldsymbol{F}_S + \boldsymbol{F}_A \cdot \boldsymbol{F}_A + 2\boldsymbol{F}_S \cdot \boldsymbol{F}_A) \Bigg\} \ , \end{aligned} \tag{2.58}$$

where the global force vectors are $\boldsymbol{F}_S = \{F^{\alpha}_{\uparrow\uparrow i}, F^{\alpha}_{\downarrow\downarrow a}\}$ and $\boldsymbol{F}_A = \{F^{\alpha}_{\uparrow\downarrow i}, F^{\alpha}_{\uparrow\downarrow a}\}$ and $e^L = -(f'' + (d-1)f'/r)/f$ is the local kinetic energy of the two-body problem in units of $2D$. The last term can be also written equivalently as $\frac{1}{4}\boldsymbol{F} \cdot \boldsymbol{F}$, where the scalar product is meant as a sum over the coordinates of all the particles. See the PhD thesis [68] for the details of the calculation.

In the case of Bose-Fermi mixtures we identify fermions (F) with $\uparrow$ particles and bosons (B) with $\downarrow$ particles. The Jastrow wavefunction is now simpler than the general case (2.56) because we assume that the short-range fermion-fermion interaction is negligible, since the fermions are polarized and the usually dominant zero-temperature s-wave correlations are thus prevented by Pauli principle [3]. Thus it reads as

$$\psi_J(\boldsymbol{R}) = J_{BB}(\boldsymbol{R})J_{FB}(\boldsymbol{R}) = \prod_{a<b} f_{BB}(r_{ab}) \prod_{i,a} f_{FB}(r_{ia}) \ . \tag{2.59}$$

Jastrow-Slater wavefunction

In the study of fermionic systems the Jastrow wavefunction cannot be used alone, since it is symmetric in the exchange of particles. The simplest antisymmetric wavefunction that one can use is a *Slater determinant*. The antisymmetry of this type of functions comes directly from the properties of the determinant (i.e., by interchanging any pair of

columns or rows a minus sign appears). Slater determinants can be constructed using different functions depending on the system that one is studying. For dilute systems, non-interacting single particle wavefunctions (i.e., plane waves) proved to be good enough for comparison with experimental results (see [67, 69]).

We can then couple the Jastrow function and the Slater determinant in order to obtain a more refined wavefunction, called *Jastrow-Slater wavefunction*, which is now able to describe interacting systems containing both bosons and fermions. In the particular case of Bose-Fermi mixtures, it can be written as the following product:

$$\psi_{JS} = \psi_J D_F \ , \tag{2.60}$$

where the determinant is defined as

$$D_F(\boldsymbol{R}_F) = \det S_{Fpi} = \det[\phi_{\boldsymbol{k}_p}(\boldsymbol{r}_i)] \ . \tag{2.61}$$

The $\phi_{\boldsymbol{k}_p}$ orbitals are single particle wavefunctions corresponding to eigenvectors of momentum in a box with periodic boundary conditions (see Section 2.7 for further details on the periodicity of the system). In order to have a real wavefunction we used the $cos(\boldsymbol{kr})$ and $sin(\boldsymbol{kr})$ functions. For the $\boldsymbol{k}$ vectors we choose the eigenvalues of momentum starting from the zero vector up to the Fermi wavevector fixed by the number of particles and the volume of the box (in the thermodynamic limit only by the density).

We will now derive some useful relations for the calculation of the drift force and of the local kinetic energy for the Slater term D_F. It is convenient to introduce the inverse Slater matrix $\bar{S}$, whose properties are:

$$\sum_i S_{pi}\bar{S}_{iq} = \sum_i \phi_{\boldsymbol{k}_p}(\boldsymbol{r}_i)\bar{S}_{iq} = \delta_{pq} \qquad \sum_p \bar{S}_{jp}\phi_{\boldsymbol{k}_p}(\boldsymbol{r}_i) = \sum_p \bar{S}_{jp}S_{pi} = \delta_{ij} \ .$$

Since the iterative calculation of the determinant involves the cofactors A_{pi} in the equation $D_F = \sum_i S_{ip}A_{pi}$ (cofactor expansion of the determinant), for any p, the inverse matrix is related to the cofactors in the following way: $\bar{S}_{pi} = A_{pi}/D_F$. Two useful properties can therefore be deduced, concerning the derivatives of the Slater determinant:

$$\frac{1}{D_F}\frac{\partial D_F}{\partial S_{ip}} = \bar{S}_{pi} \qquad \frac{\partial \bar{S}_{pi}}{\partial S_{jq}} = -\bar{S}_{qi}\bar{S}_{pj} \ .$$

It is now possible to derive the drift force for the Slater determinant

$$F_i^\alpha = \frac{2}{D_F}\partial_{\alpha_i} D_F = \frac{2}{D_F}\sum_p \frac{\partial D_F}{\partial S_{ip}}\frac{\partial S_{ip}}{\partial \alpha_i} = 2\sum_p \bar{S}_{pi}\partial_{\alpha i}\phi_{\boldsymbol{k}_p}(\boldsymbol{r}_i) \ , \tag{2.62}$$

and the local kinetic energy

$$
\begin{aligned}
K &= -\frac{D}{D_F}\sum_i\sum_\alpha \partial^2_{\alpha_i} D_F = -\frac{D}{D_F}\sum_i\sum_\alpha \partial_{\alpha_i}\left[D_F\sum_p \bar{S}_{pi}\frac{\partial S_{ip}}{\partial\alpha_i}\right] \\
&= -D\sum_i\sum_\alpha\left[\left(\sum_{pq}\bar{S}_{qi}\frac{\partial S_{iq}}{\partial\alpha_i}\bar{S}_{pi}\frac{\partial S_{ip}}{\partial\alpha_i}\right) - \left(\sum_{pq}\bar{S}_{qi}\frac{\partial S_{iq}}{\partial\alpha_i}\bar{S}_{pi}\frac{\partial S_{ip}}{\partial\alpha_i}\right)\right. \\
&\left. + \sum_p \bar{S}_{pi}\partial^2_{\alpha_i}\phi_{\boldsymbol{k}_p}(\boldsymbol{r}_i)\right] = -D\sum_{i,p}\sum_\alpha \bar{S}_{pi}\partial^2_{\alpha_i}\phi_{\boldsymbol{k}_p}(\boldsymbol{r}_i)\ ,
\end{aligned}
\tag{2.63}
$$

where the index $\alpha = x, y$ refers again to the spatial coordinate. In the homogeneous system which we consider, the functions $\phi_{\boldsymbol{k}_p}$ are just plane waves. Thus, the last expression simply turns into $K = D\sum_p k_p^2$, where k_p is the modulus of the p-th eigenvector of momentum. Going back to the complete wavefunction (2.60), let us now use the superscript S, J to refer to the Slater determinants or the Jastrow factors respectively. The total drift force is simply $\boldsymbol{F} = \boldsymbol{F}^J + \boldsymbol{F}^S_F$ (where again the indices of these vectors correspond to the ordered coordinates of all the particles). The total local kinetic energy is instead given by

$$
K^{JS} = -\frac{D}{\psi^{JS}}\left(\sum_{i,\alpha}\partial_{\alpha_i}\psi_{JS} + \sum_{a,\alpha}\partial_{\alpha_a}\psi_{JS}\right) = K^J + K^S_F - \frac{D}{2}(\boldsymbol{F}^J\cdot\boldsymbol{F}^S)\ . \tag{2.64}
$$

We now have all the elements to construct the necessary quantities required by both VMC and DMC algorithms.

2.7 Finite-size systems

When dealing with extended systems we cannot attempt the simulation with an infinite number of particles. The usual way of dealing with these systems, inherited from Statistical Mechanics [37, 70], consists in representing the system in a simulation cell with appropriate periodic boundary conditions (PBC). For a general d-dimensional system, the simulation cell is a d-dimensional hypercube with linear size L so that $L^d = N/n$, where n is the particle density. The implementation of PBC requires a regular behavior of the trial wavefunctions at the boundary of the simulation box: in the case of Slater determinants, the single particle orbitals must have a period for which L is an integer multiple; in the case of Jastrow factors, one requires that at the distance $r = L/2$ the function goes to a constant and its derivative goes to zero.

The implementation of PBC implies also additional conditions on the Monte Carlo moves. In fact, every time a particle comes out from the elementary cell, it must be

brought back inside by subtracting or adding an integer number of times the length L. Moreover, when calculating properties involving a pair of particles, such as Jastrow factors, one has to consider the closest replica of the particles (see Fig. 2.2).

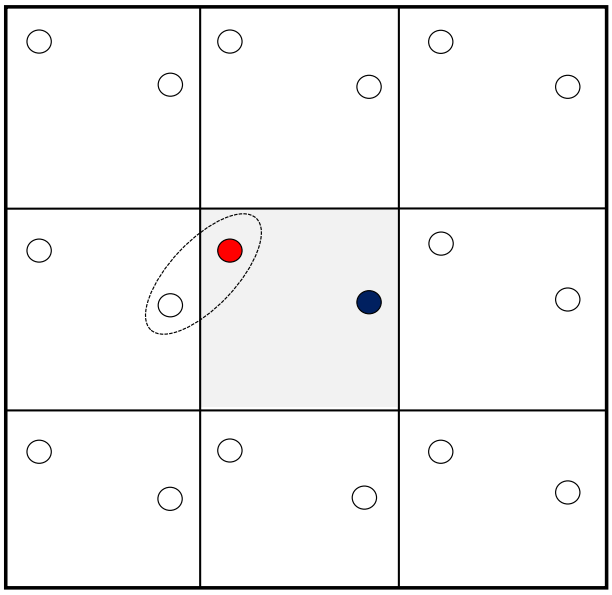

Figure 2.2: Periodic boundary conditions and closest replica.

Even if the fixed and limited number of particles implies an accessible computational time, the finite size of the systems could be a problem. This is evident when one wants to calculate, using QMC techniques, the properties of a system in the thermodynamic limit. It is therefore necessary to study how these finite-size effects negatively affect our results in order to find a way, if any, to mitigate them. However, it is clear from the outset, that finite-size errors cannot be completely erased, introducing a systematic error in our simulations that will have to be appropriately estimated (see Sec. 3.2.2).

The finite-size error can be reduced by choosing particular particle numbers. In case of bosonic systems, this idea is tied to the possibility of allowing the system *crystallize*, i.e. , when particles prefer to place themselves around an ordered and periodic structure. Instead, in case of fermionic systems there is a set of *magical* numbers which are related to the concept of closed shell and to the ability to emulate the properties of the system in the thermodynamic limit. In the following, we will devote our attention to this second case as in our B-F mixtures bosons constitute only a small fraction of the total particles.

By imposing the periodic boundary conditions discussed above on the two-dimensional simulation cell with side L, we are implicitly fixing the discrete values of the wavevectors

$\boldsymbol{k}$ of the particles. Thus, possible values of $\boldsymbol{k}$ must follow the rule

$$\boldsymbol{k} = \frac{2\pi}{L}(n_x, n_y) \ ,$$

where the n are positive or negative integer numbers. At this point one can notice that there are some combinations of the allowed wavevectors which better describe the thermodynamic limit. These combinations are those that form the so called closed shells (i.e. , combinations where the sum of all $\boldsymbol{k}$ is zero). In fact, in the thermodynamic limit, the average value of $\boldsymbol{k}$ is just zero. Furthermore, one constructs configurations of fermions that respect discrete rotational symmetries, which are expected in the thermodynamic limit. For these reasons it can be deduced that to realize such configurations only some particular numbers are able to satisfy all the previous requests, that are, in two dimensions: 5, 9, 13, 21, 29, 37, 45, 49, 57, 61, ... Figure 2.3 provides an example of how these closed shells must be built to respect the properties described above.

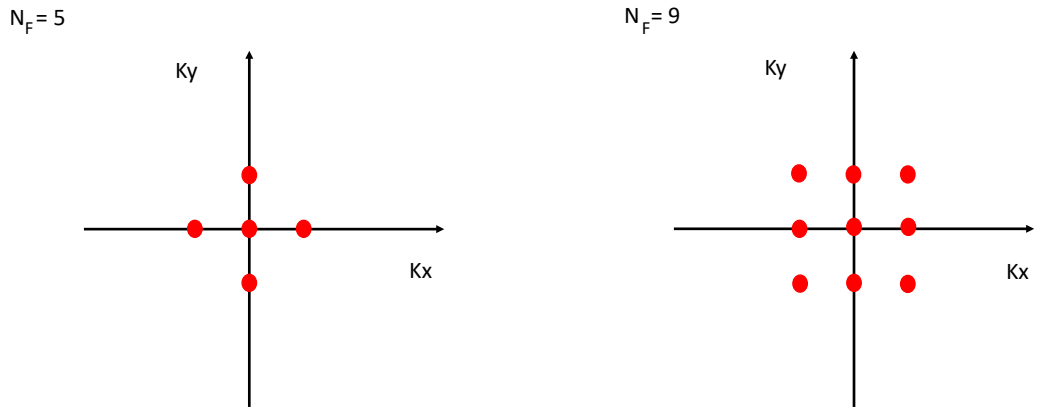

Figure 2.3: Construction of the first two non-trivial closed shells for a fermionic system.

Chapter 3

Quantum Monte Carlo simulations

In this Chapter we apply the QMC techniques described in Chapter 2 to the two-dimensional Bose-Fermi mixture described in Section 1.3. Our simulations are based on a QMC code written by G. Bertaina (from INRiM, Torino, Italy). The code has already been used to address many different physical systems (we mention Refs. [6, 71, 72, 73] as examples of some recent applications of the code), but it has never been applied so far to Bose-Fermi mixtures in two dimensions. The simulations of the present work have being carried out by using the parallel computing cluster of the Open Physics Hub (https://site.unibo.it/openphysicshub/en) at the Physics and Astronomy Department in Bologna.

The present chapter is organized as follows. A first introductory section points out the conventions adopted during the simulations. Then, we show how the VMC simulations and the DMC simulations must be carried out in order to take into account all the systematic errors introduced by the approximations used. Finally, we compare the results of our simulations with the perturbative predictions.

3.1 Input parameters and conventions

The QMC code used in our simulations is a general purpose algorithm adaptable to many different physical systems. It is thus important to highlight what are the input parameters to be specified and which are the conventions used in our simulations.

Let us begin by describing the parameters necessary for the correct functioning of the program. We can divide the entire set of parameters into two distinct classes which are independently specified through two different input files: the Monte Carlo parameters and the physical parameters. The former are strictly related to the type of MC algorithm used and to the type of analysis conducted. In case of VMC simulations the number of walkers, the number of MC moves and the length of the transient must be specified. Also, a factor related to the acceptance ratio is necessary in order to ensure the correct

movement of the Markov chain. The case of DMC simulations is, instead, slightly more complicated than the previous one. Of course, the number of walkers, the number of MC moves and the length of the transient have to be fixed again, but now one must specify also the reference energy E_{ref} and the time step. Other parameters of a more technical nature are introduced, such as the cutoff factor (see Sec. 3.3.2 for further details) or the number of copies allowed in the branching process, in order to control the often unstable diffusion-branching process of the DMC algorithm. The physical parameters required, on the other hand, do not distinguish between VMC and DMC. We need then to specify the main characteristics of the system that we want to study. Before going into details, it is important to stress that almost all physical parameters, with the exception of the number of components and the number of particles of each type, are physical quantities and therefore have a unit of measure. However, the values we enter as input in the program must be dimensionless quantities, therefore we will have to divide or multiply the previous quantities by suitable reference values (indicated with the subscript R). So, the first parameters are the number of different species present in the mixture and the relative numbers of particles. Then we need to specify the mass of the particles

$$\text{mass}_i = \frac{m_i}{m_R} \,, \tag{3.1}$$

where the index i refers to the type of species considered. In our case, we have only two species with equal mass, thus we always fix for our simulations

$$\frac{m_F}{m_R} = \frac{m_B}{m_R} = 1 \,,$$

in order to have the relation $m_F = m_B = m_R$. Other parameters are the total density of particles $n = n_F + n_B$, given by

$$dens = n\, R_R^2 \,, \tag{3.2}$$

and the following constant

$$h2o2mRl2 = \frac{\frac{\hbar^2}{2m_R R_R^2}}{E_R} \,, \tag{3.3}$$

that allows us to fix the unit of energy and of time step. The interactions between bosons and fermions and those between bosons and bosons are regulated by two pairs of parameters

$$\left(\widetilde{R}^{BF} = \frac{R^{BF}}{R_R} \,, \;\; R_P^{BF} = \frac{R^{BF}}{\widetilde{a}^{BF}} \right) \tag{3.4}$$

$$\left(\widetilde{R}^{BB} = \frac{R^{BB}}{R_R} \,, \;\; R_P^{BB} = \frac{R^{BB}}{\widetilde{a}^{BB}} \right) \,, \tag{3.5}$$

where $\widetilde{a}^{BF}$ and $\widetilde{a}^{BB}$ are the scattering lengths which follow the convention described in the Appendix C and R^{BB} and R^{BF} are the radii of the potential disks that we consider as model potentials. In particular, by choosing different values of $\widetilde{R}$ we can vary the magnitude of the interaction, while changing the value of R_P we modify the structure of the potential, in the sense that for $R_P = 1.0$ we have a hard disk potential, instead for $R_P > 1.0$ we have a soft disk potential. In our simulations we are only interested in the soft disk case, thus we fix, without ever changing, $R_P^{BB} = R_P^{BF} = 2.0$. This choice is irrelevant in the weakly interacting regime, where what matters is only the ratio between the scattering lengths and the average particle distance, however results can depend on this parameter for strong interactions.

As can be seen from the previous expressions, the values of the physical parameters entered in the program depend on the choice of the reference constants (R_R, E_R) used. This arbitrariness can very easily lead to misunderstandings and errors. For this reason, it is important to establish a convention that will then be used for the duration of the simulations. We thus fix the reference length R_R as the mean distance between fermions $l_m^{(F)}$, which, in two dimensions, is given by

$$R_R = l_m^{(F)} = \frac{1}{\sqrt{n_F}} \,, \tag{3.6}$$

where n_F is the fermion density. Furthermore, we require that the reference energy E_R is equal to the Fermi energy ε_F:

$$E_R = \varepsilon_F = \frac{\hbar^2 k_F^2}{2m_F} \,, \tag{3.7}$$

where m_F is the fermionic mass (in our convention $m_F = m_R$) and k_F is the Fermi wavevector which in two dimensions is given by $k_F = \sqrt{4\pi n_F}$. This choice of R_R and E_R imposes some conditions on the physical parameters *dens* and *h2o2mRl2* . In particular,

$$\begin{aligned} dens = n \left(\frac{1}{\sqrt{n_F}} \right)^2 = \frac{n}{n_F} = \frac{n_F + n_B}{n_F} \\ = 1 + \frac{n_B}{n_F} \equiv 1 + x \,, \end{aligned} \tag{3.8}$$

where n_B is the boson density and $x = n_B/n_F = N_B/N_F$ is the boson concentration. We also use

$$h2o2mRl2 = \frac{\hbar^2 n_F}{2m_R} \frac{2m_F}{\hbar^2 k_F^2} = \frac{n_F}{k_F^2} = \frac{n_F}{4\pi n_F} = \frac{1}{4\pi} \,. \tag{3.9}$$

The adopted convention has two useful consequences: the first is that the time step of the DMC will be in units of the inverse Fermi energy of the fermions ($\hbar/\varepsilon_F$); the second is that the energies resulting from the QMC simulations will be in units of ε_F.

Although the physical parameters described above are one of the most convenient choices in the implementation of the QMC code, they are not necessarily as effective in the theoretical description of the physical system. In fact, in Quantum Many-Body theory, for two dimensional systems, it is more convenient to describe the BF and the BB coupling strength in terms of the dimensionless parameters g_{BF} and g_{BB} respectively:

$$g_{BF} = -\frac{1}{\log(k_F a_{BF})} \qquad g_{BB} = -\frac{1}{\log\left(n_B a_{BB}^2\right)}\,, \tag{3.10}$$

where a_{BF} and a_{BB} are the scattering lengths which respect the convention described in Appendix C. The coupling parameters (3.10) are related to the input parameters $\widetilde{R}$ and R_P by the following relations (see Appendix D for further details on the derivation):

$$g_{BF} = -\frac{1}{\log(k_F a_{BF})} = -\frac{1}{\log\left[\sqrt{4\pi}\,\frac{e^\gamma}{2}\left(\frac{\widetilde{R}^{BF}}{R_P^{BF}}\right)\right]}\,, \tag{3.11}$$

$$g_{BB} = -\frac{1}{\log\left(n_B a_{BB}^2\right)} = -\frac{1}{\log\left[x\,\frac{e^{2\gamma}}{4}\left(\frac{\widetilde{R}^{BB}}{R_P^{BB}}\right)^2\right]}\,, \tag{3.12}$$

where $\gamma \simeq 0.577...$ is Euler-Mascheroni constant.

Due to these relations, in the following we can find the interactions described in terms of the coupling parameters or in terms of the input parameters.

Before concluding this section, in the input file one has also to specify the boundary conditions chosen (PBC) and the trial wavefunction to use in the simulations (Jastrow-Slater).

3.2 VMC simulations

Before obtaining the VMC results shown in Section 3.4 several preliminary analyses must be conducted. The purpose of this section is therefore to summarize and report all the simulations that were necessary to obtain consistent and precise results. In particular, the main issue addressed concerns the finite size of the system simulated with the QMC techniques. For this reason, the simulations were repeated considering different closed shells, with an ever larger number of fermions (and bosons).

The Bose-Fermi mixture under study is mainly composed of fermions, since we consider low bosonic concentrations. Therefore the BF interaction is the most relevant term of the total interaction energy. For this reason, we decide to fix a small value of the BB interaction (in terms of the input parameters we set $\widetilde{R}^{BB} = 0.001$ and $R_P^{BB} = 2.0$) and we then consider several values of the BF interaction by varying $\widetilde{R}^{BF}$ (Table 3.1 reports the interactions considered in terms of both input and coupling parameters).

$\widetilde{R}^{BF}$	R_P^{BF}	g_{BF}	$\widetilde{R}^{BB}$	R_P^{BB}	g_{BB}
1.0×10^{-9}	2.0	0.0493	1.0×10^{-3}	2.0	0.0594
1.0×10^{-5}	2.0	0.0904	1.0×10^{-3}	2.0	0.0594
1.0×10^{-3}	2.0	0.1550	1.0×10^{-3}	2.0	0.0594
5.0×10^{-3}	2.0	0.2065	1.0×10^{-3}	2.0	0.0594
1.0×10^{-2}	2.0	0.2410	1.0×10^{-3}	2.0	0.0594
3.0×10^{-2}	2.0	0.3278	1.0×10^{-3}	2.0	0.0594
5.0×10^{-2}	2.0	0.3938	1.0×10^{-3}	2.0	0.0594
1.0×10^{-1}	2.0	0.5417	1.0×10^{-3}	2.0	0.0594
2.0×10^{-1}	2.0	0.8673	1.0×10^{-3}	2.0	0.0594

Table 3.1: List of the values of the interactions considered in terms of both input and coupling parameters. Each row represents a particular configuration of interactions studied. The coupling parameter g_{BB} is obtained from Eq. 3.12 for $x = 12/49$.

3.2.1 Optimization of the variational parameters

In section 2.4 we have described the variational method and how it can be used to obtain an upper bound for the ground state energy. However, until now, we have not yet described any variational parameters in our trial wavefunction. We therefore decided to introduce the parameters $\bar{R}^{BF}$ and $\bar{R}^{BB}$, which are used to parametrize, in the Jastrow factors, the distance at which the trial wavefunction goes to a constant (examine Section 2.7 to see how PBC are implemented for Jastrow-Slater wavefunctions). In this way, the energy becomes a functional of the two variational parameters $\bar{R}^{BF}$ and $\bar{R}^{BB}$. Thus, for distinct values of these parameters, several simulations must be carried out in order to find the minimum of the energy.

Clearly, the optimal values of $\bar{R}^{BF}$ and $\bar{R}^{BB}$ are affected by the considered interactions. It is therefore necessary to optimize these variational parameters for each possible value of the interactions. Since the BB interaction is kept constant, the first analysis we conducted was to identify an optimal $\bar{R}^{BB}$ parameter to be used in all subsequent simulations. In particular, we fixed $\widetilde{R}^{BF} = 0.01$, $\widetilde{R}^{BB} = 0.001$ and $R_P^{BF} = R_P^{BB} = 2.0$ and we performed several simulations by varying $\bar{R}^{BB}$. The resulting energies were then fitted with a parabola in order to identify the minimum of the energy and the corresponding optimized value for $\bar{R}^{BB}$ (see Fig. 3.1).

Once we found the optimized variational parameter $\bar{R}^{BB}$, for each value of the BF interaction, we conducted similar analyses by identifying the respective optimized $\bar{R}^{BF}$ (see Fig. 3.2). The results of the optimization of the variational parameters are reported in Table 3.2 and are then used in all subsequent simulations. It should be pointed out that these analyses were conducted for the smallest closed shell studied (13 fermions + 3 bosons) and the results were then extended to the subsequent larger closed shells by

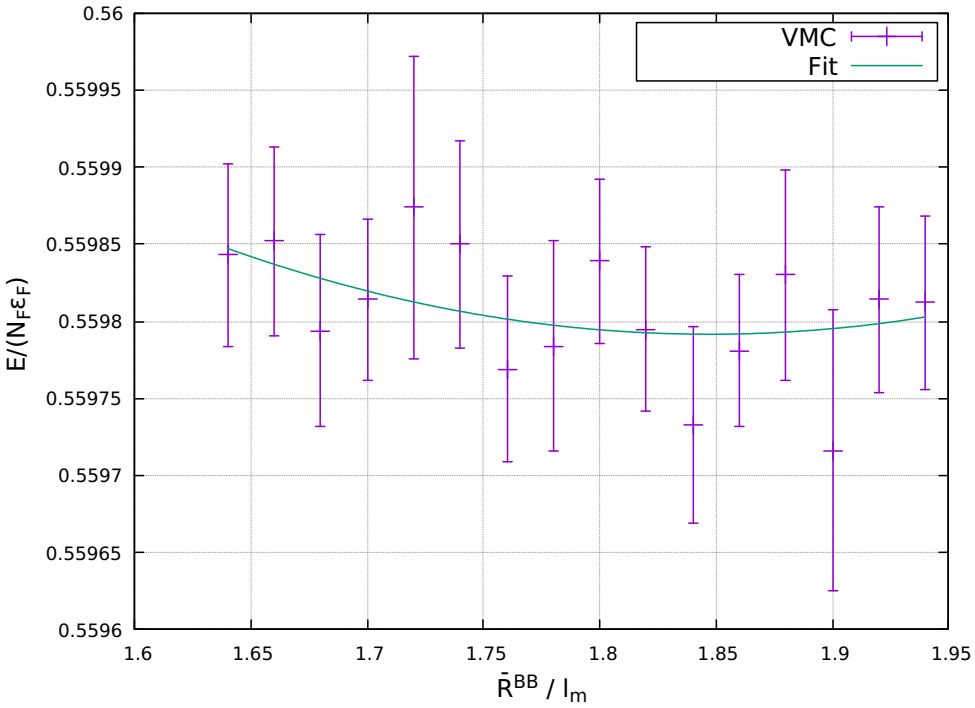

Figure 3.1: Optimization of the variational parameter $\bar{R}^{BB}$. The energy per fermion, in units of Fermi energy, is plotted with respect to the variational parameter, which is in units of the mean interparticle distance l_m. The error bars are given by the statistical error of the Monte Carlo simulations. The extrapolated optimal value for the variational parameter is $\bar{R}^{BB} = 1.85$. We notice that there is only a very mild dependence on this parameter.

implicitly assuming the independence of the variational parameters from the finite-size effects.

3.2.2 Finite-size correction

In order to study finite-size effects, for each interaction listed in Table 3.1, we consider several closed shells trying to keep a constant concentration of bosons ($x \simeq 0.238$). The allowed combinations of bosons and fermions (N_B, N_F) that we have analysed are reported in Table 3.3.

The procedure used to estimate the finite-size effects can be described as follows. First, for each fermionic closed shell, we have calculated the difference in energy per particle between a finite system of non-interacting fermions and an infinite one:

$$\Delta K = E^N_{x=0} - E^\infty_{x=0} \ ,$$

$\widetilde{R}^{BF}$	$\widetilde{R}^{BB}$	$\bar{R}^{BF}$	$\bar{R}^{BB}$
1.0×10^{-9}	1.0×10^{-3}	1.08	1.85
1.0×10^{-5}	1.0×10^{-3}	1.26	1.85
1.0×10^{-3}	1.0×10^{-3}	1.40	1.85
5.0×10^{-3}	1.0×10^{-3}	1.45	1.85
1.0×10^{-2}	1.0×10^{-3}	1.50	1.85
3.0×10^{-2}	1.0×10^{-3}	1.68	1.85
5.0×10^{-2}	1.0×10^{-3}	1.80	1.85
1.0×10^{-1}	1.0×10^{-3}	2.00	1.85
2.0×10^{-1}	1.0×10^{-3}	1.99	1.85

Table 3.2: Combinations of the optimal variational parameters for each interaction configuration. $\bar{R}^{BF}$ and $\bar{R}^{BB}$ are obtained by following the procedure described in Sec. 3.2.1. These variational parameters are expressed in units of the mean interparticle distance l_m.

N_B	N_F	x	ΔK
3	13	0.2308	-0.020501
5	21	0.2381	$+0.015582$
7	29	0.2414	-0.008034
9	37	0.2432	$+0.004321$
11	45	0.2444	$+0.003551$
12	49	0.2449	-0.002445

Table 3.3: Configurations of bosons and fermions analysed. The number of fermions is chosen in order to have closed fermionic shells. The last column represents the difference in energy per particle between a finite system of non-interacting fermions (with N_F fermions) and an infinite one. This difference ΔK typically decreases as N_F grows, however with oscillations.

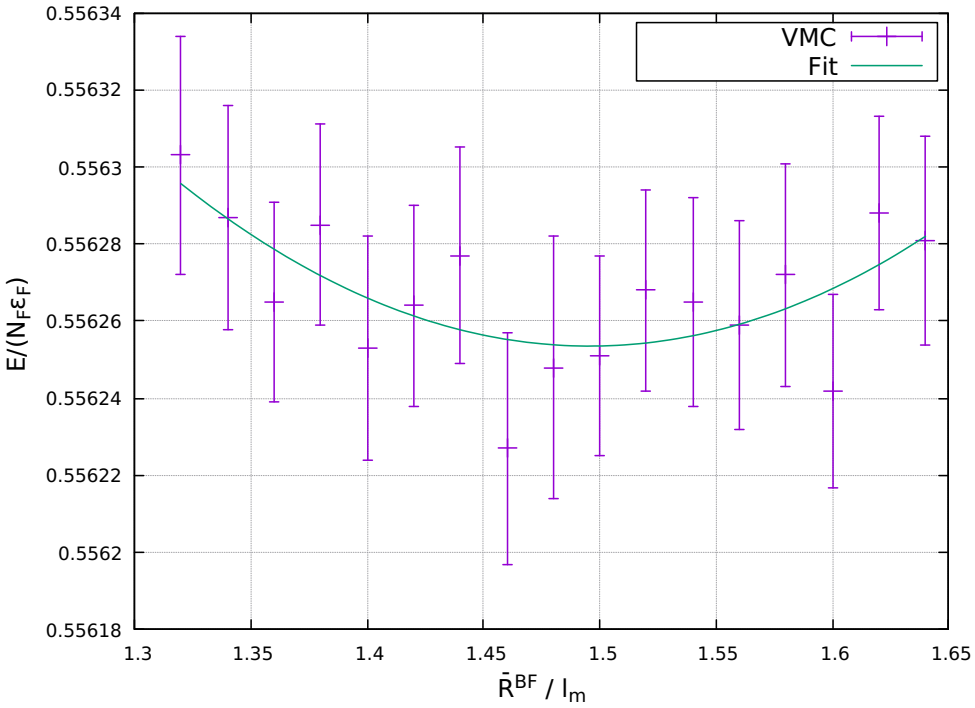

Figure 3.2: Example of optimization of the variational parameter $\bar{R}^{BF}$ for the interaction configuration $\widetilde{R}^{BF} = 0.01$ and $\widetilde{R}^{BB} = 0.001$. The energy per fermion, in units of Fermi energy, is plotted with respect to the variational parameter, which is in units of the mean interparticle distance l_m. The error bars are given by the statistical error of the Monte Carlo simulations. The extrapolated optimal value for the variational parameter is $\bar{R}^{BF} = 1.50$.

where $E^N_{x=0}$ is obtained from preliminary VMC simulations and $E^\infty_{x=0}$ is the energy per particle in the thermodynamic limit, which, in two dimensions, is given by $\varepsilon_F/2$. ΔK (see Tab. 3.3) can then be interpreted as the finite-size correction in case of a non-interacting fermionic system. Our first attempt at reducing finite-size effects was to use ΔK as a finite-size correction also for the interacting Bose-Fermi mixture. However, this choice turned out not to be a valid solution, since ΔK is a good approximation only for weakly interacting systems. We therefore decided to introduce a multiplicative factor b in front of ΔK (following [74]), which depends on the interactions. Thus, we assume that the energy per fermion of the finite B-F mixture is given by:

$$E^N_{QMC} = E^\infty - b\,\Delta K \ ,$$

where E^∞ is the energy per fermion in the thermodynamic limit for a fixed value of boson concentration x. Although in our simulations we try to keep x constant, as the

number of fermions grows, considering the constraints imposed by the closed shells, the concentration of bosons will slightly increase (See Table 3.3). This leads to an increase in the interaction energy, as it depends on the number of bosons present in the mixture. This dependence on boson concentration must be somehow introduced in the previous formula if we want to compare the VMC results obtained for different closed shells. This can be done by treating E^{∞} as the sum of two terms:

$$E^{\infty} = E^{\infty}_{x=0} + c\,x\ .$$

The first term in the sum is x-independent and it is again the energy per particle for a non-interacting fermionic system in the thermodynamic limit, the second instead contains the interaction part and it is proportional to the boson concentration by the constant c. We can then replace this expression for E^{∞} in the equation above, obtaining:

$$E^{N}_{QMC} = E^{\infty}_{x=0} + c\,x - b\,\Delta K\ . \tag{3.13}$$

Parameters b and c can be estimated, for each interaction, by performing several simulations for all the studied closed shells and by fitting the resulting energies per fermion with Eq. (3.13). This is a two-dimensional fit, in terms of x and ΔK. The parameter b can then be used for the finite-size correction of the QMC simulations (see Fig. 3.3), meanwhile c can be used as a further check of the correctness of the results. In particular, the finite-size error can be taken into account by adding the term $b\,\Delta K$:

$$E^{N\,(C)}_{QMC} = E^{N}_{QMC} + b\,\Delta K\ . \tag{3.14}$$

The error on parameter b obtained from the fit, multiplied by ΔK, will then be added to the statistical uncertainty of the QMC simulations.

This apparently heuristic method for the estimation of the finite-size effects can be justified from a theoretical point of view. The procedure implemented above is just a particular application of a more general method developed by Kwon, Ceperley and Martin [75], which relies on the identification of the fermions present in the mixture with a Fermi liquid. The authors of the previous paper show also that the b parameter that we have estimated corresponds to the inverse of the effective mass. Without going into details of Fermi liquid theory, which is not the purpose of this thesis, we limit ourselves to reporting in Tab. 3.4 the resulting values of b.

3.3 DMC simulations

The DMC simulations were conducted for the same interactions already considered with VMC. The energies resulting from the VMC simulations, together with the final positions of the walkers, were used to fix the reference energies E_{ref} and the initial positions of the walkers, respectively.

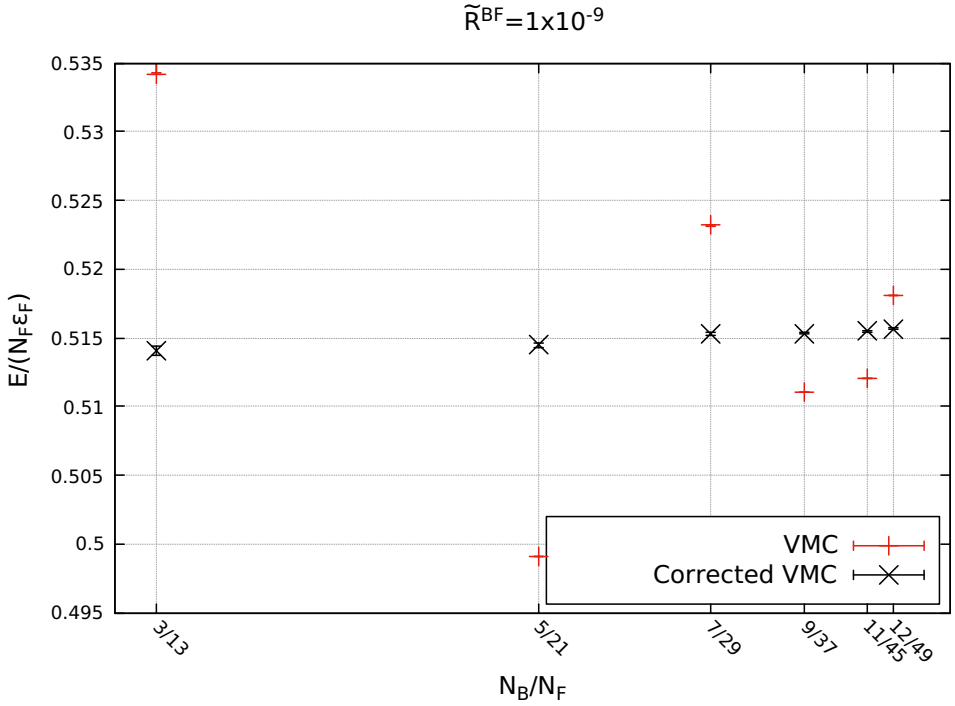

Figure 3.3: Effects of the finite-size correction, described in Sec. 3.2.2, on VMC results for a particular value of the interaction. The energy per fermion, in unit of the Fermi energy, is plotted with respect to the boson concentration $x = N_B/N_F$. The finite-size correction becomes smaller and smaller as we analyse larger and larger closed shells. Notice that the finite-size corrected results display an expected linear dependence on the concentration.

Also in this case, before obtaining the final results shown in Section 3.4, several preliminary analyses must be conducted. First of all, we choose as our trial wavefunction the previous optimized Jastrow-Slater function. This is clearly an advantage of having run VMC simulations first. Secondly, we exploit the results for the finite-size effects, obtained from the Variational Monte Carlo, also for the DMC method. It must be underlined that, in principle, one would have to perform again the same finite-size analyses, described in Section 3.2.2, also for the DMC as they could give slightly different results. In practice, since DMC simulations are much more computationally expensive than VMC, we simply assumed that the finite-size effects are not affected by the type of QMC algorithm used. Furthermore, as we have seen in the previous chapter, DMC depends on the time step ($d\tau$) used in the simulations. Consequently, a time-step analysis must be performed to understand how a non-zero $d\tau$ affects our simulations.

$\widetilde{R}^{BF}$	g_{BF}	$\widetilde{R}^{BB}$	b
1.0×10^{-9}	0.0493	1.0×10^{-3}	0.983 ± 0.013
1.0×10^{-5}	0.0904	1.0×10^{-3}	0.982 ± 0.014
1.0×10^{-3}	0.1550	1.0×10^{-3}	0.978 ± 0.014
5.0×10^{-3}	0.2065	1.0×10^{-3}	0.974 ± 0.015
1.0×10^{-2}	0.2410	1.0×10^{-3}	0.971 ± 0.015
3.0×10^{-2}	0.3278	1.0×10^{-3}	0.962 ± 0.014
5.0×10^{-2}	0.3938	1.0×10^{-3}	0.948 ± 0.015
1.0×10^{-1}	0.5417	1.0×10^{-3}	0.917 ± 0.012
2.0×10^{-1}	0.8673	1.0×10^{-3}	0.853 ± 0.016

Table 3.4: Resulting values of b obtained following the procedure described in Sec. 3.2.2. This parameter, according to Refs. [75, 74], corresponds to the inverse of the Fermi liquid effective mass.

3.3.1 Evidence of clustering

During our DMC simulations we experienced some issues regarding the block analysis (see Section 2.3.3 and Appendix A). In particular, we have found that for high BF interactions, even if we performed longer and longer simulations, the correlation lengths were much bigger than the maximum block lengths assumed. Also, by plotting the resulting energies per particle with respect to the MC iterations, we have observed large fluctuations even at the end of the simulations, a behavior that typically occurs when the transient is not yet concluded. These issues could be interpreted in two different ways. One possibility, more technical in nature, could be that the simulations were not long enough. The second option, instead, could be related to some lack of knowledge regarding our physical system. The first hypothesis was immediately discarded: we performed simulations ten times longer than those with low interaction finding the same problem. We then conjectured that, for strong BF repulsion, bosons are affected by an effective attractive interaction, thus forming bosonic clusters within the mixture. In this way, the Bose-Fermi mixture loses its homogeneity and can no longer be efficiently simulated with a Jastrow-Slater function, which is unable to describe the presence of bosonic clusters.

In order to prove the correctness of this conjecture, we decided to perform a qualitative study of the pair distribution function for bosons. The pair distribution function $g_{\sigma,\sigma'}(\boldsymbol{r}, \boldsymbol{r}')$ is proportional to the probability density of finding a σ particle at position $\boldsymbol{r}$ when a σ' particle is at position $\boldsymbol{r}'$. For a translationally invariant and isotropic fluid, as in our case, the pair distribution function depends just on the relative distance $|\boldsymbol{r} - \boldsymbol{r}'|$. One can then set $\boldsymbol{r}' = 0$, and introduce the shorter notation $g_{\sigma,\sigma'}(r) \equiv g_{\sigma,\sigma'}(\boldsymbol{r}, \boldsymbol{r}' = 0)$.

In the second quantization formalism one has (see e.g [76]))

$$g_{\sigma,\sigma'}(r) = \frac{\langle \hat{\Psi}^\dagger_\sigma(\boldsymbol{r})\hat{\Psi}^\dagger_{\sigma'}(0)\hat{\Psi}_{\sigma'}(0)\hat{\Psi}_\sigma(\boldsymbol{r})\rangle}{n_\sigma n_{\sigma'}} \,, \tag{3.15}$$

where $\hat{\psi}^\dagger_\sigma(\boldsymbol{r})$ is the field operator creating a σ particle at position $\boldsymbol{r}$, while n_σ and $n_{\sigma'}$ are the number densities of σ and σ' particles, respectively. Here, we focus on the boson-boson pair distribution function $g_{B,B}(r)$. The BB repulsion will suppress the probability of finding two bosons close to each other, so we expect $g_{B,B}(r)$ to be small at short distances. By increasing the distance, the probability density will increase until it will reach a plateau value (which, due to the normalization in Eq. (3.15), is 1 in the thermodynamic limit, and $1 - 1/N_B$ for a finite-size system: in our case with $N_B = 12$ the plateau value is ≈ 0.92). However, if the BF repulsion is strong enough to introduce an effective attraction between the bosons, what is expected is that a maximum in the probability density will occur for some intermediate distance, and then decrease to a plateau value for $r \to \infty$. The pair distribution function for bosons can be calculated with both VMC and DMC algorithms (we refer again to Refs. [68] and [76]). So we analysed $g_{B,B}(r)$ for all the interaction configurations, using both VMC and DMC methods (we performed our simulations for the biggest closed shell studied, i.e., 12 bosons plus 49 fermions). The main results are shown in Figs. 3.4, 3.5.

Looking at the Figures 3.4 and 3.5, what emerges is that in the DMC results we observe the typical behaviour that occurs following the formation, from a certain BF interaction onwards, of bosonic clusters. Instead, in the VMC results, this behaviour is not so evident. This diversity is due to the different nature of the two algorithms. VMC simulations cannot yield more physical information than what is already present in the trial wavefunction, so if the bosonic clusters are not included in the trial wavefunction, they will not even be present in the observables. This is reflected only in a small variation of the pair distribution function with respect to the case of a homogeneous system. The situation is different in the DMC algorithm where a real physical evolution is carried out as a function of the imaginary time. In this case, the system will evolve towards the true ground state containing the bosonic clusters regardless of the chosen trial wavefunction, thus explaining the peculiar behavior of $g_{B,B}(r)$. However, the diffusion-branching process of the DMC is highly influenced by the chosen trial wavefunction. In fact, if it is very different from the true ground state, the sampling will be carried out in sparsely populated areas of the configuration space, resulting in energy peaks that compromise the convergence of the energy.

Thus, thanks to this qualitative analysis, we can say that, for sufficiently strong BF repulsion (see Figs. 3.5e, 3.5f), bosonic clusters occur even if there is a repulsive interaction between bosons and between bosons and fermions. The Bose-Fermi mixture then loses its homogeneity and a new trial wavefunction is needed if we want to study the cases $\widetilde{R}^{BF} = 0.1$ and $\widetilde{R}^{BF} = 0.2$ which correspond to $g_{BF} = 0.5417$ and $g_{BF} = 0.8673$, respectively. We therefore limited our DMC simulations only to cases where $\widetilde{R}^{BF} \leq 0.05$.

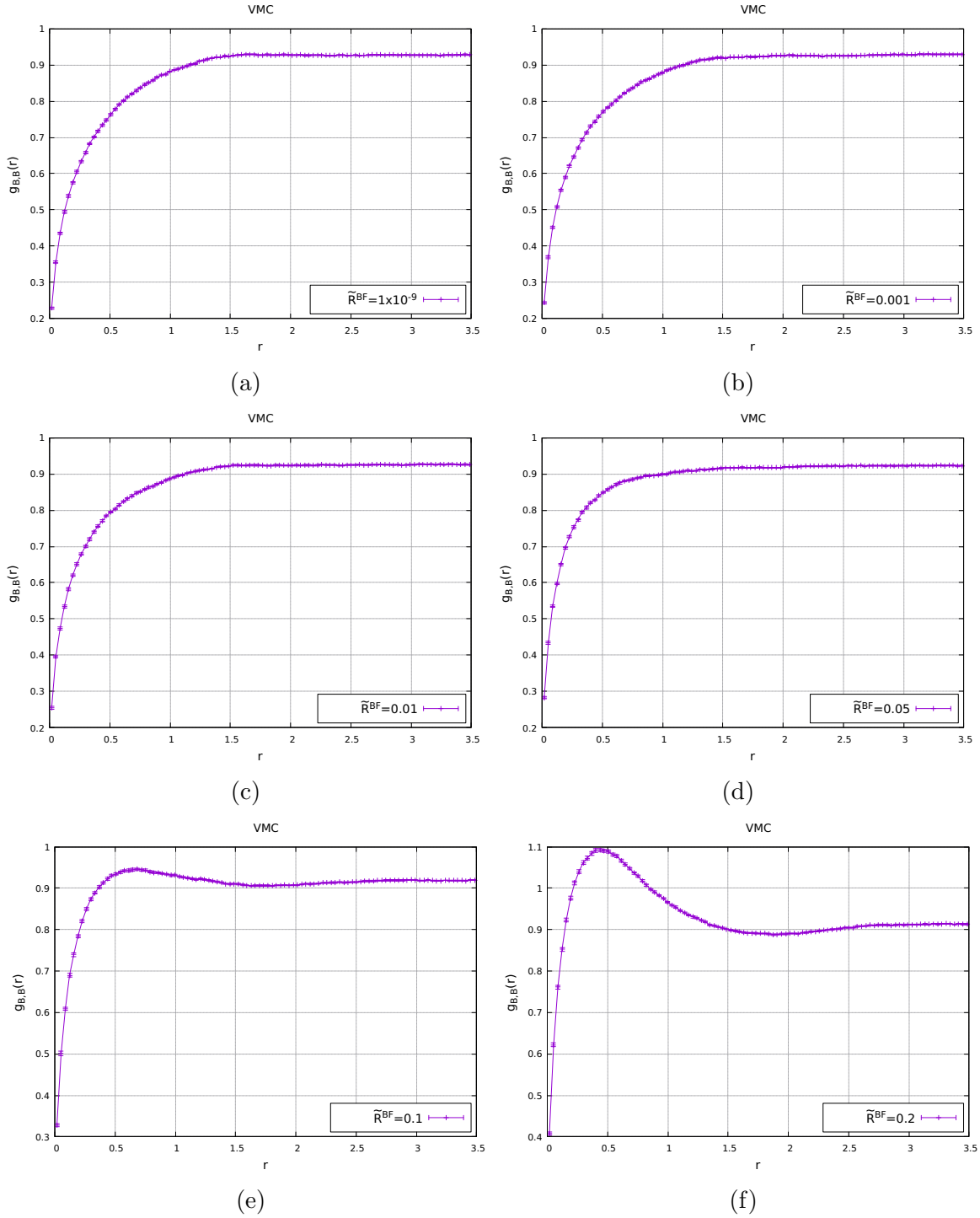

Figure 3.4: VMC results of $g_{B,B}(r)$, varying the BF interaction, for the biggest closed shell studied (12B + 49F).

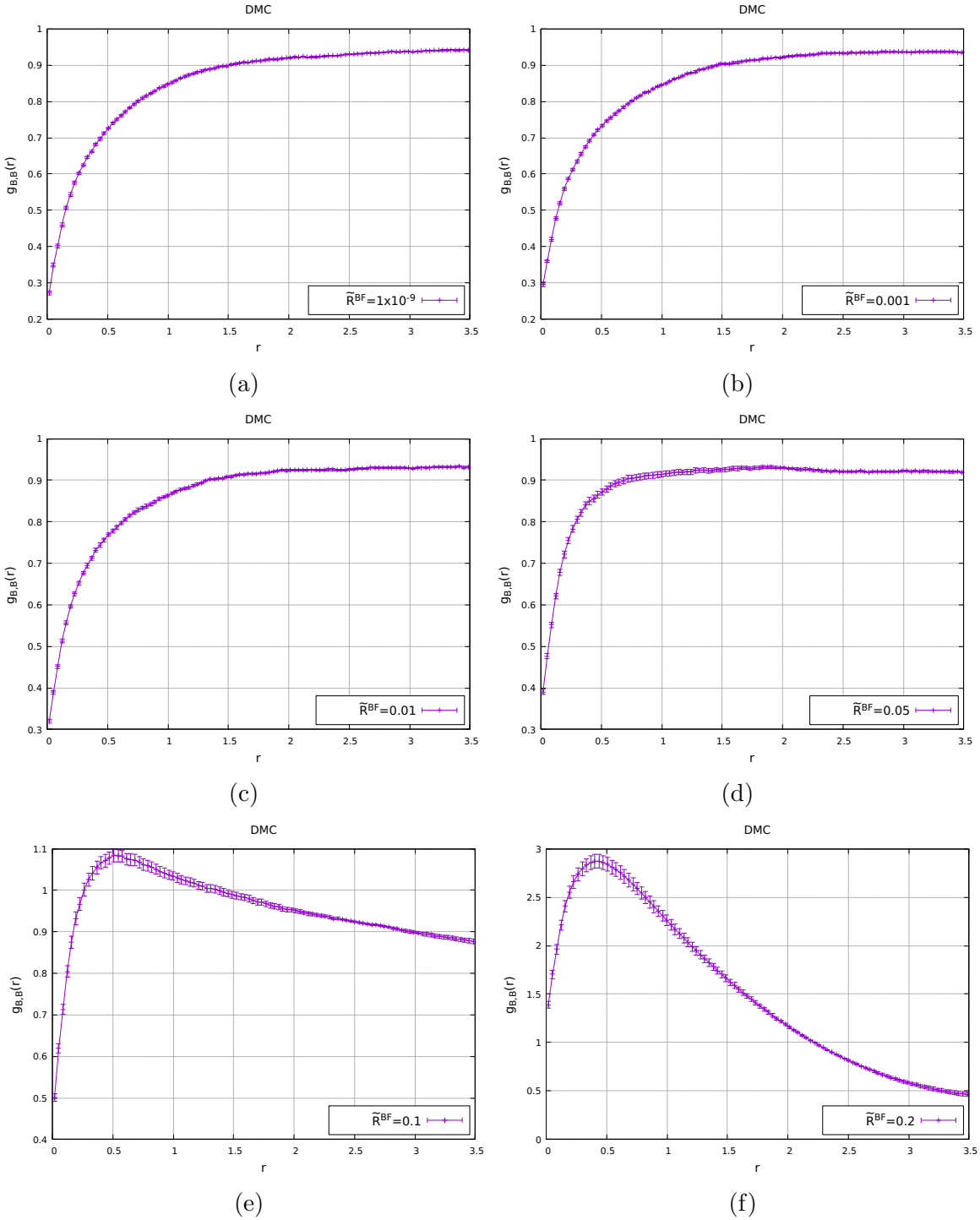

Figure 3.5: DMC results of $g_{B,B}(r)$, varying the BF interaction, for the biggest closed shell studied (12B + 49F).

It is worth stressing that, based on the limited data we have, we cannot assert the presence of a phase transition between the "homogeneous phase" and the "clustered" one. In particular, if such phase transition exists, we have not properly characterized what type it is. Of course, further analyses are required, especially in the intermediate interaction region ($0.05 < \widetilde{R}^{BF} < 0.1$).

3.3.2 Time-step analysis and systematic errors

In Section 2.5 we have described the main ideas and approximations behind the DMC method. We have seen that, in order to obtain an explicit form for the total Green's function, we have to use the small-time approximation. Thus, in principle, if one wants more and more accurate results, the time step $d\tau$ must be reduced. However, by reducing the time step, the duration of the simulation increases as well as the computational resources required. The choice of the time step is therefore a matter of fundamental importance in the implementation of DMC simulations. Furthermore, an analysis on the systematic effects caused by the choice of a finite time step must be conducted.

What is usually done in the context of the DMC method is to perform a time-step analysis, in the sense that, once the interaction configuration and the closed shell have been fixed, one performs several simulations for a sequence of decreasing values of $d\tau$. Then, the resulting energies are fitted with a linear function in order to extrapolate the corrected value for null time step. The error obtained from the fit on the extrapolated result is then added to the statistical uncertainty of the DMC algorithm as a systematic time-step error. Of course, this analysis is very expensive from a computational point of view, since several DMC simulations are required for a single interaction configuration. For this reason, we decided to analyse only the lowest ($\widetilde{R}^{BF} = 1.0 \times 10^{-9}$, $g_{BF} = 0.0493$) and the highest ($\widetilde{R}^{BF} = 0.05$, $g_{BF} = 0.3938$) interaction configurations. The results of the time-step analyses are shown in the Figures 3.6 and 3.7.

For the intermediate interaction configurations, where a time-step analysis has not been carried out, the contribution due to the finite $d\tau$ must be estimated. Thus, we set an intermediate time step ($d\tau = 0.012$) that would provide a good compromise between accuracy of the results and duration of the simulations. Then we compared the DMC results for time step $d\tau = 0.012$ of the lowest interaction configuration ($g_{BF} = 0.0493$) and of the highest interaction configuration ($g_{BF} = 0.3938$) with their respective extrapolated results from the time-step analysis. We used these two discrepancies as boundaries of the corrections for finite time step. At this point, exploiting the fact that the DMC energies depend linearly on the time step (see Refs. [68, 58]), we estimated, through a linear interpolation process, the finite time-step correction for each intermediate interaction value g_{BF}. Then, looking at the effect of the time-step extrapolation for the lowest and the highest interaction configurations (see Figs. 3.6 and 3.7), which consists in a shift towards higher energy values, we decided to sum the finite step correction to the DMC results. As finite step error, to be added to the QMC statistical uncertainty

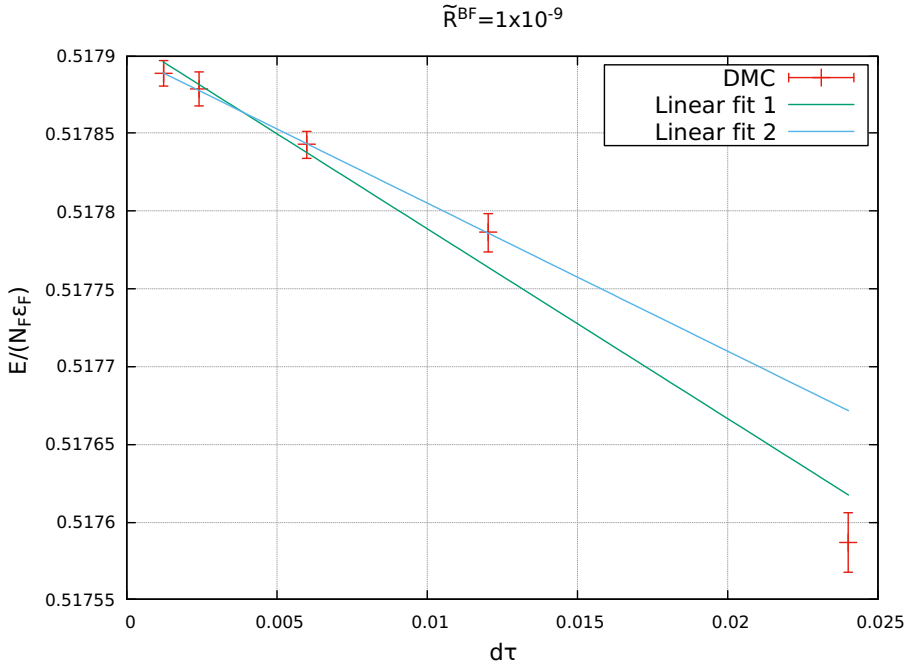

Figure 3.6: Time-step analysis for the biggest closed shell studied (12B + 49B). The time step is measured in units of $\hbar/\varepsilon_F$. Fit number 1 was obtained by considering all time-step points, fit number 2, instead, by excluding the highest time-step point. The extrapolated values of the energy per fermion from fit 1 and fit 2, in units of ε_F, as $d\tau \to 0$ are given by 0.517911 ± 0.000010 and 0.517900 ± 0.000001, respectively. These values must then be adjusted with the finite-size correction. The error bars are given by the statistical uncertainty of DMC simulations.

and the finite-size error, we assigned arbitrarily half of the finite step correction.

During our DMC simulations, we introduced an energy cutoff in the algorithm, in order to control and simplify the diffusion-branching process, thus avoiding energy peaks that slow down the convergence to a precise value of energy. This cutoff is of the form $\Delta E = c/\sqrt{d\tau}$, where ΔE is the maximum allowed difference between the sampled local energy and a reference energy which we take as the result of a converged VMC simulation, and c is a free parameter. This modification of the algorithm implies, according to Ref. [77], the introduction of a systematic bias that must be appropriately estimated in order to have consistent and precise results. A possible way to estimate this error, once a time step, a closed shell and an interaction configuration are fixed, is to perform several simulations varying the cutoff factor and then extrapolate the energy value for cutoff $\to \infty$ (absence of cutoff). However, studying how the cutoff acts in the DMC algorithm allowed us to understand that this systematic bias introduced is actually already contained within the finite time-step error. Going into details, the energy peaks

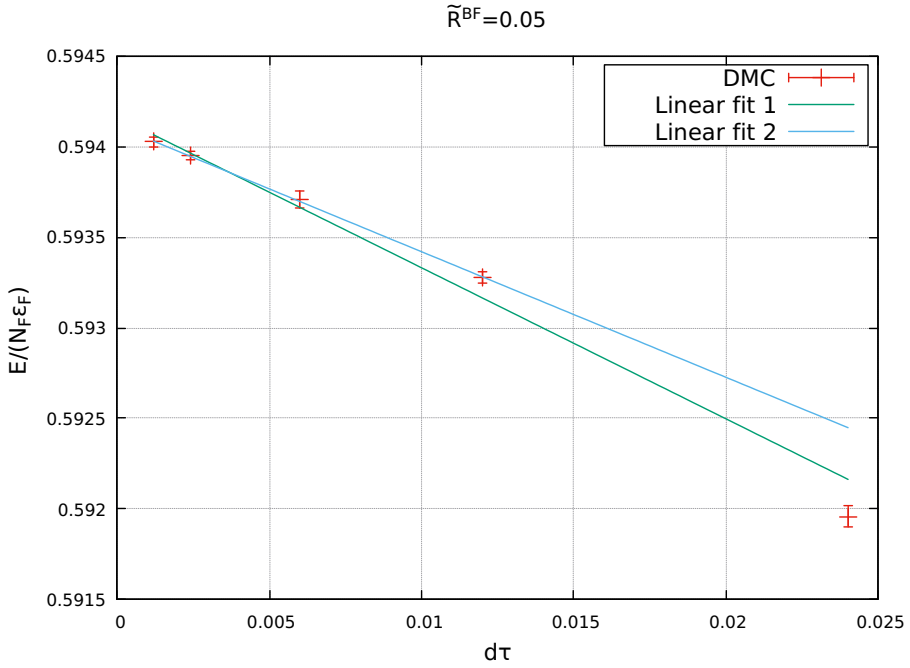

Figure 3.7: Time-step analysis for the biggest closed shell studied (12B+49B). The time step is measured in units of $\hbar/\varepsilon_F$. Fit number 1 was obtained by considering all time-step points, fit number 2, instead, by excluding the highest time-step point. We considered fit number 2 because it best represents small time-step points. The extrapolated values of the energy per fermion from fit 1 and fit 2, in units of ε_F, as $d\tau \to 0$ are given by 0.594164 ± 0.000062 and 0.594112 ± 0.000004, respectively. These values must then be adjusted with the finite-size correction. The error bars are given by the statistical uncertainty of DMC simulations.

suppressed by the cutoff occur when the sampling is done near the nodal surface or in sparsely populated areas of the configuration space. It is therefore the task of the drift force (see Sec. 2.5.4) to move away the sampling from these regions. The time step, instead, regulates the step of MC moves. However, the drift force acts only at the end of the MC step, thus, if one chooses a large time step it could arrive near the nodal surface (generating a peak in the energy value) and only at the end of the move it is pushed back by the drift force. Then, by choosing an ever smaller time step we reduce the width of the MC step so that the repeated action of the drift force will not bring the sampling close to the nodal surface, avoiding the generation of energy peaks (i.e., avoiding the action of the introduced cutoff). Moreover, the cutoff scales as $d\tau^{-1/2}$. For these reasons, it is clear that if we perform the $d\tau \to 0$ extrapolation, described in the previous section, the systematic error due to the cutoff will be null. The case of intermediate interaction configurations, where time-step analyses were not conducted, is different. We did not

perform a cutoff analysis such that described above, thus we are not able to estimate this systematic error. However we understand that this systematic bias is included in the finite time-step error.

Given the sizeable role of the finite time-step bias at the chosen time-step for intermediate interactions, a full time-step analysis will be needed in future work to more accurately determine the equation of state.

3.4 Final results

In this Section we compare the final results of the VMC and DMC simulations with analytic predictions. We focus our attention on the second order perturbative correction in the coupling parameter g_{BF}.

3.4.1 Perturbative predictions

A perturbative calculation for the energy of a two-dimensional Bose-Fermi mixture to second order in the coupling parameter g_{BF} is available from a previous master thesis' work [8], yielding for the energy density the expression:

$$\frac{E}{V} = -\frac{k_F^2 n_B}{4m_R \log(k_F a_{BF})}\left[1 - \frac{1}{2\log(k_F a_{BF})}\left(\frac{w+1}{w-1}\log w + \log\left(\frac{w}{(w+1)^2}\right) - 1\right)\right] + \frac{k_F^2}{2m_F}\frac{n_F}{2} + \mathcal{E}_B \,, \tag{3.16}$$

where m_R is the reduced mass of the system, $w = m_B/m_F$ is the mass ratio and we have set $\hbar = 1$. The term $\mathcal{E}_B$ is the energy density of the boson component in the absence of coupling with the fermion component, i.e., for $g_{BF} = 0$. Equation (3.16) was obtained in [8] by assuming the coupling parameters g_{BF} and g_{BB} to be both small, neglecting terms of order higher than two in g_{BF}, g_{BB}, or their combinations. Under this assumption, terms involving simultaneously g_{BF} and g_{BB} do not contribute. An accurate perturbative expansion for $\mathcal{E}_B$ has been obtained in [78], and verified with QMC calculations shortly after [79]. Here, since in our simulations the boson-boson parameter g_{BB} has been kept fixed to a very small value, it will be sufficient to retain the lowest order expression for $\mathcal{E}_B$, namely

$$\mathcal{E}_B = -\frac{2\pi n_B^2}{m_B \log\left(n_B a_{BB}^2\right)} \,. \tag{3.17}$$

The novelty of Eq. (3.16) lies however in the second order perturbative term in the BF coupling parameter, which we will check against our QMC simulations.

In our Bose-Fermi mixture, we assumed that the mass of the bosons (m_B) was equal to that of the fermions (m_F), so that the mass ratio (w) simplifies to one and the reduced mass becomes $m_R = m_B/2 = m_F/2$. Thus, taking the $w \to 1$ limit, Eq. (3.16), together with Eq. (3.17), becomes:

$$\frac{E}{V} = -\frac{k_F^2 n_B}{4\frac{m_F}{2}\log(k_F a_{BF})}\left[1 - \frac{(1-\log 4)}{2\log(k_F a_{BF})}\right] - \frac{2\pi n_B^2}{m_B \log\left(n_B a_{BB}^2\right)} + \frac{k_F^2}{2m_F}\frac{n_F}{2}\,. \tag{3.18}$$

We now want to compare the theoretical predictions with the QMC results. To do this, it is necessary to rewrite the previous formula in order to obtain an energy per fermion in units of ε_F.
We then multiply the above energy density for $(n_F\varepsilon_F)^{-1}$, obtaining:

$$\frac{E}{N_F\varepsilon_F} = \frac{E}{V}\cdot\frac{1}{n_F\varepsilon_F} = -\frac{x}{\log(k_F a_{BF})}\left[1 - \frac{1-\log 4}{2\log(k_F a_{BF})}\right] - \frac{x^2}{\log(n_B a_{BB}^2)} + \frac{1}{2}\,, \tag{3.19}$$

where we have introduced the boson concentration $x = n_B/n_F$ and we used $\varepsilon_F = \frac{\hbar^2 k_F^2}{2m_F}$ (with $\hbar = 1$) and the fact that in two dimensions $k_F = \sqrt{4\pi n_F}$. Eq. (3.19) can be expressed in terms of the coupling parameters g_{BF} and g_{BB} introduced in Sec. 3.1 :

$$\frac{E}{N_F\varepsilon_F} = x\, g_{BF}\left[1 + g_{BF}\frac{1-\log 4}{2}\right] + x^2 g_{BB} + \frac{1}{2}\,, \tag{3.20}$$

where the second order perturbative correction in terms of g_{BF} is given by

$$\frac{\Delta E}{N_F\varepsilon_F} = x\, g_{BF}^2\frac{1-\log 4}{2}\,. \tag{3.21}$$

It is also useful to express Eq. (3.19) in terms of the MC input parameters. Using the expressions obtained in Appendix D, we have that

$$\frac{E}{N_F\varepsilon_F} = -\frac{x}{\frac{1}{2}\log\left[4\pi\left(\frac{\widetilde{R}^{BF}}{R_P^{BF}}\right)^2\right]}\left[1 - \frac{1-\log 4}{\log\left[4\pi\left(\frac{\widetilde{R}^{BF}}{R_P^{BF}}\right)^2\right]}\right] - \frac{x^2}{\log\left[x\left(\frac{\widetilde{R}^{BB}}{R_P^{BB}}\right)^2\right]} + \frac{1}{2}\,. \tag{3.22}$$

3.4.2 Comparison between analytic and QMC results

We now compare the results of VMC and DMC with the analytic prediction expressed by Eq. (3.19). Once the biggest closed shell studied has been chosen (12B + 49F), thus fixing the boson concentration in the mixture ($x = 12/49$), several QMC simulations were performed varying the BF repulsive interaction. In particular, we fixed the BB repulsive interaction by setting $\widetilde{R}^{BB} = 1.0 \times 10^{-3}$ and $R_P^{BB} = 2.0$ corresponding to $g_{BB} = 0.0594$.

We set $R_P^{BF} = 2.0$ and we allowed $\widetilde{R}^{BF}$ to vary, thus fixing the structure of the potential (soft disk potential) but changing the magnitude of the interaction. This corresponds, in terms of the coupling parameter, to varying g_{BF} according to the values reported in Tab. 3.1. The comparison between theoretical and QMC results is then shown in Fig. 3.8 and in Tables 3.5, 3.6.

From Figure 3.8 it appears that the QMC results are in agreement with theoretical predictions for $g_{BF} < 0.4$. In particular, for $g_{BF} < 0.3$, DMC and VMC results differ slightly while for greater BF interactions the two algorithms give different results. However the energy scale is too large to allow us to accurately compare the results. Furthermore, we are mainly interested in the second order perturbative correction in g_{BF}. Thus, in Fig. 3.9 and in Tables 3.7, 3.8, we compare Eq. (3.21) with the corresponding QMC results.

From Table 3.7 one can see that VMC results are in agreement with the perturbative predictions only for the first point with lower interaction. In particular, for $g_{BF} > 0.05$, one can see that the VMC results are no longer compatible with either the DMC results or the perturbative predictions. This is because the trial wavefunction ψ_T is just an approximation to the exact ground state wavefunction. It is however reassuring that the VMC provides higher values than the others, being an upper bound of the ground state energy. The agreement between the DMC results and the theoretical predictions extends instead up to $g_{BF} \simeq 0.3278$. At the interaction point $g_{BF} = 0.3938$ the three different results are all in disagreement. The most reliable result is the one provided by the DMC, which we have also seen to be an upper bound of the true energy. This makes sense, considering that the value of the BF coupling parameter is relatively large to expect the perturbative approach to be valid. For $g_{BF} > 0.5$, we are unable to make definite conclusions on the accuracy of the DMC results, due to the convergence problems related to apparent clustering of bosons, as we discussed in Sec. 3.3.1. In this regime of strong repulsion, we also expect that the details of the chosen model potential start to matter, and a future analysis will be needed to understand the universality of our DMC results close to the phase separation transition.

g_{BF}	VMC	Corrected VMC	Prediction
0.0493	0.518079(13)	0.515675(46)	0.515570
0.0904	0.528081(17)	0.525681(52)	0.525363
0.1550	0.543558(48)	0.541166(81)	0.540434
0.2065	0.555619(24)	0.553237(61)	0.552165
0.2410	0.563501(27)	0.561126(64)	0.559884
0.3278	0.582602(34)	0.580249(67)	0.578806
0.3938	0.596258(34)	0.593941(72)	0.592716
0.5417	0.623620(42)	0.621378(71)	0.622392
0.8673	0.670372(67)	0.668287(106)	0.680431

Table 3.5: Resulting values of energy per fermion, in units of ε_F, obtained with VMC method. In the third column the effects of the finite size correction (see Sec. 3.2.2) have been considered.

g_{BF}	DMC	Extracted DMC	Corrected DMC	Prediction
0.0493	0.517786(15)	0.515506(43)	0.515506(110)	0.515570
0.0904	0.527492(22)	–	0.525296(160)	0.525363
0.1550	0.542478(29)	–	0.540422(230)	0.540434
0.2065	0.554133(34)	–	0.552192(292)	0.552165
0.2410	0.561656(33)	–	0.559793(326)	0.559884
0.3278	0.580120(38)	–	0.578459(417)	0.578806
0.3938	0.593278(38)	0.591794(47)	0.591794(493)	0.592716

Table 3.6: Resulting values of energy per fermion, in units of ε_F, obtained with DMC method. In the second and third columns the effects of the finite size correction (see Sec. 3.2.2) and of the finite time-step correction (see Sec. 3.3.2) have been considered. In particular, in the second column a full time-step analysis was conducted, while in the third, the finite time-step correction was obtained through a linear interpolation process (see again Sec. 3.3.2).

g_{BF}	VMC	Corrected VMC	Prediction
0.0493	+0.002394(13)	−0.000010(46)	−0.000115
0.0904	+0.002331(17)	−0.000069(52)	−0.000387
0.1550	+0.001988(48)	−0.000404(81)	−0.001136
0.2065	+0.001437(24)	−0.000945(61)	−0.002017
0.2410	+0.000870(27)	−0.001505(64)	−0.002747
0.3278	−0.001287(34)	−0.003640(67)	−0.005082
0.3938	−0.003794(34)	−0.006111(72)	−0.007335
0.5417	−0.012652(42)	−0.014894(71)	−0.013880
0.8673	−0.045639(67)	−0.047724(106)	−0.035581

Table 3.7: Resulting values of the second order perturbative correction ΔE (per fermion), in units of ε_F, obtained with VMC method. In the third column the effects of the finite size correction (see Sec. 3.2.2) have been considered.

g_{BF}	DMC	Extracted DMC	Corrected DMC	Prediction
0.0493	+0.002102(15)	−0.000179(43)	−0.000179(110)	−0.000115
0.0904	+0.001742(22)	–	−0.000454(160)	−0.000387
0.1550	+0.000907(29)	–	−0.001148(230)	−0.001136
0.2065	−0.000050(34)	–	−0.001990(292)	−0.002017
0.2410	−0.000976(33)	–	−0.002838(326)	−0.002747
0.3278	−0.003769(38)	–	−0.005430(417)	−0.005082
0.3938	−0.006774(38)	−0.008258(47)	−0.008258(493)	−0.007335

Table 3.8: Resulting values of the second order perturbative correction ΔE (per fermion), in units of ε_F, obtained with DMC method. In the second and third columns the effects of the finite size correction (see Sec. 3.2.2) and of the finite time-step correction (see Sec. 3.3.2) have been considered. In particular, in the second column a full time-step analysis was conducted, while in the third, the finite time-step correction was obtained through a linear interpolation process (see again Sec. 3.3.2).

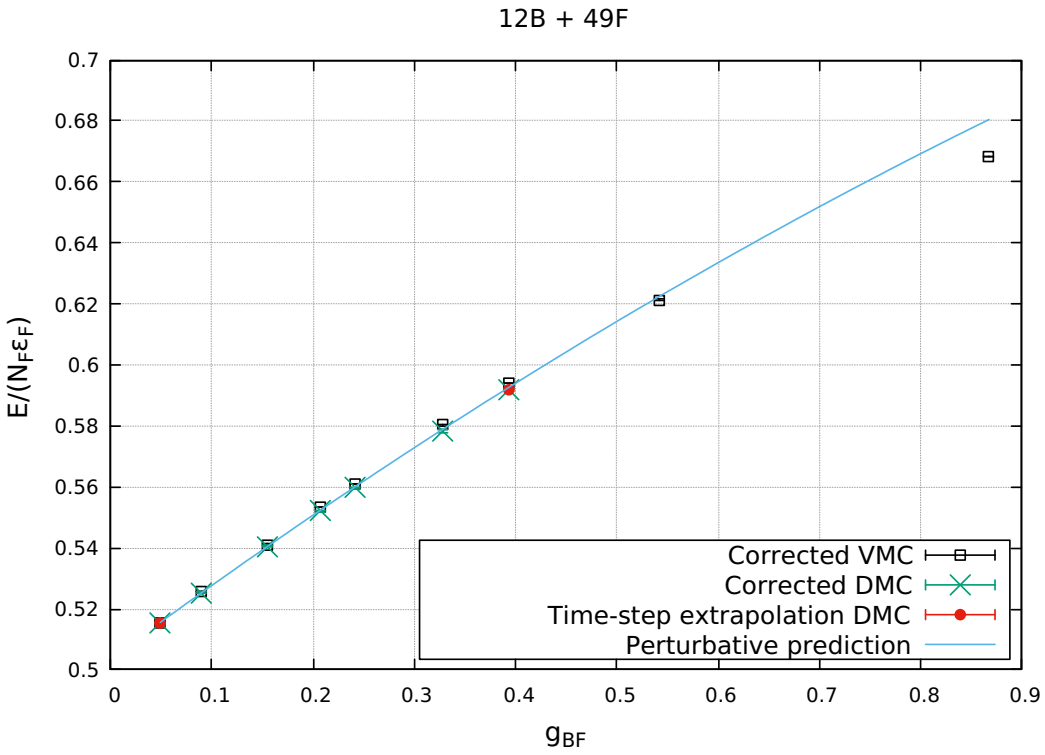

Figure 3.8: Comparison between theoretical and QMC results. The energy per fermion, in units of ε_F, is expressed as a function of the coupling parameter g_{BF}, introduced in Sec. 3.1. Errorbars are smaller than symbol size. VMC results (black squares) are adjusted with finite-size corrections described in Sec. 3.2.2. The respective errors are the sum of the statistical fluctuations of VMC algorithm and of the finite-size errors. DMC results (green crosses) are adjusted with finite-size corrections and finite time-step corrections (see Sec. 3.3.2). The respective errors contain also the finite time-step contribution. The DMC results (red circles) differ from the green ones because an exhaustive time-step analysis is conducted. In this case the DMC points are given by the $d\tau \to 0$ extrapolated results and only the finite-size correction is performed. The respective errors are obtained in a similar way to the green case, but this time the time-step uncertainties are given by the errors on the fit of the extrapolated results. For $g_{BF} > 0.4$, DMC simulations cannot be conducted (see Sec. 3.3.1).

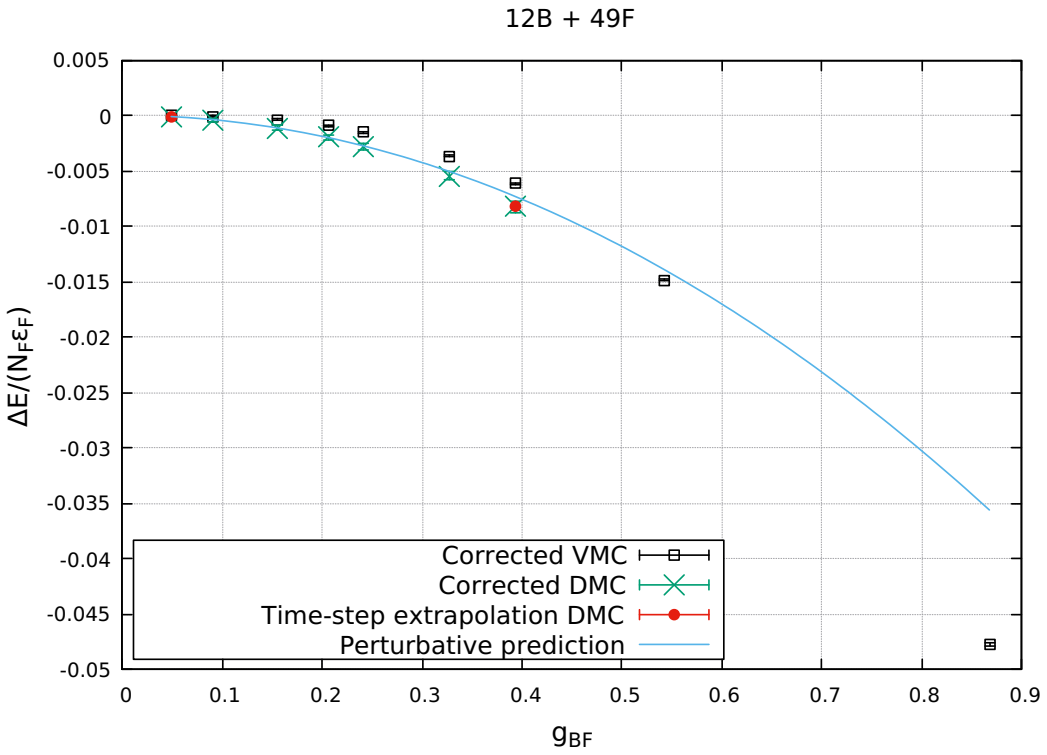

Figure 3.9: Comparison between theoretical and QMC results. The second order perturbative correction ΔE (per fermion), in units of ε_F, is expressed as a function of the coupling parameter g_{BF}. Errorbars are smaller than symbol size. VMC results (black squares) are adjusted with finite-size corrections described in Sec. 3.2.2. The respective errors are the sum of the statistical fluctuations of VMC algorithm and of the finite-size errors. DMC results (green crosses) are adjusted with finite-size corrections and finite time-step corrections (see Sec. 3.3.2). The respective errors contain also the finite time-step contribution. The DMC results (red circles) differ from the green ones because an exhaustive time-step analysis is conducted. In this case the DMC points are given by the $d\tau \to 0$ extrapolated results and only the finite-size correction is performed. The respective errors are obtained in a similar way to the green case, but this time the time-step uncertainties are given by the errors on the fit of the extrapolated results. For $g_{BF} > 0.4$, DMC simulations cannot be conducted (see Sec. 3.3.1).

Conclusions and perspectives

In this master degree thesis we have studied a two-dimensional Bose-Fermi mixture, with both BF and BB repulsive interactions, using Quantum Monte Carlo techniques. We have extended the methodology developed for a three-dimensional Bose-Fermi mixture to two dimensions. Our simulations were performed for a mixture of bosons and fermions of equal mass, fixed boson concentration $x = 12/49$ and BB repulsive interaction (which in terms of the BB coupling parameter is given by $g_{BB} = 0.0594$), and exploring several values of the BF repulsive interaction, from the weak to the strong-coupling limit. In particular, the Quantum Monte Carlo study was developed at zero-temperature, through the use of two particular techniques: Variational Monte Carlo and Fixed-Node Diffusion Monte Carlo. We have considered a short-range soft-disk potential and used a Jastrow-Slater function as a trial wavefunction.

More specifically, concerning the VMC simulations, we have first optimized the variational parameters introduced in our trial wavefunction, by extrapolating the minimum energies through parabolic fits. Then, we studied how finite-size effects affect our results, finding an effective method to accurately estimate finite-size corrections. These corrections are also used to adjust the DMC results, assuming that the two algorithms depend in the same way on finite-size effects. During the simulations we experienced some issues in the strong-coupling limit (for $g_{BF} > 0.4$). We therefore carried out some analyses, evaluating the pair distribution function of bosons for both the VMC and the DMC methods. Even if this was a qualitative analysis, we have found that, for large values of the BF interaction ($g_{BF} > 0.4$), bosons experience an effective attractive interaction which drives the formation of bosonic clusters. The system then loses its homogeneity and can no longer be described through a Jastrow-Slater wavefunction, which does not foresee the presence of clusters. Based on the limited data we have, we cannot assert the presence of a phase transition and, even more, we cannot establish the possible type of transition. Several possible outlooks are provided by this result. Of course, further analyses are required, especially in the intermediate interaction region ($0.3938 < g_{BF} < 0.5417$) but also in the strong-coupling limit, where a new trial wavefunction is needed in order to properly describe the bosonic clusters. Furthermore, it may be worth to study the dependence of the hypothetical transition with respect to the details of the potential, which are probably relevant in that regime.

On the other hand, considering the DMC simulations, we studied how the choice of a finite time step affects the results. In particular, we performed a time-step ($\mathrm{d}\tau$) analysis for the point with the largest BF interaction and for the one with the least BF interaction. This allowed us to obtain the corrected results for $d\tau \to 0$. The time-step corrections to the intermediate interaction points were obtained through a linear interpolation process.

We have then compared the corrected QMC results with analytic perturbative calculations. In particular we were interested in the second order perturbative correction. We obtained an agreement between the QMC and the theoretical results in the weak-coupling limit (for $g_{BF} < 0.05$). For larger BF interactions, VMC results differ from the DMC and theoretical ones. At the interaction point $g_{BF} = 0.3938$, there is no longer an agreement between the results. DMC result is then the most reliable one, being an upper bound of the true energy.

Several future extensions of the present work are foreseen. First of all, focusing on repulsive Bose-Fermi mixtures, a more thorough analysis of the perturbative regime would require one to consider also different values of the boson concentration n_B/n_F, as well as different mass ratios m_B/m_F. Away from the perturbative regime, it would then be interesting to analyze more in depth the formation of bosonic clusters induced by the Bose-Fermi repulsion. In particular, a stronger Bose-Bose repulsion is expected to suppress the clustering: the interplay between the two kind of interactions should be analyzed in detail. A further important question to be considered is the dependence of the results on the details of the interaction potentials (e.g., the soft-core vs hard-core character of the interaction).

Finally, one could tackle the attractive 2D Bose-Fermi mixtures of relevance to the recent theoretical proposal by Bazak and Petrov [7]. From weak to moderate Bose-Fermi attraction VMC and DMC simulations could be performed with the same trial wavefunction used in the present work, while the strong-coupling case will require using a different trial wavefunction, taking into account the formation of molecules in the system.

Appendix A

Estimation of correlation length and variance

In a Monte Carlo calculation the principal source of statistical error in the measured value of a quantity is usually the fluctuation of that quantity between two successive steps. This is of course due to the innate randomness and statistical nature of MC methods.
If we make N independent measurements of a certain quantity h, it is straightforward to estimate the statistical error associate to such quantity, which is the error on the mean. The true average of h is simply the mean $\bar{h}$ of those N measurements, meanwhile the best estimate of the standard deviation on the mean is given by

$$\sigma = \sqrt{\frac{\frac{1}{N}\sum_{i=1}^{N}(h_i - \bar{h})^2}{N-1}} = \sqrt{\frac{1}{N-1}(\overline{h^2} - \bar{h}^2)} \tag{A.1}$$

However this is not the case we will be dealing with in our Monte Carlo simulations. In fact, due to the generation of random numbers through the Metropolis-Hastings algorithm, correlations between quantities estimated in subsequent steps arise.

Several error estimation methods can be used in case of correlated measurements, among which the simplest is the *blocking method* (see Ref. [80] for other general-purpose error estimation methods). Let us consider N iterations of a stochastic process that produces a series of random values for the observable of interest h_x, where x is the index of the iteration. We can divide the series into n blocks of length $M = N/n$ and calculate the estimator of the mean for each block j, $\langle h_x \rangle_j = \bar{h}_j = \frac{1}{M}\sum_{x\in j} h_x$. If the block length M is sufficiently large (i.e. bigger than the correlation time), each block is independent and, consequently, the $\bar{h}_j$ are independent of each other. Then the expectation value of the observable h is simply given by the average of all $\bar{h}_j$

$$\langle h \rangle = \bar{h} = \frac{1}{n}\sum_j \bar{h}_j = \frac{1}{n}\frac{1}{M}\sum_j \sum_{x\in j} h_x = \frac{1}{N}\sum_x h_x \ , \tag{A.2}$$

whereas the error on the mean is given again by Eq. (A.1), except that N is now replaced by the number n of blocks

$$\sigma = \sqrt{\frac{1}{n(n-1)} \sum_j (\bar{h}_j - \bar{h})^2} \ . \tag{A.3}$$

This method is intuitive and will give a reasonable estimate of the error. However, it strongly depends on the number of different blocks the data are divided into (thus depending on the block length). It is then necessary to perform a *block analysis*, in the sense that the variance associated to the mean (given by the square of Eq. (A.3)) is plotted with respect to different block lengths. So one expects that the variance goes to the previous wrong estimate (the square of Eq. (A.1)) for $M \to 0$, then increases up to a steady value, after $M \approx M_c$, which provides the correct estimate of the (square) error, then possibly decreases again if M is too large and there are too few blocks (see Fig. A.1). The value M_C indicates the correlation length, after which both the correlation effects have disappeared and the central limit theorem starts to be valid.

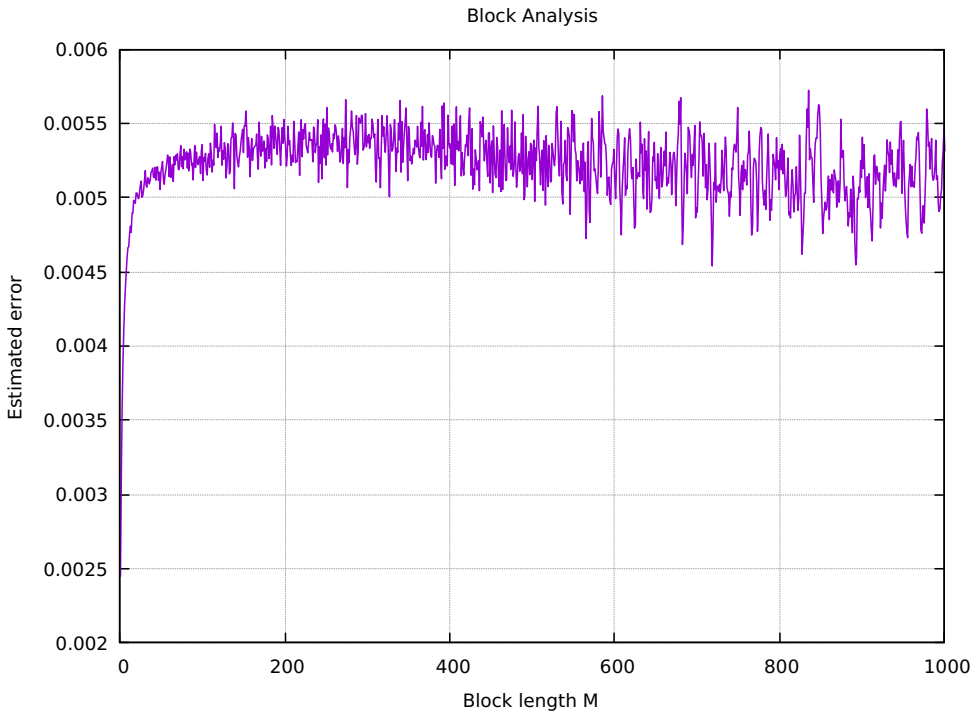

Figure A.1: Example of error estimated with the standard deviation of the block averages as explained in the text (arb. units). In this case we would set $Error = 0.006$, and we would notice that the correlation length is $M_C \approx 100$.

Appendix B

Estimators of observables

The estimators of the observables calculated with VMC are called variational estimators

$$\langle \hat{O} \rangle_V = \frac{\langle \psi_T | \hat{O} | \psi_T \rangle}{\langle \psi_T | \psi_T \rangle} \,, \tag{B.1}$$

while those calculated with DMC are called mixed estimators

$$\langle \hat{O} \rangle_M = \frac{\langle \psi_T | \hat{O} | \phi_0 \rangle}{\langle \psi_T | \phi_0 \rangle} \,. \tag{B.2}$$

We can also define the pure estimator as

$$\langle \hat{O} \rangle_P = \frac{\langle \phi_0 | \hat{O} | \phi_0 \rangle}{\langle \phi_0 | \phi_0 \rangle} \,, \tag{B.3}$$

which corresponds to the true quantum-mechanical equilibrium value at zero temperature.

If the operator $\hat{O}$ commutes with the Hamiltonian $\hat{H}$, i.e. $[\hat{O}, \hat{H}] = 0$, the corresponding mixed estimator can be exact (a trivial example is the case $\hat{O} = \hat{H}$). In general the mixed estimator is an approximation of the pure one (see [81] for the direct calculation of pure estimators in DMC). One can write $\phi_0 = \psi_T + \delta\psi$ and the pure estimator can be approximated with the extrapolated estimator:

$$\langle \hat{O} \rangle_P = \frac{\langle \phi_0 | \hat{O} | \phi_0 \rangle}{\langle \phi_0 | \phi_0 \rangle} = \frac{\langle \psi_T + \delta\psi | \hat{O} | \psi_T + \delta\psi \rangle}{\langle \psi_T + \delta\psi | \psi_T + \delta\psi \rangle} \approx 2\langle \hat{O} \rangle_M - \langle \hat{O} \rangle_V = \langle \hat{O} \rangle_E \,, \tag{B.4}$$

provided $\delta\psi \ll \psi$. Conversely, if we observe that $\langle \hat{O} \rangle_M$ is significantly different from $\langle \hat{O} \rangle_V$, we can infer that the used trial wavefunction is not accurate. An example of this situation is described in Section 3.3.1 where we notice that the variational and mixed estimators of the pair distribution functions of bosons are very different in a certain regime of strong repulsion, and we argue that the used trial wavefunction is not capable to describe the clustering of bosons.

Appendix C

Two-body problem and scattering length in two dimensions

In classical mechanics, the two-body problem consists in determining the motion of two massive objects which are abstractly viewed as point particles. Furthermore, the problem assumes that the two objects interact only with each other, excluding the presence of any external force. In quantum mechanics, things get more complicated due to Heisenberg's uncertainty principle, which prevents to define precisely, at the same time, both the position and the momentum of particles. In this context, the two-body problem is understood as solving the Schroedinger equation for two particles which interact through a certain potential. This problem, therefore, falls within the general framework of scattering theory.

Let us then consider the scattering of two particles (1 and 2) in two dimensions. The starting point is certainly the Schroedinger equation, with the following Hamiltonian:

$$\hat{H} = \frac{\hat{\boldsymbol{P}}_1^2}{2m_1} + \frac{\hat{\boldsymbol{P}}_2^2}{2m_2} + \hat{U}(|\boldsymbol{x}_1 - \boldsymbol{x}_2|) \,, \tag{C.1}$$

where we have assumed a central potential (i.e., a potential that depends only on the distance between the two particles) and we have indicated with $\boldsymbol{x}_1$ and $\boldsymbol{x}_2$ the coordinate vectors of particles 1 and 2 respectively. It is convenient to express the previous Hamiltonian in terms of the center of mass $\overline{\boldsymbol{x}}$ and of the relative position $\boldsymbol{r}$. Let us introduce

$$\begin{aligned} \hat{\overline{\boldsymbol{P}}} &= \hat{\boldsymbol{P}}_1 + \hat{\boldsymbol{P}}_2 \qquad && \text{(total momentum)} \\ \hat{\boldsymbol{P}} &= \frac{m_2\hat{\boldsymbol{P}}_1 - m_1\hat{\boldsymbol{P}}_2}{m_1 + m_2} \qquad && \text{(relative momentum)} \end{aligned} \tag{C.2}$$

which are respectively the conjugate momenta of

$$\begin{aligned} \overline{\boldsymbol{x}} &= \frac{m_1\boldsymbol{x}_1 + m_2\boldsymbol{x}_2}{m_1+m_2} \\ \boldsymbol{r} &= \boldsymbol{x}_1 - \boldsymbol{x}_2 \ . \end{aligned} \tag{C.3}$$

The Hamiltonian thus becomes:

$$\begin{aligned} \hat{H} =& \ \frac{\hat{\boldsymbol{P}}_1^2}{2m_1} + \frac{\hat{\boldsymbol{P}}_2^2}{2m_2} + \hat{U}(|\boldsymbol{x}_1 - \boldsymbol{x}_2|) \\ =& \ \frac{1}{2}\frac{\hat{\boldsymbol{P}}_1^2 m_2(m_1+m_2) + \hat{\boldsymbol{P}}_2^2 m_1(m_1+m_2)}{m_1m_2(m_1+m_2)} + \hat{U}(|\boldsymbol{x}_1 - \boldsymbol{x}_2|) \\ =& \ \frac{1}{2}\frac{m_1m_2(\hat{\boldsymbol{P}}_1^2 + \hat{\boldsymbol{P}}_2^2 + 2\hat{\boldsymbol{P}}_1\hat{\boldsymbol{P}}_2)}{m_1m_2(m_1+m_2)} + \frac{1}{2}\frac{m_1^2\hat{\boldsymbol{P}}_2^2 + m_2^2\hat{\boldsymbol{P}}_1^2 - 2m_1m_2\hat{\boldsymbol{P}}_1\hat{\boldsymbol{P}}_2}{m_1m_2(m_1+m_2)} + \hat{U}(|\boldsymbol{x}_1 - \boldsymbol{x}_2|) \\ =& \ \frac{1}{2}\frac{(\hat{\boldsymbol{P}}_1 + \hat{\boldsymbol{P}}_2)^2}{m_1+m_2} + \frac{1}{2}\left(\frac{m_2\hat{\boldsymbol{P}}_1 - m_1\hat{\boldsymbol{P}}_2}{m_1+m_2}\right)^2 \cdot \left(\frac{m_1+m_2}{m_1m_2}\right) + \hat{U}(|\boldsymbol{x}_1 - \boldsymbol{x}_2|) \\ =& \ \frac{\hat{\overline{\boldsymbol{P}}}^2}{2M} + \left[\frac{\hat{\boldsymbol{P}}^2}{2m_R} + \hat{U}(|\boldsymbol{r}|)\right] \equiv \hat{H}_{CM} + \hat{H}_{rel} \ , \end{aligned} \tag{C.4}$$

where $M = m_1 + m_2$ is the total mass and $m_R = (m_1m_2)/(m_1+m_2)$ is the reduced mass. From now on we assume that the two particles have the same mass $m_1 = m_2 = m$, thus the reduced mass becomes simply $m_R = m/2$. The total Hamiltonian $\hat{H}$ can then be divided into two independent pieces $\hat{H}_{CM}$ and $\hat{H}_{rel}$ which describe respectively the motion of the center of mass $\overline{\boldsymbol{x}}$ and the evolution of the relative position $\boldsymbol{r}$. In particular, since $\hat{H}_{CM}$ contains only the kinetic term, the center of mass moves like a free particle of mass M. These results suggest the following ansatz for the solution of the Schroedinger equation:

$$\psi(\overline{\boldsymbol{x}}, \boldsymbol{r}) = \phi(\overline{\boldsymbol{x}})\varphi(\boldsymbol{r}) \ . \tag{C.5}$$

Assuming now that the external forces are zero, which makes sense in the context of a two-body problem, the total momentum $\overline{\boldsymbol{P}}$ of the center of mass is conserved, and the center-of-mass wavefunction has the free particle form: $\phi(\overline{\boldsymbol{x}}) = e^{i\overline{\boldsymbol{P}}\cdot\overline{\boldsymbol{x}}}$. There is arbitrariness in the choice of $\overline{\boldsymbol{P}}$. For simplicity we choose $\overline{\boldsymbol{P}} = 0$ whereby the above wavefunction becomes

$$\psi(\overline{\boldsymbol{x}}, \boldsymbol{r}) = \varphi(\boldsymbol{r}) \ . \tag{C.6}$$

The previous choice regarding the value of the total momentum $\overline{\boldsymbol{P}}$ allows to simplify the Hamiltonian $\hat{H}$ by ignoring the center of mass term:

$$\hat{H} = \hat{H}_{rel} = \frac{\hat{\boldsymbol{P}}^2}{2m_R} + \hat{U}(|\boldsymbol{r}|) = -\frac{\hbar^2}{m}\nabla^2_{\boldsymbol{r}} + U(|\boldsymbol{r}|) \; . \tag{C.7}$$

We have thus obtained an Hamiltonian which now depends only on the two-dimensional vector of the relative position $\boldsymbol{r}$. At this point, in two-dimensional scattering theory, the next step consists in performing a change of variables going into polar coordinates:

$$\boldsymbol{r} = (r_x, r_y) \longrightarrow (x, \theta)$$
$$\varphi(\boldsymbol{r}) = \varphi(r_x, r_y) \longrightarrow \varphi(x, \theta) \; ,$$

where we have indicated the modulus of the relative position $\boldsymbol{r}$ with the variable x (i.e., $|\boldsymbol{r}| = x$). Expressing the Laplacian in polar coordinates, the Schroedinger equation becomes:

$$\left[\frac{\partial^2}{\partial x^2} + \frac{1}{x}\frac{\partial}{\partial x} + \frac{1}{x^2}\frac{\partial^2}{\partial \theta^2} + \frac{m}{\hbar^2}(E - U)\right]\varphi(x, \theta) = 0 \; . \tag{C.8}$$

Since the Hamiltonian is invariant upon rotation, it is advantageous to perform a *partial wave expansion*, which consists in considering the wavefunction φ as a sum of products, where each term is separated into a radial and an angular part. Let us then plug this

$$\varphi(x, \theta) = \sum_{l=0}^{\infty} R_l(x) Y_l(\theta) = \sum_{l=0}^{\infty} R_l(x) e^{il\theta} \tag{C.9}$$

into the Schroedinger equation (C.8). We thus obtain

$$\begin{aligned}
&\left[\frac{\partial^2}{\partial x^2} + \frac{1}{x}\frac{\partial}{\partial x} + \frac{1}{x^2}\frac{\partial^2}{\partial \theta^2} + \frac{m}{\hbar^2}(E - U)\right]\sum_{l=0}^{\infty} R_l(x) e^{il\theta} = 0 \quad \Longrightarrow \\
&\sum_{l=0}^{\infty}\left[\frac{\partial^2 R_l}{\partial x^2}e^{il\theta} + \frac{1}{x}\frac{\partial R_l}{\partial x}e^{il\theta} + \frac{1}{x^2}R_l(-l^2)e^{il\theta} + \frac{m}{\hbar^2}(E - U)R_l e^{il\theta}\right] = 0 \quad \Longrightarrow \\
&\sum_{l=0}^{\infty}\left[\frac{\partial^2}{\partial x^2} + \frac{1}{x}\frac{\partial}{\partial x} - \frac{l^2}{x^2} + \frac{m}{\hbar^2}(E - U)\right] R_l(x) e^{il\theta} = 0 \; .
\end{aligned} \tag{C.10}$$

For each of the values of l it is possible to solve separate radial Schroedinger equations. In case of s-wave scattering we consider only the $l = 0$ partial wave (which is the leading term for low energy scattering) and the previous equation becomes:

$$\left[\frac{\partial^2}{\partial x^2} + \frac{1}{x}\frac{\partial}{\partial x} + \frac{m}{\hbar^2}(E - U)\right] R_0(x) = 0 \; . \tag{C.11}$$

This is now a one-dimensional Schroedinger equation. Let us call $\frac{m}{\hbar^2}E = k^2$ and $\frac{m}{\hbar^2}U = \widetilde{U}$, then the Eq. (C.11) can be written as

$$\frac{d^2R_0}{dx^2} + \frac{1}{x}\frac{dR_0}{dx} + (k^2 - \widetilde{U})R_0 = 0 \,. \tag{C.12}$$

We can make a substitution, introducing the reduced radial function $u(x)$ which is related to R_0 by the expression $R_0(x) = u(x)/\sqrt{x}$, thus

$$\frac{d^2u}{dx^2} + \left(k^2 + \frac{1}{4x^2} - \widetilde{U}\right)u = 0 \,. \tag{C.13}$$

At this point, in order to solve the Schroedinger equation, it is necessary to make explicit the shape of the potential U. Of course, the choice of U is arbitrary and depends on the system that we are studying. Several potentials can be used, where for each of them it is possible to have a different solution to the problem. In QMC, for a two-dimensional system with repulsive interactions, the most used potentials are:

$$\text{(Hard disk)} \qquad U(x) = \begin{cases} +\infty & x < R \\ 0 & x \geq R \quad (x < L/2) \end{cases} \tag{C.14}$$

$$\text{(Soft disk)} \qquad U(x) = \begin{cases} V_0 & x < R \\ 0 & x \geq R \quad (x < L/2) \end{cases} \tag{C.15}$$

We now consider the case of a soft disk potential, which is the one that we have used for our simulations (the hard disk case can then be derived by the solution taking the $V_0 \to +\infty$ limit for $x < R$). Furthermore, we have to distinguish between two other cases, which are

$$\begin{cases} k^2 \geq \widetilde{U} \\ k^2 < \widetilde{U} \,. \end{cases}$$

We only consider the second option because in our simulations we only deal with repulsive potentials (i.e., $\widetilde{U} > 0$). By introducing $-\widetilde{k}^2 \equiv k^2 - \widetilde{U} = k^2 - \frac{m}{\hbar^2}V_0$, the differential equation (C.13) becomes

$$\frac{d^2u}{dx^2} + \left(-\widetilde{k}^2 + \frac{1}{4x^2}\right)u = 0 \,, \tag{C.16}$$

which is a Bessel's equation whose solution is given by a linear combination of Bessel functions (see [82] for details regarding Bessel's equations and functions). Thus, going back to the radial function $R_0(x)$ we have

$$R_0(x) = \begin{cases} b_1 I_0(\widetilde{k}x) + b_2 K_0(\widetilde{k}x) & \text{for } x < R \\ c_1 J_0(kx) + c_2 Y_0(kx) & \text{for } R \leq x \leq L/2 \\ 1 & \text{for } x > L/2 \end{cases} \tag{C.17}$$

where I_0 and K_0 are the modified Bessel functions of the first and second kind while J_0 and Y_0 are the usual Bessel functions of the first and second kind. The constant solution for $x > L/2$ is a consequence of the periodic boundary conditions to which the system under study is subjected (see Section 2.7 for more clarifications). At this point, the solution to the two-body problem is determined once the values of the coefficients appearing in the above system have been found. This can be done by imposing appropriate boundary conditions. First of all, we need that R_0 goes to zero for $x \to 0$. Studying the behaviour of the modified Bessel functions I_0 and K_0, one finds that the only possibility to satisfy this condition is to require that the coefficient b_2 be zero. Thus the solution simplifies to

$$R_0(x) = \begin{cases} b_1 I_0(\widetilde{k}x) & \text{for } x < R \\ c_1 J_0(kx) + c_2 Y_0(kx) & \text{for } R \leq x \leq L/2 \\ 1 & \text{for } x > L/2\,. \end{cases} \tag{C.18}$$

Now we impose the continuity of R_0 and its first derivative in $x = R$ and $x = L/2$. These conditions will produce four equations, which with the addition of the definition of $\widetilde{k}$, will form a system of five equations for five unknown variables $\left(b_1, c_1, c_2, k, \widetilde{k}\right)$:

$$\begin{cases} c_1 J_0(kR) + c_2 Y_0(kR) - b_1 I_0(\widetilde{k}R) = 0 & (A) \\ c_1 k J_1(kR) + c_2 k Y_1(kR) + b_1 \widetilde{k} I_1(\widetilde{k}R) = 0 & (B) \\ c_1 J_0(kL/2) + c_2 Y_0(kL/2) = 1 & (C) \\ c_1 J_1(kL/2) + c_2 Y_1(kL/2) = 0 & (D) \\ (k^2 - \widetilde{U}) = -\widetilde{k}^2 & (E) \end{cases} \tag{C.19}$$

From (E) we can see that we are able to obtain $\widetilde{k}$ once k is known. Equation (D) can be written as

$$c_1 = -c_2 \frac{Y_1(kL/2)}{J_1(kL/2)}$$

and then can be inserted in (A)

$$-c_2 \frac{Y_1(kL/2)}{J_1(kL/2)} J_0(kR) + c_2 Y_0(kR) = b_1 I_0(\widetilde{k}R) \quad \Longrightarrow$$

$$b_1 = c_2 \left(\frac{Y_0(kR)}{I_0(\widetilde{k}R)} - \frac{Y_1(kL/2)}{J_1(kL/2)} \frac{J_0(kR)}{I_0(\widetilde{k}R)} \right)\,.$$

Now, by plugging (D) and (A) in (B) we get

$$c_2\frac{Y_1(kL/2)}{J_1(kL/2)}kJ_1(kR) - c_2kY_1(kR) - c_2\left(\frac{Y_0(kR)}{I_0(\widetilde{k}R)} - \frac{Y_1(kL/2)}{J_1(kL/2)}\frac{J_0(kR)}{I_0(\widetilde{k}R)}\right)\widetilde{k}I_1(\widetilde{k}R) = 0\ .$$

This is an equation for k (since $\widetilde{k}$ is related to k), which can be solved using numerical algorithms (e.g., *bisection algorithm*) after a qualitative function study. We therefore find a solution $k = k^*$ (or, equivalently, $\widetilde{k} = \widetilde{k}^*$). At this point we insert (D) in (C):

$$-c_2\frac{Y_1(kL/2)}{J_1(kL/2)}J_0(kL/2) + c_2Y_0(kL/2) = 1 \quad \Longrightarrow$$

$$c_2 = \frac{1}{Y_0(kL/2) - \frac{Y_1(kL/2)}{J_1(kL/2)}J_0(kL/2)}\ .$$

Computing this last equation with $k = k^*$ we find the coefficient c_2. Then through (A) we find b_1 and finally using (D) we determine the last unknown coefficient c_1, definitively solving the two-body problem.

Asymptotic behaviour and scattering length

The continuity condition of the logarithmic derivative calculated in R allows us to obtain the ratio between the coefficients c_2 and c_1, which, as we will see in the following, is closely related to the scattering length. Thus, we have that

$$\frac{b_1\widetilde{k}I_1(\widetilde{k}R)}{b_1I_0(\widetilde{k}R)} = \frac{-c_1kJ_1(kR) - c_2kY_1(kR)}{c_1J_0(kR) + c_2Y_0(kR)} \quad \Longrightarrow$$

$$\widetilde{k}\,\frac{I_1(\widetilde{k}R)}{I_0(\widetilde{k}R)}(c_1J_0(kR) + c_2Y_0(kR)) = -c_1kJ_1(kR) - c_2kY_1(kR) \quad \Longrightarrow$$

$$\frac{c_2}{c_1}\left(\widetilde{k}\,\frac{I_1(\widetilde{k}R)}{I_0(\widetilde{k}R)}Y_0(kR) + kY_1(kR)\right) = -kJ_1(kR) - \widetilde{k}\frac{I_1(\widetilde{k}R)}{I_0(\widetilde{k}R)}J_0(kR) \quad \Longrightarrow$$

$$\frac{c_2}{c_1} = \frac{-kJ_1(kR) - \widetilde{k}\frac{I_1(\widetilde{k}R)}{I_0(\widetilde{k}R)}J_0(kR)}{\widetilde{k}\,\frac{Y_0(kR)}{I_0(\widetilde{k}R)}I_1(\widetilde{k}R) + kY_1(kR)}\ . \tag{C.20}$$

At this point we can study the asymptotic behaviour, considering small k. The main reference for the asymptotic form of Bessel functions is still book [82]. The previous expression thus becomes:

$$\frac{c_2}{c_1} = \frac{\pi}{2\,\frac{k^2-\widetilde{U}}{\widetilde{U}}\left[\log(\frac{kR}{2})+\gamma\right]+\frac{4}{\widetilde{U}R^2}} \tag{C.21}$$

$$= -\frac{\pi}{2\,\log\left(k\,Re^{-\frac{2}{\widetilde{U}R}}\,\frac{e^\gamma}{2}\right)} + \mathcal{O}(k^2)\;, \tag{C.22}$$

where γ is the Euler-Mascheroni constant. But, on the other hand, from the scattering theory we know that for small k and at large distances the wavefunction will be that of a free wave shifted by a certain phase shift dependent on l (in our case $l = 0$). In particular, one has that:

$$\frac{c_2}{c_1} = -\frac{A\sin\delta_0}{A\cos\delta_0} = -\tan\delta_0 \;\xrightarrow[k\to 0]{}\; \frac{\pi}{2\log(ka)}\;, \tag{C.23}$$

where a is the so called *scattering length*. By comparing (C.22) with (C.23) we can extract the expression for the scattering length in two dimensions for soft disk potentials:

$$a = R\,e^{-2/\widetilde{U}R}\,\frac{e^\gamma}{2}\;. \tag{C.24}$$

One can notice that, in two dimensions, the scattering length is always positive. It is also very important to stress that, in scattering theory, there is some ambiguity regarding the definition of the scattering length. In fact, there are two different conventions which are distinguished from each other according to the constants included in the definition. The first convention is the one seen above in Eq. (C.24) where all the constant factors are included, the second one, instead excludes the constant term $e^\gamma/2$ from the definition. To avoid confusion, we will indicate the second convention by putting a tilde on the letter a, so that

$$\widetilde{a} = R\,e^{-2/\widetilde{U}R} = \frac{2}{e^\gamma}a\;. \tag{C.25}$$

The hard disk potential case can be obtained by the previous expressions by simply taking the limit $\widetilde{U}\to+\infty$. The convention of (C.25) is then natural when considering the hard-disk potential, since in this case $\tilde{a}$ is equal to the radius of the potential. However, in the case of ultracold gases where the focus is often on attractive interactions, the convention (C.24) is more customary, because it is related to the energy of the universal bound state by $E_b = -\frac{\hbar^2}{ma^2}$, and we therefore use it in order to compare our QMC simulations with perturbative predictions.

Appendix D

Relation between physical and input parameters

In this Appendix we show that there is a connection between the coupling parameters introduced in (3.10) and the input parameters $\widetilde{R}$ and R_P. Let us begin with some algebraic manipulations:

$$\ln(k_F a_{BF}) = \ln[(k_F a_{BF})^2]^{1/2} = \frac{1}{2}\ln(k_F^2 a_{BF}^2) = \frac{1}{2}\ln(4\pi n_F a_{BF}^2) = \frac{1}{2}\ln\left[4\pi n_F \frac{e^{2\gamma}}{4}(\widetilde{a}^{BF})^2\right] ,$$

where in the last equality we have used the relation obtained in Appendix C that links the two different conventions in the definition of the scattering length. At this point we perform the mathematical trick of multiplying and dividing by the same quantity the argument of the logarithm, thus we have

$$\begin{aligned}\frac{1}{2}\ln\left[4\pi n_F \frac{e^{2\gamma}}{4}(\widetilde{a}^{BF})^2\right] &= \frac{1}{2}\ln\left[4\pi n_F \frac{e^{2\gamma}}{4} R_R^2 \left(\frac{R^{BF}}{R_R}\right)^2 \left(\frac{\widetilde{a}^{BF}}{R^{BF}}\right)^2\right] \\ &= \frac{1}{2}\ln\left[4\pi n_F \frac{e^{2\gamma}}{4} R_R^2 \left(\frac{\widetilde{R}^{BF}}{R_P^{BF}}\right)^2\right] ,\end{aligned}$$

using the definitions (3.4) of $\widetilde{R}^{BF}$ and of R_P^{BF}. Then we recall that by the conventions chosen for the reference parameters, the reference length $R_R = 1/\sqrt{n_F}$. So the previous expression becomes

$$\frac{1}{2}\ln\left[4\pi n_F \frac{e^{2\gamma}}{4} R_R^2 \left(\frac{\widetilde{R}^{BF}}{R_P^{BF}}\right)^2\right] = \ln\left[\sqrt{4\pi}\,\frac{e^{\gamma}}{2}\left(\frac{\widetilde{R}^{BF}}{R_P^{BF}}\right)\right] .$$

Thus, we can finally express the coupling parameter g_{BF} in terms of the input parameters:

$$g_{BF} = -\frac{1}{\ln(k_F a_{BF})} = -\frac{1}{\ln\left[\sqrt{4\pi}\,\frac{e^\gamma}{2}\left(\frac{\widetilde{R}^{BF}}{R_P^{BF}}\right)\right]} \quad . \tag{D.1}$$

Similar procedure can be also applied for the calculation of the BB counterpart. Thus, given the logarithm of $n_B a_{BB}^2$, we use again the trick of multiplying and dividing by a same quantity:

$$\ln(n_B a_{BB}^2) = \ln\left[n_B\,\frac{e^{2\gamma}}{4}R_R^2\left(\frac{R^{BB}}{R_R}\right)^2\left(\frac{\widetilde{a}^{BB}}{R^{BB}}\right)^2\right] \ ,$$

where we exploit the relation between the two definitions of scattering length (Appendix C). Then, using the definitions of the input parameters $\widetilde{R}^{BB}$ and R_P^{BB}, we can rewrite the previous expression as

$$\ln\left[n_B\,\frac{e^{2\gamma}}{4}R_R^2\left(\frac{R^{BB}}{R_R}\right)^2\left(\frac{\widetilde{a}^{BB}}{R^{BB}}\right)^2\right] = \ln\left[n_B\,\frac{e^{2\gamma}}{4}R_R^2\left(\frac{\widetilde{R}^{BB}}{R_P^{BB}}\right)^2\right] \quad .$$

At this point, we replace R_R^2 with $1/n_R$ and we introduce the boson concentration $x = n_B/n_F$. So, we obtain

$$\ln\left[n_B\,\frac{e^{2\gamma}}{4}R_R^2\left(\frac{\widetilde{R}^{BB}}{R_P^{BB}}\right)^2\right] = \ln\left[x\,\frac{e^{2\gamma}}{4}\left(\frac{\widetilde{R}^{BB}}{R_P^{BB}}\right)^2\right] \quad .$$

Using the last result we can express the coupling parameter g_{BB} in terms of the input parameters as

$$g_{BB} = -\frac{1}{\ln\left(n_B a_{BB}^2\right)} = -\frac{1}{\ln\left[x\,\frac{e^{2\gamma}}{4}\left(\frac{\widetilde{R}^{BB}}{R_P^{BB}}\right)^2\right]} \ . \tag{D.2}$$

Bibliography

[1] J. Bardeen, L. N. Cooper, and J. R. Schrieffer. "Theory of Superconductivity". In: *Physical Review* **108**, 5 (1957), pp. 1175–1204.

[2] C. Chin, R. Grimm, P. Julienne, and E. Tiesinga. "Feshbach resonances in ultracold gases". In: *Reviews of Modern Physics* **82**, 2 (2010), pp. 1225–1286.

[3] G. Bertaina, E. Fratini, S. Giorgini, and P. Pieri. "Quantum Monte Carlo Study of a Resonant Bose-Fermi Mixture". In: *Physical Review Letters* **110**, 11 (2013), p. 115303.

[4] A. Guidini, G. Bertaina, D. E. Galli, and P. Pieri. "Condensed phase of Bose-Fermi mixtures with a pairing interaction". In: *Physical Review A* **91**, 2 (2015), p. 023603.

[5] G. Bertaina and S. Giorgini. "BCS-BEC Crossover in a Two-Dimensional Fermi Gas". In: *Physical Review Letters* **106**, 11 (2011), p. 110403.

[6] S. Pilati, G. Orso, and G. Bertaina. "Quantum Monte Carlo simulations of two-dimensional repulsive Fermi gases with population imbalance". In: *Physical Review A* **103**, 6 (2021), p. 063314.

[7] B. Bazak and D. S. Petrov. "Stable p-Wave Resonant Two-Dimensional Fermi-Bose Dimers". In: *Physical Review Letters* **121**, 26 (2018), p. 263001.

[8] L. Cardarelli. "Ground state properties of dilute Bose-Fermi mixtures in two and three dimensions". MA thesis. University of Camerino, 2014.

[9] F. Dalfovo, S. Giorgini, L. P. Pitaevskii, and S. Stringari. "Theory of Bose-Einstein condensation in trapped gases". In: *Reviews of Modern Physics* **71**, 3 (1999), pp. 463–512.

[10] I. Bloch, J. Dalibard, and W. Zwerger. "Many-body physics with ultracold gases". In: *Reviews of Modern Physics* **80**, 3 (2008), pp. 885–964.

[11] S. Giorgini, L. P. Pitaevskii, and S. Stringari. "Theory of ultracold atomic Fermi gases". In: *Reviews of Modern Physics* **80**, 4 (2008), pp. 1215–1274.

[12] M. H. Anderson, J. R. Ensher, M. R. Matthews, C. E. Wieman, and E. A. Cornell. "Observation of Bose-Einstein Condensation in a Dilute Atomic Vapor". In: *Science* **269**, 5221 (1995), pp. 198–201.

[13] K. B. Davis, M. -O. Mewes, M. R. Andrews, N. J. van Druten, D. S. Durfee, D. M. Kurn, and W. Ketterle. "Bose-Einstein Condensation in a Gas of Sodium Atoms". In: *Physical Review Letters* **75**, 22 (1995), pp. 3969–3973.

[14] J. R. Taylor. *Scattering Theory: The Quantum Theory of Nonrelativistic Collisions*. Dover Pubns, 2006.

[15] C. J. Pethick and H. Smith. *Bose–Einstein Condensation in Dilute Gases*. Cambridge University Press, 2008.

[16] C. Ospelkaus, S. Ospelkaus, L. Humbert, P. Ernst, K. Sengstock, and K. Bongs. "Ultracold Heteronuclear Molecules in a 3D Optical Lattice". In: *Physical Review Letters* **97**, 12 (2006), p. 120402.

[17] J. J. Zirbel, K.-K. Ni, S. Ospelkaus, J. P. D'Incao, C. E. Wieman, J. Ye, and D. S. Jin. "Collisional Stability of Fermionic Feshbach Molecules". In: *Physical Review Letters* **100**, 14 (2008), p. 143201.

[18] M.-S. Heo, T. T. Wang, C. A. Christensen, T. M. Rvachov, A. Cotta, J.-H. Choi, Y.-R Lee, and W. Ketterle. "Formation of ultracold fermionic NaLi Feshbach molecules". In: *Physical Review A* **86**, 2 (2012), p. 021602.

[19] C.-H. Wu, J. W. Park, P. Ahmadi, S. Will, and M. W. Zwierlein. "Ultracold Fermionic Feshbach Molecules of ^{23}Na^{40}**K**". In: *Physical Review Letters* **109**, 8 (2012), p. 085301.

[20] L. Viverit, C. J. Pethick, and H. Smith. "Zero-temperature phase diagram of binary boson-fermion mixtures". In: *Physical Review A* **61**, 5 (2000), p. 053605.

[21] X. X. Yi and C. P. Sun. "Phase separation of a trapped Bose-Fermi gas mixture: Beyond the Thomas-Fermi approximation". In: *Physical Review A* **64**, 4 (2001), p. 043608.

[22] R. Roth and C. P. Sun. "Mean-field instability of trapped dilute boson-fermion mixtures". In: *Physical Review A* **65**, 2 (2002), p. 021603.

[23] S. Simonucci, P. Pieri, and G. C. Strinati. "Broad vs. narrow Fano-Feshbach resonances in the BCS-BEC crossover with trapped Fermi atoms". In: *Europhysics Letters* **69**, 5 (2005), pp. 713–718.

[24] A. P. Albus, S. A. Gardiner, F. Illuminati, and M. Wilkens. "Quantum field theory of dilute homogeneous Bose-Fermi mixtures at zero temperature: General formalism and beyond mean-field corrections". In: *Physical Review A* **65**, 5 (2002), p. 053607.

[25] L. Viverit and S. Giorgini. "Ground-state properties of a dilute Bose-Fermi mixture". In: *Physical Review A* **66**, 6 (2002), p. 063604.

[26] K. Helfrich, H.-W. Hammer, and D. S. Petrov. "Three-body problem in heteronuclear mixtures with resonant interspecies interaction". In: *Physical Review A* **81**, 4 (2010), p. 042715.

[27] E. Fratini and P. Pieri. "Pairing and condensation in a resonant Bose-Fermi mixture". In: *Physical Review A* **81**, 5 (2010), p. 051605.

[28] W. Feller. *An introduction to probability theory and its applications*. New York: J. Wiley, 1957.

[29] B. Gnedenko. *The theory of Probability*. Moscow: Mir Publ., 1975.

[30] J. M. Hammersley and D. C. Handscomb. *Monte Carlo Methods*. Norwich: Methuen, 1965.

[31] S. Sorella and F. Becca. *SISSA Lecture notes on Numerical methods for strongly correlated electrons*. June 2016.

[32] R. Guardiola. *Monte Carlo Methods in Quantum Many-Body Theories*. Springer, 1998.

[33] D. E. Knuth. *The Art of Computer Programmer, Vol. II Seminumerical Algorithms*. New York: Addison Wesley, 1971.

[34] G. E. P. Box and M. E. Muller. "A Note on the Generation of Random Normal Deviates". In: *The Annals of Mathematical Statistics* **29**, 2 (1958), pp. 610–611.

[35] P. G. Hoel, S. C. Port, and C. J. Stone. *Introduction to stochastic processes*. Boston: Houghton Mifflin Company, 1972.

[36] M. Gardner. *Circo Matemático*. Madrid: Alianza, 1985.

[37] N. Metropolis, A. W. Rosenbluth, M. N. Rosenbluth A. H. Teller, and E. W. Teller. "Equation of State Calculations by Fast Computing Machines". In: *The Journal of Chemical Physics* **21**, 6 (1953), pp. 1087–1092.

[38] W. K. Hastings. "Monte Carlo sampling methods using Markov chains and their applications". In: *Biometrika* **57**, 1 (1970), pp. 97–109.

[39] M. H. Kalos and P.A. Whitlock. *Monte Carlo Methods*. Wiley-VCH, 2nd edition, 2008.

[40] W. A. Press, S. A. Teukolsky, W. T. Vettering, and B. P. Flannery. *Numerical Recipes in Fortran*. Cambridge: Cambridge University Press, 2nd edition, 1992.

[41] N. Metropolis and S. Ulam. "The Monte Carlo Method". In: *Journal of the American Statistical Association* **44**, 247 (1949), pp. 335–341.

[42] W. McMillan. "Ground State of Liquid ^4He". In: *Physical Review* **138**, A442 (1965).

[43] J. B. Anderson. "A random-walk simulation of the Schrödinger equation: H_3^+". In: *The Journal of Chemical Physics* **63**, 4 (1975).

[44] D. M. Ceperley and B. J. Alder. "Ground State of the Electron Gas by a Stochastic Method". In: *Physical Review Letters* **45**, 7 (1980), pp. 566–569.

[45] P. J. Reynolds, D. M. Ceperley, B. J. Alder, and W. A. Lester. "Fixed-node quantum Monte Carlo for molecules". In: *The Journal of Chemical Physics* **77**, 11 (1982), pp. 5593–5603.

[46] D. M. Ceperley. "Metropolis Methods for Quantum Monte Carlo Simulations". In: *AIP Conference Proceedings* **690** (2003), pp. 85–98.

[47] D. Ceperley, G. V. Chester, and M. H. Kalos. "Monte Carlo simulation of a many-fermion study". In: *Physical Review B* **16**, 7 (1977), pp. 3081–3099.

[48] B. H. Bransden and C. J. Joachain. *Physics of Atoms and Molecules*. Harlow: Prentice Hall, 2nd edition, 2003.

[49] J. B. Anderson. "Quantum chemistry by random walk. $H\ ^2P$, $H_3^+\ D_{3h}\ ^1A_1'$, $H_2\ ^3\Sigma_u^+$, $H_4\ ^1\Sigma_g^+$, $Be\ ^1S$". In: *The Journal of Chemical Physics* **65**, 10 (1976), pp. 4121–4127.

[50] B. L. Hammond, W. A. Jr Lester, and P. J. Reynolds. *Monte Carlo Methods in Ab Initio Quantum Chemistry*. Singapore: World Scientific, 1994.

[51] I. Kosztin, B. Faber, and K. Schulten. "Introduction to the diffusion Monte Carlo method". In: *American Journal of Physics* **64**, 5 (1996), pp. 633–644.

[52] W. M. C. Foulkes, L. Mitas, R. J. Needs, and G. Rajagopal. "Quantum Monte Carlo simulations of solids". In: *Reviews of Modern Physics* **73**, 1 (2001), pp. 33–83.

[53] J. Boronat. *Monte Carlo simulations at zero temperature: Helium in one, two and three dimensions*. World Scientific Publishing Co. Pte. Ltd., 2002.

[54] N. Hatano and M. Suzuki. "Finding Exponential Product Formulas of Higher Orders". In: *Lecture Notes in Physics* **679** (2005), pp. 37–68.

[55] R. Assaraf, M. Caffarel, and A. Khelif. "Diffusion Monte Carlo methods with a fixed number of walkers". In: *Physical Review E* **61**, 4 (2000), pp. 4566–4575.

[56] M. H. Kalos, D. Levesque, and L. Verlet. "Helium at zero temperature with hard-sphere and other forces". In: *Physical Review A* **9**, 5 (1974), pp. 2178–2195.

[57] J. Vrbik and S. M. Rothstein. "Quadratic accuracy diffusion Monte Carlo". In: *Journal of Computational Physics* **63**, 1 (1986), pp. 130–139.

[58] C. J. Umrigar, M. P. Nightingale, and K. J. Runge. "A diffusion Monte Carlo algorithm with very small time-step errors". In: *The Journal of Chemical Physics* **99**, 4 (1993), pp. 2865–2890.

[59] M. Lee, K. Schmidt, M. Kalos, and G. Chester. "Green's Function Monte Carlo Method for Liquid ^3He". In: *Physical Review Letters* **46**, 11 (1981), pp. 728–731.

[60] D. M. Ceperley and B. J. Alder. "Quantum Monte Carlo for molecules: Green's function and nodal release". In: *The Journal of Chemical Physics* **81**, 12 (1984), pp. 5833–5844.

[61] D. M. Ceperley and B. Bernu. "The calculation of excited state properties with quantum Monte Carlo". In: *The Journal of Chemical Physics* **89**, 10 (1988), pp. 6316–6328.

[62] M. Troyer and U.-J. Wiese. "Computational Complexity and Fundamental Limitations to Fermionic Quantum Monte Carlo Simulations". In: *Physical Review Letters* **94**, 17 (2005), pp. 170201–170205.

[63] J. Moskowitz, K. E. Schmidt, M. A. Lee, and M. H. Kalos. "A new look at correlation energy in atomic and molecular systems. II. The application of the Green's function Monte Carlo method to LiH". In: *The Journal of Chemical Physics* **77**, 1 (1982), pp. 349–355.

[64] S. Giorgini, J. Boronat, and J. Casulleras. "Ground state of a homogeneous Bose gas: A diffusion Monte Carlo calculation". In: *Physical Review A* **60**, 6 (1999), pp. 5129–5132.

[65] J. P. Bouchaud, A. Georges, and C. Lhuillier. "Pair wave functions for strongly correlated fermions and their determinantal representation". In: *Journal de Physique* **49**, 4 (1988), pp. 553–559.

[66] J. Carlson, S.-Y. Chang, V. R. Pandharipande, and K. E. Schmidt. "Superfluid Fermi Gases with Large Scattering Length". In: *Physical Review Letters* **91**, 5 (2003), p. 050401.

[67] G. Astrakharchik, J. Boronat, J. Casulleras, and S. Giorgini. "Equation of State of a Fermi Gas in the BEC-BCS Crossover: A Quantum Monte Carlo Study". In: *Physical Review Letters* **93**, 20 (2004), p. 200404.

[68] G. Bertaina. "Study of Ultracold Fermi Gases in the BCS-BEC Crossover: Quantum Monte Carlo Methods, Hydrodynamics and Local Density Approximation". PhD thesis. Università degli Studi di Trento, 2010.

[69] S. Pilati and S. Giorgini. "Phase Separation in a Polarized Fermi Gas at Zero Temperature". In: *Physical Review Letters* **100**, 3 (2008), p. 030401.

[70] W. W. Wood and F. R. Parker. "Monte Carlo Equation of State of Molecules Interacting with the Lennard-Jones Potential. I. A Supercritical Isotherm at about Twice the Critical Temperature". In: *The Journal of Chemical Physics* **27**, 3 (1957), pp. 720–733.

[71] R. Bombín, T. Comparin, G. Bertaina, F. Mazzanti, S. Giorgini, and J. Boronat. "Two-dimensional repulsive Fermi polarons with short- and long-range interactions". In: *Physical Review A* **100**, 2 (2019), p. 023608.

[72] S. Rossotti, M. Teruzzi, D. Pini, D. E. Galli, and G. Bertaina. "Quantum Critical Behavior of One-Dimensional Soft Bosons in the Continuum". In: *Physical Review Letters* **119**, 21 (2017), p. 215301.

[73] G. Bertaina, M. Motta, M. Rossi, E. Vitali, and D. E. Galli. "One-Dimensional Liquid ^{4}He: Dynamical Properties beyond Luttinger-Liquid Theory". In: *Physical Review Letters* **116**, 13 (2016), p. 135302.

[74] B. Tanatar and D. M. Ceperley. "Ground state of the two-dimensional electron gas". In: *Physical Review B* **39**, 8 (1989), pp. 5005–5016.

[75] Y. Kwon, D. M. Ceperley, and R. M. Martin. "Quantum Monte Carlo calculation of the Fermi-liquid parameters in the two-dimensional electron gas". In: *Physical Review B* **50**, 3 (1994), pp. 1684–1694.

[76] G. E. Astrakharchik. "Quantum Monte Carlo study of ultracold gases". PhD thesis. Università degli Studi di Trento, 2004.

[77] M. F. DePasquale, S. M. Rothstein, and J. Vrbik. "Reliable diffusion quantum Monte Carlo". In: *The Journal of Chemical Physics* **89**, 6 (1988), pp. 3629–3637.

[78] C. Mora and Y. Castin. "Ground State Energy of the Two-Dimensional Weakly Interacting Bose Gas: First Correction Beyond Bogoliubov Theory". In: *Physical Review Letters* **102**, 18 (2009), p. 180404.

[79] G. E. Astrakharchik, J. Boronat, I. L. Kurbakov, Yu. E. Lozovik, and F. Mazzanti. "Low-dimensional weakly interacting Bose gases: Nonuniversal equations of state". In: *Physical Review A* **81**, 1 (2010), p. 013612.

[80] M. E. J. Newman and G. T. Barkema. *Monte Carlo Methods in Statistical Physics*. Oxford: Clarendon Press, 1999.

[81] A. Sarsa, J. Boronat, and J. Casulleras. "Quadratic diffusion Monte Carlo and pure estimators for atoms". In: *The Journal of Chemical Physics* **116**, 14 (2002), pp. 5956–5962.

[82] M. Abramowitz and I. A. Stegun. *Handbook of Mathematical Functions, With Formulas, Graphs, and Mathematical Tables*. Dover Pubns, 1965.